

Lagrangian ocean analysis: fundamentals and practices

Erik van Sebille^{a,b}, Stephen M. Griffies^c, Ryan Abernathey^d, Thomas P. Adams^e, Pavel Berloff^f, Arne Biastoch^g, Bruno Blanke^h, Eric P. Chassignetⁱ, Yu Cheng^j, Colin J. Cotter^f, Eric Deleersnijder^{k,l}, Kristofer Döösⁿ, Henri Drake^{o,p}, Sybren Drijfhout^q, Stefan F. Gary^e, Arnold W. Heemink^l, Joakim Kjellsson^{r,t}, Inga Monika Koszalka^g, Michael Lange^{a,s}, Camille Lique^h, Graeme A. MacGilchrist^u, Robert Marsh^q, C. Gabriela Mayorga Adame^v, Ronan McAdam^a, Francesco Nencioli^w, Claire B. Paris^j, Matthew D. Piggott^s, Jeff A. Polton^v, Siren Rühs^g, Syed H. A. M. Shah^{m,l}, Matthew D. Thomas^x, Jinbo Wang^y, Phillip J. Wolfram^z, Laure Zanna^t, Jan D. Zika^a

^a Grantham Institute & Department of Physics, Imperial College London, UK

^b Institute for Marine and Atmospheric Research, Utrecht University, Utrecht, Netherlands

^c NOAA / Geophysical Fluid Dynamics Laboratory, Princeton, USA

^d Department of Earth and Environmental Sciences, Columbia University, NY, USA

^e Scottish Association for Marine Science, Oban, UK

^f Department of Mathematics, Imperial College London, UK

^g GEOMAR Helmholtz Centre for Ocean Research Kiel, Kiel, Germany

^h Laboratoire d'Oceanographie Physique et Spatiale, UMR 6523,

CNRS-IFREMER-IRD-UBO, Brest, France

ⁱ Center for Ocean-Atmospheric Prediction Studies, Florida State University, Tallahassee, FL, USA

^j Department of Ocean Sciences, Rosenstiel School of Marine and Atmospheric Science, University of Miami, USA

^k Université catholique de Louvain, Institute of Mechanics, Materials and Civil Engineering (IMMC) & Earth and Life Institute (ELI), Louvain-la-Neuve, Belgium

^l Delft Institute of Applied Mathematics (DIAM), Delft University of Technology, Netherlands

^m Department of Mathematics, Sukkur Institute of Business Administration, Pakistan

ⁿ Department of Meteorology, Bolin Centre for Climate Research, Stockholm University, Sweden

^o Department Atmospheric and Oceanic Sciences, Princeton University, USA

^p Currently at Massachusetts Institute of Technology and Woods Hole Oceanographic Institution Joint Program in Oceanography, USA

^q University of Southampton, UK

^r British Antarctic Survey, Cambridge, UK

^s Department of Earth Science and Engineering, Imperial College London, UK

^t Department of Physics, University of Oxford, UK

^u Department of Earth Sciences, University of Oxford, UK

^v National Oceanography Centre, Liverpool, UK

^w Remote Sensing Group, Plymouth Marine Laboratory, Plymouth, UK

^x School of Geology and Geophysics, Yale University, USA

^y*Jet Propulsion Laboratory, California Institute of Technology, USA*

^z*T-3 (Climate, Ocean and Sea Ice Modeling), Los Alamos National Laboratory, USA*

Abstract

Lagrangian analysis is a powerful way to analyse the output of ocean circulation models and other ocean velocity data such as from altimetry. In the Lagrangian approach, large sets of virtual particles are integrated within the three-dimensional, time-evolving velocity fields. Over several decades, a variety of tools and methods for this purpose have emerged. Here, we review the state of the art in the field of Lagrangian analysis of ocean velocity data, starting from a fundamental kinematic framework and with a focus on large-scale open ocean applications. Beyond the use of explicit velocity fields, we consider the influence of unresolved physics and dynamics on particle trajectories. We comprehensively list and discuss the tools currently available for tracking virtual particles. We then showcase some of the innovative applications of trajectory data, and conclude with some open questions and an outlook. The overall goal of this review paper is to reconcile some of the different techniques and methods in Lagrangian ocean analysis, while recognising the rich diversity of codes that have and continue to emerge, and the challenges of the coming age of petascale computing.

Key words: Ocean circulation, Lagrangian analysis, Connectivity, Particle tracking, Future modeling

Contents

1	Introduction	4
1.1	Estimating pathways	4
1.2	Overview of Lagrangian ocean analysis	5
1.3	Structure of this paper	8
2	Kinematic framework	8
2.1	Lagrangian and Eulerian reference frames	8
2.2	Trajectories or material pathlines	9
2.3	The material time derivative without trajectories	10
2.4	Steady-state volume transport pathways defined by streamtubes	11

2.5	An introduction to tracer transport pathways	12
2.5.1	The tracer equation with subgrid scale transport	13
2.5.2	Introducing the Fokker-Planck equation	15
2.5.3	Using particles to track a tracer patch	16
3	Computing Lagrangian particle trajectories	16
3.1	Basic needs for Lagrangian trajectory calculations	16
3.2	Temporal integration of the virtual particle trajectory equation	18
3.2.1	Explicit time stepping methods	20
3.2.2	Time-implicit discrete integration schemes	21
3.2.3	An analytical discrete streamtube method	21
3.3	Computing stochastic trajectories to simulate diffusion and unresolved physics	23
3.3.1	Stochastic trajectories using the Fokker-Planck equation	24
3.3.2	A hierarchy of Markov models for stochastic trajectories	26
3.3.3	When and how to add stochastic terms?	28
3.4	Spatial interpolation	29
3.5	Available tools	30
4	Applications of Lagrangian particle trajectories	31
4.1	Dispersion and diffusivity	31
4.2	Lagrangian Coherent Structures	35
4.3	Probability distributions	38
4.4	Water mass ages and transit times	41
4.5	Volume transport and Lagrangian streamfunctions	43
4.6	Biological connectivity	45
5	Outlook	46
5.1	The next generation of particle tools	46
5.2	A case for standard tests of particle tools	47
5.3	Whole-Earth System and Water Cycle Modelling	48
6	Concluding remarks	51
A	Community tools for Lagrangian Ocean Analysis	52
A.1	Community-based offline 3D Lagrangian codes	52
A.1.1	Ariane	52
A.1.2	TRACMASS	53

A.1.3	Octopus	54
A.1.4	LAMTA software package	54
A.1.5	The Connectivity Modeling System (CMS)	55
A.1.6	Other Biotic-particle models	56
A.1.7	Parcels	56
A.2	Online tools within OGCMs	56
A.2.1	LIGHT within MPAS-O	56
A.2.2	NEMO	57
A.2.3	MITgcm	57
A.2.4	HYCOM	58
A.2.5	ROMS	58
B	Tracer trajectories with isopycnal diffusion	59
C	Diffusion in two-dimensional models and associated Lagrangian tracer trajectories	61

1 1. Introduction

2 The ocean exhibits a huge range of dynamical motions, spanning scales
3 from millimeters to thousands of kilometers. As seawater moves, each fluid
4 particle carries tracers such as salt, nutrients, heat, as well as particulate
5 matter such as plankton and marine debris. For various theoretical and
6 practical applications, we are interested in how water moves between ocean
7 regions. That is, we are interested in mapping out pathways of seawater
8 motion, since the transport of seawater and its tracer content, as well as the
9 pathways and timescales for that transport, are key facets in how the ocean
10 plays a role in climate and marine ecology.

11 1.1. Estimating pathways

12 There are two general methods for estimating pathways in the ocean. One
13 method makes use of tracers, such as the multitude of age tracers described
14 by Mouchet et al. (2016) and references therein. Tracer studies are well suited
15 for Eulerian methods, which make direct use of ocean velocity fields on their
16 native grids.

17 The second approach makes exclusive use of the Lagrangian perspective
18 of fluid dynamics (e.g., Bennett, 2006). This method employs an ensemble of
19 virtual (passive) Lagrangian particles of zero spatial extent whose trajectories

20 are determined by the velocity field.¹ The velocity fields that are used to
21 move the particles often come from OGCMs, although there are interesting
22 application using observational-based velocities such as surface geostrophic
23 velocities based on satellite altimetry (e.g. d'Ovidio et al., 2009; Klocker and
24 Abernathey, 2014), or measured by high frequency (HF) radar (e.g. Ullman
25 et al., 2006).

26 Trajectories for virtual particles map out pathlines of the velocity field,
27 often including the effect of subgrid scale diffusion. Statistics of the trajectories
28 then define particle pathways and their associated time scales. By following
29 the flow of virtual particles, and possibly assigning non-zero transports and
30 other properties to them in post-processing, questions about pathways and
31 flow connectivity can be addressed.

32 This review focuses on Lagrangian analysis methods facilitated by virtual
33 particles in the open ocean. We are partly motivated by the growing array
34 of floating instruments in the ocean along with the improving Lagrangian
35 simulation capabilities. There is a corresponding need to review the methods
36 and foster new ideas for extracting information about the ocean circulation
37 from the entangled trajectories of floats and/or simulated particles. We
38 thus aim to summarize the state of the science in Lagrangian modelling and
39 analysis, focussing on the large scale open ocean circulation, hoping to support
40 a new generation of scientists contributing to the development and use of the
41 methods.

42 Our presentation is aimed at graduate students, though any large-scale
43 oceanographer or mathematician with an interest in virtual particle analysis
44 could use this paper as a starting point. In that sense, this paper is intended
45 as an accompanying paper to Griffies et al. (2000), which provided an intro-
46 duction to primitive equation ocean models and to Ådlandsvik et al. (2009),
47 which gave an overview of Lagrangian modelling practice from a marine
48 biology perspective.

49 *1.2. Overview of Lagrangian ocean analysis*

50 Observationalists have been tracking the ocean in a Lagrangian fashion
51 since the very early ages of oceanography. Movements of the currents were
52 documented using either ship drift or the drift of purposely built (subsurface)

¹Lagrangian particles are also sometimes called ‘e-floats’ by, for example, Bower et al. (2009).

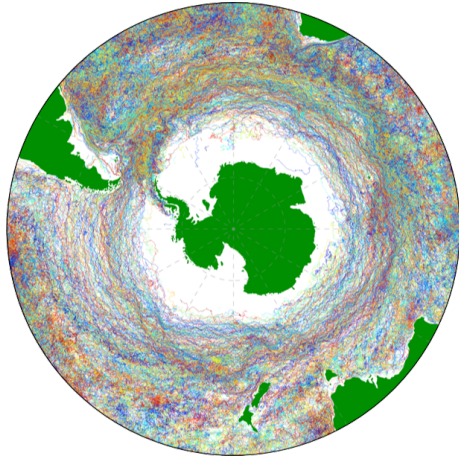


Figure 1: Map of all the Southern Ocean observational Lagrangian surface drifters in the NOAA GDP Data Set (Lumpkin and Pazos, 2007). Each drifter is geo-located every 6 hours and has a randomly assigned colour.

53 floats (e.g., Swift and Riser, 1994). Many observations remain inherently
 54 Lagrangian, such as the trajectories of surface drifters shown in Figure 1
 55 (Lumpkin and Pazos, 2007), the subsurface Argo floats (Lebedev et al., 2007;
 56 Ollitrault and Rannou, 2013), and the tracking of fish larvae (Paris et al.,
 57 2013a) and turtle hatchlings (Scott et al., 2014).

58 Lagrangian analysis through virtual particle tracking within OGCMs began
 59 in the 1980s, on small-scale structures, with studies on a theoretical box-model
 60 (Awaji et al., 1980) as well as a model that incorporated hydrographic data
 61 and realistic topography (Imasato et al., 1980). The Lagrangian framework
 62 of these small-scale examples was then applied to the velocity-field output
 63 of basin-scale, three-dimensional numerical experiments. Examples include
 64 regional deep ocean circulation (Fujio and Imasato, 1991), western boundary
 65 currents (Imasato and Qiu, 1987), fronts (Pavia and Cushman-Roisin, 1988)
 66 and gyre transport (Böning and Cox, 1988). Particle trajectories in global
 67 ocean circulation models, driven by global hydrographic and wind observations,
 68 were first achieved in the 1990s (Fujio et al., 1992; Döös, 1995; Drijfhout et al.,
 69 1996; Blanke and Raynaud, 1997).

70 In recent years, more than 100 articles per year are published with the
 71 words ‘Lagrangian Ocean Modelling’ as the topic, according to the Web of
 72 Science. These papers include studies on the pathways of virtual particles
 73 that simulate sea water pathways, as well as explicit tracking of tracers such

as nutrients (e.g. Chenillat et al., 2015; Jönsson et al., 2011) and particulates such as larvae (e.g. Cowen et al., 2006; Paris et al., 2005; Teske et al., 2015; Cetina-Heredia et al., 2015; Phelps et al., 2015), plastics (e.g. Lebreton et al., 2012), microbes (e.g. Hellweger et al., 2014), planktic foraminifera (e.g. van Sebille et al., 2015), jellyfish (e.g. Dawson et al., 2005), icebergs (e.g. Marsh et al., 2015), surface drifters (e.g. Kjellsson and Döös, 2012b), oil droplets (e.g. Paris et al., 2012), eel (e.g. Baltazar-Soares et al., 2014), pumice (e.g. Jutzeler et al., 2014) and many more.

The ocean circulation covers an enormous range of scales and regions. As said above, in this review we focus primarily on applications on the basin and global scales. However, it should be noted that there is also extensive Lagrangian analysis work done on smaller scales, such as in coastal zones and recently in the Gulf of Mexico through interest in dispersion of the DeepWater Horizon oil spill (e.g. Beron-Vera and LaCasce, 2016; Haza et al., 2016).

The Lagrangian framework is not only used to analyse velocity fields by computing their integral curves, but also to directly solve for the trajectory by casting the equations of motion in a Lagrangian framework (Bennett, 2006). Lagrangian methods are widely used in engineering, including Discrete Element Methods (e.g. Kruggel-Emden et al., 2008) and Smoothed Particle Hydrodynamics (e.g. Cummins et al., 2012). While advances in this field have been made in large scale oceanography, both for sub-components of ocean models (e.g. Bates et al., 2012) and for fully Lagrangian ocean models (Haertel and Randall, 2002; Haertel and Fedorov, 2012), this topic is not the focus of this review. Instead, we focus on Lagrangian diagnostic methods to identify oceanic pathways.

The Lagrangian framework for analysing pathways is complementary to the analysis of tracers. One of the key differences is the computational cost. For each time step, movement of a Lagrangian particle takes only one set of computations. In contrast, the advection-diffusion of a tracer concentration takes N sets of computation, where N is the number of discrete ocean grid cells. While one Lagrangian particle trajectory does not allow for meaningful analysis of ocean pathways, this comparison does show that the computational scaling of the two methods is very different.

Furthermore, the experimental design is different for tracer and particle experiments. Exclusive to particle experiments is that the entire trajectory history of the virtual particles can in principle be stored. This history allows for *a posteriori* analysis of ‘connectivity’ between different regions of the ocean (e.g., sections 4.5 and 4.6) and ‘conditional statistics’ (e.g. Koszalka et al.,

112 2013b; van Sebille et al., 2013, 2014; von Appen et al., 2014; Gary et al., 2014;
113 Durgadoo et al., 2017), where subsets of particles can be analysed that obey
114 certain conditions based on their properties. For example, in van Sebille et al.
115 (2013), particles in the Southern Ocean were analysed for how often they
116 looped around Antarctica in their journey from the Antarctic slope to the
117 deep subtropical basins. Such an analysis would be hard to do with tracer
118 fields, although the latter has its own advantages, including a more natural
119 alignment with the treatment of advection and diffusion within models.

120 Finally, another great advantage of Lagrangian particle experiments is
121 that particles can be advected, at least in offline mode when velocity fields are
122 stored, backwards in time. This reverse-time analysis allows one to investigate
123 where water masses found within a model at a certain location come from.

124 *1.3. Structure of this paper*

125 This paper is structured as follows. In Section 2 we introduce a kinematic
126 framework used for thinking about Lagrangian particles. In Section 3 we detail
127 how to compute and interpret Lagrangian particles, including an overview
128 of the available Lagrangian diagnostic tools. In Section 4, we highlight
129 applications of how virtual particle trajectories can be analysed to reveal
130 quantitative and qualitative information about the flow. In Section 5, we
131 conclude the main part of the paper with future outlooks. A selection of
132 appendices then provide examples and detailed discussion of topics introduced
133 earlier in the paper, as well as brief descriptions of the different numerical
134 codes introduced in Section 3.

135 **2. Kinematic framework**

136 We here introduce a kinematic framework to describe fluid motions. The
137 ideas are fundamental to how we make use of both Eulerian and Lagrangian
138 methods for analyzing ocean circulation. We make connections to Lagrangian
139 analysis methods, though reserve algorithmic details for later sections.

140 *2.1. Lagrangian and Eulerian reference frames*

141 A Lagrangian kinematic approach is based on a description of the fluid in a
142 reference frame that is moving with an infinitesimal fluid particle (equivalently
143 a “fluid parcel”). Fluid motion is thus the accumulation of continuum particle
144 motion. The fluid particle framework that forms the basis for Lagrangian
145 kinematics offers a powerful conceptual picture of fluid motion (e.g., Salmon,

146 1998; Bennett, 2006), with this picture taken as the basis for Lagrangian
147 methods of analysis.

148 Eulerian kinematics is a complement to Lagrangian kinematics. The
149 Eulerian approach is based on describing fluid motion in a reference frame
150 that is fixed in space. Eulerian kinematics is the basis for most numerical
151 ocean circulation models, in which the horizontal position of grid cells is
152 held fixed in time². Quite generally, the technical aim of Lagrangian ocean
153 analysis is to estimate the trajectory of virtual fluid particles by making use
154 of Eulerian fluid information, i.e., the velocity field.

155 *2.2. Trajectories or material pathlines*

156 The motion of a classical point particle is described by knowledge of its
157 position vector, $\mathbf{X}(t)$, which provides the position of the particle at time
158 t . As the particle moves, it traces out a curve in space referred to as a
159 *trajectory*. When describing N discrete particles, we add a discrete label
160 to each of the particle positions, $\mathbf{X}^{(n)}(t)$. For continuum matter, such as
161 seawater, the discrete label n becomes a continuous vector, $\mathbf{X}(\mathbf{a}, t)$, with
162 $\mathbf{a} = \mathbf{X}(t = t_0)$ a common (though not necessary) choice. In general, the label
163 vector, \mathbf{a} , is referred to as the *material* coordinate (e.g., Salmon, 1998), since
164 this coordinate distinguishes between infinitesimal particles comprising the
165 continuum.

166 A fluid particle is conceived of as a microscopically large collection of
167 many molecules, whose velocity is formally determined as a mass weighted
168 mean of the velocity of the individual molecules (i.e., *barycentric* velocity
169 as defined in Section II.2 of DeGroot and Mazur (1984) and Section 1.9 of
170 Salmon (1998)). Alternatively, by making the continuum hypothesis, we
171 dispense with molecular degrees of freedom, so that a particle is considered
172 a macroscopically small material fluid volume, treated as a mathematical
173 continuum and labelled by the material coordinate \mathbf{a} . For an incompressible
174 fluid, the fluid particle has constant volume; however, its constituents do
175 not remain fixed, as they are generally exchanged with adjacent particles
176 through mixing, thus changing the particle's tracer content (e.g., water, salt,

2The top and bottom faces of grid cells are generally moving, since the general vertical coordinates defining these surfaces need not be static. For example, these cell faces may be defined according to constant pressure, constant potential density, or constant rescaled ocean depth.

177 nutrients), as well as altering its heat, all the while maintaining a constant
178 volume.

179 The velocity of a fluid particle is the time derivative of the trajectory,
180 computed with the material coordinate held fixed. The mathematical connec-
181 tion between Lagrangian and Eulerian descriptions is enabled by equating the
182 particle velocity crossing a point in space, $\mathbf{X}(\mathbf{a}, t) = \mathbf{x}$, to the fluid velocity
183 field at that point

$$\left(\frac{\partial \mathbf{X}(\mathbf{a}, t)}{\partial t} \right)_{\mathbf{a}} = \mathbf{v}(\mathbf{x}, t) \quad \text{where } \mathbf{X}(\mathbf{a}, t) = \mathbf{x}. \quad (1)$$

184 The relation (1) provides a starting point for Lagrangian fluid analysis. Note
185 that the resulting fluid particle trajectories are sometimes called material
186 pathlines in the fluid mechanics literature (e.g., Aris, 1962; Batchelor, 1967).

187 2.3. The material time derivative without trajectories

188 A kinematic description requires time changes of an arbitrary function, Ψ ,
189 evaluated along trajectories, $\Psi[\mathbf{X}(\mathbf{a}, t), t]$. Use of the chain rule leads to

$$\frac{\partial \Psi[\mathbf{X}(\mathbf{a}, t), t]}{\partial t} = \left[\left(\frac{\partial}{\partial t} \right)_{\mathbf{x}} + \mathbf{v}[\mathbf{X}(\mathbf{a}, t), t] \cdot \nabla \right] \Psi[\mathbf{X}(\mathbf{a}, t), t]. \quad (2)$$

190 Note that, when trajectories are dispensed with (as in the Eulerian descrip-
191 tion), we recover the more succinct expression for the material time derivative

$$\frac{D\Psi(\mathbf{x}, t)}{Dt} = \left(\frac{\partial}{\partial t} + \mathbf{v}(\mathbf{x}, t) \cdot \nabla \right) \Psi(\mathbf{x}, t), \quad (3)$$

192 where all expressions on the right hand side are taken with respect to the fixed
193 Eulerian reference frame.³ The symbol D is commonly used to distinguish
194 the material time derivative from a more general time derivative that is not
195 necessarily following a material fluid particle. To illustrate this formalism,
196 consider $\Psi(\mathbf{x}, t) = \mathbf{x}$. In this case, the material time derivative is given by
197 the velocity field at that point

$$\frac{D\mathbf{x}}{Dt} = \mathbf{v}(\mathbf{x}, t). \quad (4)$$

³An alternative derivation of equation (3), which is arguably more straightforward mathematically, dispenses with trajectories from the start, in which case we express the total differential of a function as $d\Psi(\mathbf{x}, t) = dt \partial_t \Psi + d\mathbf{x} \cdot \nabla \Psi$. Specifying the spatial increment to correspond to movement of a fluid particle, $d\mathbf{x} = \mathbf{v}(\mathbf{x}, t) dt$, leads to equation (3). We prefer the derivation using particle trajectories, as it exposes the relation between Lagrangian and Eulerian reference frames.

198 2.4. Steady-state volume transport pathways defined by streamtubes

199 Within Lagrangian Ocean Analysis, there is a long history of interpreting
200 particle trajectories as streamtubes, and using this interpretation to compute
201 volume transports (Döös, 1995; Blanke and Raynaud, 1997, see also section
202 3.2.3). Formally, the equivalence between streamtubes and material pathways
203 is only valid for steady-state flows (i.e. where the flow is constant in time).
204 Originally, the streamtube calculations were indeed performed on time-mean,
205 steady-state velocity fields, but they were soon extended to time-varying
206 flows, for example by assuming piecewise steady flow (Blanke and Raynaud,
207 1997, cf. Section 3.2.3). Over the last two decades, however, the approach has
208 been widely used in studies of large-scale ocean transports (see e.g. section
209 4.5), justifying a discussion of the mathematical underpinning of streamtubes
210 for steady-state flows here in this review manuscript.

211 The ocean is a nearly incompressible fluid. Thus, for this review we
212 consider an incompressible (Boussinesq) fluid, which means that the velocity
213 field is non-divergent

$$\nabla \cdot \mathbf{v} = 0. \quad (5)$$

214 Consequently, the volume of a material fluid particle remains constant (i.e.,
215 it is incompressible).

216 A streamtube is a bundle of streamlines, so that streamtube sides are
217 parallel to the velocity (see e.g. Figure 3.6 in Kundu et al., 2012)⁴. For a
218 steady flow, streamlines are equivalent to material pathlines, in which case
219 streamtubes are material tubes. It is for the steady case that we can make use
220 of streamtubes to map out volume transport pathways in an incompressible
221 fluid. We see this property by integrating the non-divergence constraint,
222 equation (5), over the streamtube, and making use of Gauss's Law. Doing so
223 reveals that volume transport (volume per time) through the two streamtube
224 ends balances exactly

$$\int_{A_1} \mathbf{v} \cdot \hat{\mathbf{n}} dA + \int_{A_2} \mathbf{v} \cdot \hat{\mathbf{n}} dA = 0, \quad (6)$$

225 where $\hat{\mathbf{n}}$ is the outward normal at the respective end, and dA the corresponding
226 area. By construction, $\mathbf{v} \cdot \hat{\mathbf{n}} = 0$ on the streamtube sides, so the sides do
227 not contribute to the balance in equation (6). Hence, the volume transport

⁴One may think of streamtubes as the “communication cable lines” within an incompressible fluid, transmitting volume signals within a steady flow.

228 entering one streamtube end equals to that leaving the other end. Furthermore,
229 the area of the streamtube is inversely proportional to the local normal velocity.

230 The transport constraint (6) holds regardless of whether there is diffusive
231 tracer mixing in the Boussinesq fluid. It follows from the non-divergence
232 property of the velocity field in an incompressible fluid. However, in the
233 presence of diffusive tracer mixing, the actual material entering one end of
234 the streamtube is not necessarily the same as the material exiting the other
235 end (see also Section 2.5).

236 The above properties make streamtubes useful for understanding the
237 circulation in a steady incompressible fluid. In particular, they provide
238 the mathematical basis for Lagrangian analysis methods that tag particles
239 with volume transport (e.g. Eckart, 1948; Welander, 1955). The aggregated
240 integral curves for such particles define a probability density function (PDF)
241 for volume transport pathways. In the continuum and under the assumption
242 of a steady flow field, volume transport pathways deduced from streamtubes
243 are identical to pathways deduced from particle trajectories determined by
244 time stepping equation (1).

245 We can make use of the volume transport information carried by stream-
246 tubes for Lagrangian analysis. To do so, define the starting point for a
247 streamtube by assigning a volume transport to each particle. The assigned
248 volume transport is directly proportional to the transport crossing the grid cell
249 face where the particle is initialized. In principle, we can fill a non-divergent
250 flow field without void between streamtubes. Consequently, we can compute
251 streamtube derived volume transport pathways whether the flow is laminar
252 or turbulent. However, turbulent flow generally requires more streamtubes
253 to develop robust statistics for the transport pathways, and also requires
254 that the flow is assumed piecewise steady (see also section 3.2.3), as for any
255 transient flow, steady-state streamlines lose their equivalence to pathlines.

256 *2.5. An introduction to tracer transport pathways*

257 A finite-size material seawater parcel is comprised of fresh water and
258 tracers of other matter, such as salts and biogeochemical components⁵. Tracer
259 concentration, C , measures the mass of tracer per parcel mass. The velocity

⁵Conservative temperature can also be considered as the concentration of heat in a parcel. The reason is that, to a very good approximation, Conservative Temperature satisfies a source-free tracer equation analogous to salinity (McDougall, 2003; Graham and McDougall, 2013).

260 considered in fluid mechanics is the barycentric velocity (section 2.2), so
 261 that the mass (or volume for a Boussinesq fluid) of a material fluid parcel
 262 is constant. However, the mass of each trace constituent is not materially
 263 constant, since tracers are exchanged between parcels through mixing in the
 264 presence of concentration gradients. Since the small-scale motions that govern
 265 this mixing are hardly ever resolved in OGCMs, the effect of tracer mixing
 266 has to be represented as (resolution-dependent) diffusive transports based on
 267 mean distributions.

268 In Section 2.4, we defined volume transport pathways according to stream-
 269 tubes in a steady flow. Here, we introduce transport pathways defined by
 270 trace constituents. In the presence of diffusive tracer mixing, tracer and
 271 volume transport pathways are distinct. The machinery of stochastic differ-
 272 ential equations (SDEs) is required to compute tracer transport pathways,
 273 with details deferred to Section 3.3. Our purpose here is to anticipate that
 274 discussion by introducing various forms of the tracer concentration equation.
 275 In so doing, we also introduce the residual mean velocity.

276 2.5.1. The tracer equation with subgrid scale transport

277 Molecular diffusion as well as turbulent subgrid scale transport processes
 278 give rise to irreversible (diffusive) transport as well as reversible (advective
 279 or skew diffusive) transport. Mathematically, we express the subgrid scale
 280 tracer transport through a transport tensor, \mathbf{J} . The corresponding tracer
 281 concentration equation takes the form⁶

$$\left(\frac{\partial}{\partial t} + \mathbf{v} \cdot \nabla \right) C = \nabla \cdot (\mathbf{J} \cdot \nabla C), \quad (7)$$

282 where the transport tensor \mathbf{J} has units of squared length per time. It is
 283 convenient to split the transport tensor into the sum of a symmetric and
 284 anti-symmetric tensor

$$\mathbf{J} = \mathbf{K} + \mathbf{A}. \quad (8)$$

285 The symmetric tensor, \mathbf{K} , has components satisfying⁷

$$K_{ij} = K_{ji}. \quad (9)$$

⁶We assume a Boussinesq fluid when writing the tracer equation (7).

⁷We make use of Cartesian tensors throughout this review, with results generalizable to arbitrary coordinates.

286 This tensor corresponds to diffusion so long as it is positive definite. The
 287 anti-symmetric tensor, \mathbf{A} , corresponds to skew diffusion or equivalently to
 288 advection (e.g., Middleton and Loder, 1989; Griffies, 1998).

289 Given the decomposition of the transport tensor (8), we find it useful to
 290 write the tracer equation in the form

$$\left(\frac{\partial}{\partial t} + \mathbf{v}^\dagger \cdot \nabla \right) C = \nabla \cdot (\mathbf{K} \cdot \nabla C), \quad (10)$$

291 where

$$\mathbf{v}^\dagger = \mathbf{v} + \mathbf{v}^* \quad (11)$$

292 defines the *residual-mean velocity* and

$$v_j^* = -\partial_i A_{ij} \quad (12)$$

293 is known as the eddy-induced velocity⁸. Notably, the eddy-induced velocity
 294 is non-divergent due to the anti-symmetry property

$$A_{ij} = -A_{ji} \Rightarrow \nabla \cdot \mathbf{v}^* = 0. \quad (13)$$

295 Consequently, the tracer equation (10) can be written in the flux-form

$$\frac{\partial C}{\partial t} + \nabla \cdot (\mathbf{v}^\dagger C) = \nabla \cdot (\mathbf{K} \cdot \nabla C). \quad (14)$$

296 Since both \mathbf{v} and \mathbf{v}^\dagger are divergence-free, one can define a streamtube in a
 297 steady-state flow according to either velocity field. The streamtubes defined by
 298 the residual mean velocity are often more relevant than those for the Eulerian
 299 time-mean velocity for ocean transport since the residual mean velocity
 300 \mathbf{v}^\dagger incorporates information about subgrid scale eddy advective transport.
 301 Drijfhout et al. (2003), for example, explicitly calculated particle trajectories
 302 with both Eulerian mean and residual mean velocities and discussed the
 303 differences in (overturning) pathways. Particle trajectories using the Eulerian
 304 mean exhibit motions that cross mean isopycnal surfaces, whereas trajectories
 305 making use of the residual mean better respect the adiabatic nature of the
 306 meridional overturning flow.

⁸Repeated indices are summed over their range.

307 2.5.2. *Introducing the Fokker-Planck equation*

308 Anticipating the discussion of Stochastic Differential Equations (SDEs) in
 309 Section 3.3.1, we manipulate the diffusive contribution in the tracer equation
 310 (14). The aim is to write the tracer concentration equation in the form
 311 of a Fokker-Planck equation (see equation (24)), which describes the time
 312 evolution of the probability density function of the tracer. For this purpose,
 313 we use the identity

$$\partial_i (K_{ij} \partial_j C) = \partial_i [\partial_j (K_{ij} C) - C \partial_j K_{ij}], \quad (15)$$

314 so that

$$\frac{\partial C}{\partial t} + \nabla \cdot (\mathbf{v}^{\text{drift}} C) = \partial_{ij} (K_{ij} C), \quad (16)$$

315 where we introduced the drift velocity

$$\mathbf{v}^{\text{drift}} = \mathbf{v}^\dagger + \nabla \cdot \mathbf{K}. \quad (17)$$

316 The drift velocity generally has a non-zero divergence

$$\nabla \cdot \mathbf{v}^{\text{drift}} = \partial_{ij} K_{ij}, \quad (18)$$

317 since $\partial_{ij} K_{ij}$ does not generally vanish⁹. Equation (16) is the tracer equation
 318 written in the form of a Fokker-Planck equation.

319 Tracer transport pathways differ from volume transport pathways in the
 320 following ways. First, as already mentioned, the drift velocity $\mathbf{v}^{\text{drift}}$ is generally
 321 divergent. Hence, it is not useful to define steady-state “tracer streamtubes”
 322 in terms of $\mathbf{v}^{\text{drift}}$. Second, even if $\nabla \cdot \mathbf{K} = 0$ so that the drift velocity is
 323 divergent-free (e.g., isotropic diffusion with a constant diffusivity), tracer
 324 pathways are affected by diffusive mixing between fluid particles. To represent
 325 such diffusion in a Lagrangian trajectory calculation requires a stochastic noise
 326 term weighted by the diffusion tensor (Section 3.3). Therefore, whether one
 327 considers volume transport pathways or tracer transport pathways depends on
 328 the scientific question and the information available to address that question.

⁹One notable case where $\nabla \cdot \mathbf{v}^{\text{drift}} = 0$ is isotropic diffusion with a constant diffusivity; e.g., molecular diffusion. Molecular diffusion is generally not relevant for large-scale ocean models, as models (and large-scale observations) do not resolve down to the Kolmogorov scales. Hence, large-scale models make use of the far larger, and flow dependent, eddy diffusivities.

329 *2.5.3. Using particles to track a tracer patch*

330 There is yet another way to consider tracer transport pathways using
331 Lagrangian analysis. For this approach, we represent a patch of tracer as
332 a collection of Lagrangian particles (e.g. Bennett, 2006; LaCasce, 2008). In
333 this way, Lagrangian analysis can be used to study tracer dispersion (Rossi
334 et al., 2013; Wang et al., 2016a). In principle, in the limit of infinite number
335 of particles and knowledge of the velocity field to arbitrarily fine spatial and
336 temporal resolution, the tracer dispersion from Lagrangian particles would
337 have theoretically perfect resolution and controllable numerical diffusion. How
338 achievable this is in real-world simulations remains an area of active research.

339 A tracer patch can be represented by a cloud of particles. Each particle
340 carries a portion of the total tracer content. Let c denote the tracer volume
341 per particle. The corresponding Eulerian tracer concentration, $C(\mathbf{x}, t)$, can
342 be written

$$C(\mathbf{x}, t) = \sum_{i=0}^N W(\mathbf{x} - \mathbf{x}_i(t))c_i, \quad (19)$$

343 where N is the total number of particles, \mathbf{x}_i is the particle position, and W is
344 a mapping kernel function (dimensions inverse volume) that maps the particle
345 density to tracer density. The kernel function satisfies the normalization
346 condition required to conserve volume

$$\int_{\Omega} W \, dx \, dy \, dz = 1, \quad (20)$$

347 where Ω is the integral volume in three dimensions. The form of W has been
348 extensively investigated in the Smoothed Particle Hydrodynamic approach
349 (Monaghan, 1992). Different forms of W exist with different projection errors.

350 **3. Computing Lagrangian particle trajectories**

351 In this section we discuss technical aspects of Lagrangian modelling and
352 analysis, focusing here on the computation of trajectories. We consider
353 how trajectories of virtual Lagrangian particles can be used in mapping
354 both volume transport pathways and tracer transport pathways (recall the
355 distinction discussed in Section 2.5).

356 *3.1. Basic needs for Lagrangian trajectory calculations*

357 For volume transport pathways, one needs a non-divergent velocity field.
358 A three-dimensional non-divergent velocity can be produced by sampling a

359 Boussinesq ocean model, thus offering a means to compute three-dimensional
360 trajectories. To compute tracer transport trajectories, we need both a velocity
361 field and a diffusion tensor. The diffusion tensor is a function of the often
362 poorly known subgrid scale flow, and it is generally a complex function of
363 the flow field. Consequently, the calculation of tracer transport pathways is
364 somewhat less mature than volume transport pathways (though see Tables 1
365 and 2).

366 When using an ocean model, we distinguish between two techniques of
367 Lagrangian integration. The first occurs online, whereby trajectories are
368 computed each time step that the Eulerian model is updated. Examples of
369 such online methods are available for volume transport pathways using the
370 velocity field (see Section 3.5). In contrast, we know of no example of online
371 tracer trajectory calculations making use of both the instantaneous velocity
372 field and the diffusion tensor.

373 The second method for Lagrangian analysis occurs through off-line trajec-
374 tory calculations. Off-line methods make use of stored velocity fields sampled
375 from the Eulerian model. Off-line trajectory calculations offer the ability to
376 compute trajectories in a forward mode (from their starting point forward in
377 time) or in a backward mode (from their ending point backward in time).

378 As an alternative to velocities generated by OGCMs, we may use observation-
379 based data from floats or drifters, which generally give a two dimensional
380 surface velocity (e.g., Koszalka et al., 2011). We may also diagnose a surface
381 geostrophic velocity by differentiating gridded satellite observations of the sea
382 surface height (e.g., Klocker et al., 2012b). Notably, both surface drifter/float
383 velocities and surface geostrophic velocities generally have a non-zero hori-
384 zontal divergence (surface geostrophic velocities are non-divergent only on
385 an *f*-plane), and the corresponding surface trajectories do therefore not map
386 volume transport pathways. Nonetheless, the resulting surface trajectories do
387 map preferred pathways of the surface flow, thus providing useful diagnostic
388 information.

389 Computation of particle trajectories using a velocity field requires essen-
390 tially two operations: a way to integrate the trajectory equation (1) and a
391 way to interpolate a gridded velocity field to an arbitrary point in space and
392 time. In this section, we detail these aspects.

393 3.2. Temporal integration of the virtual particle trajectory equation

394 When the n th virtual seawater particle is located at the point $\mathbf{X}^{(n)}(t) = \mathbf{x}$,
 395 we can update its position by time stepping the velocity equation (1)

$$\mathbf{X}(t + \Delta t) = \mathbf{X}(t) + \int_t^{t+\Delta t} \mathbf{v}(\mathbf{x}(\tau), \tau) d\tau, \quad (21)$$

396 where we dropped the trajectory super-script n to simplify notation. Note
 397 that the integrand involves the Eulerian velocity field $\mathbf{v}(\mathbf{x}, \tau)$, which equals
 398 to the Lagrangian velocity $d\mathbf{X}/dt$ when evaluated at $\mathbf{X}(t) = \mathbf{x}$. In
 399 some applications of Lagrangian analysis, there is an additional term on
 400 the right hand side of equation (21) that represents unresolved physics (see
 401 Section 3.3.2). We explore various flavours of this discrete time stepping (see
 402 also Figure 2) for estimating virtual particle trajectories, focussing on the
 403 most commonly used schemes. However, there are many more schemes than
 404 discussed here (e.g., Chu and Fan, 2014; Liu and Chua, 2016).

405 In general, the accuracy of trajectories computed in OGCM fields de-
 406 pends on accuracy of the time stepping scheme, as well as accuracy of the
 407 interpolation scheme used to estimate velocity at the time and position of
 408 the particle (see Section 3.4). Note that the first three methods (explicit,
 409 implicit and analytical) discussed below all result in identical trajectories
 410 in the continuum. However, the trajectories differ in numerical implemen-
 411 tations due to algorithmic differences and truncation errors. For all methods,
 412 statistical significance of the diagnosed pathways is enhanced by increasing
 413 the number of deployed particles. As a rule of thumb, one has deployed a
 414 sufficient numbers of particles when the physical results of interest do not
 415 significantly change as the number of particles is increased (e.g., Jones et al.,
 416 2016).

417 The maximum integration time in equation (21) is limited to the run time
 418 of a given model simulation. A number of oceanic processes, however, have
 419 time scales that exceed these run times (e.g., England, 1995; Stouffer, 2004;
 420 Danabasoglu, 2004). Using Lagrangian particles to temporally resolve for
 421 example the meridional overturning circulation (Blanke et al., 1999; Thomas
 422 et al., 2015b) or inter-basin connectivity (Blanke and Speich, 2002) can be
 423 difficult with many state of the art climate models. To address this problem,
 424 a commonly employed *ad hoc* method is to loop the model data in time such
 425 that the velocity and tracer fields are returned to the first time step once the

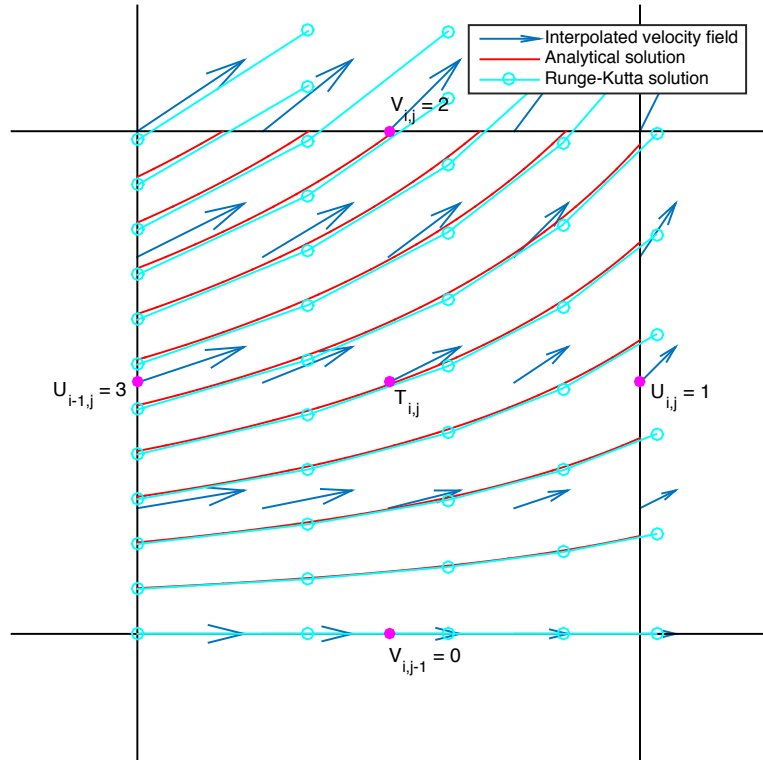


Figure 2: Illustration of time stepping solutions on an Arakawa C-grid with edges of non-dimensional length=1. Velocities (u, v) across the four edges are given in numbers at the magenta dots. The blue arrows are the linearly interpolated velocities within the grid. Assume particles are released on the $i - 1$ (left) edge. The red lines are pathlines of the analytical solution for these particles. The cyan piecewise linear lines are the solutions to RK4 timestepping with $dt = 0.1$. The two types of integration lead to similar solutions.

426 end has been reached (e.g., Döös et al., 2008; van Sebille et al., 2012; Thomas
427 et al., 2015b). This approach thus permits particles to be advected for longer
428 time scales than available from the raw data. However, particle looping can
429 only work if the model has no drift in the velocity or tracer fields, that there
430 are no large unphysical jumps in the fields between the end and the beginning
431 of the model run, and that any unphysical jumps will have a small net effect
432 on the particle pathways.

433 *3.2.1. Explicit time stepping methods*

434 One way to integrate equation (21) is to multiply the velocity at a point
435 by a time step, Δt , to estimate the displacement. This approach is known as
436 the Euler method and is correct to first order in Δt . Better accuracy of the
437 trajectories can be obtained by using higher-order methods for the integration
438 of Eq (21). One popular method is the 4th order Runge-Kutta scheme (e.g.,
439 Butcher, 2016), where information of the (interpolated) velocity field at four
440 increments between time steps t_n and t_{n+1} is used.

441 The fourth order Runge-Kutta method is a member of a family of inte-
442 grators (Dormand and Prince, 1980). One interesting extension is adaptive
443 timestepping through a RK45-method, where both a fourth order and a fifth
444 order integration are performed. The extra computational cost of a fifth
445 order computation is marginal when a fourth order is already performed. The
446 difference, $\Delta X = |X_5 - X_4|$, between the fifth order and fourth order solution
447 can be computed. If ΔX is larger than some (pre-chosen) threshold, the time
448 step Δt of equation (21) can adaptively be reduced for that particle. Doing
449 so then leads to a straightforward implementation of adaptive timestepping
450 using Runge-Kutta integrators. However, it is not *a priori* clear how the error
451 thresholds for ΔX should be chosen.

452 When working with stored velocity data, as when virtual particle tra-
453 jectories are computed offline, temporal interpolation is usually required.
454 Interpolation is needed because the interval between consecutive stored ve-
455 locity fields is generally longer than the time step, Δt , used to advance the
456 particle trajectories in equation (21). This temporal interpolation of the
457 velocity fields can be a large source of error, particularly when the interval
458 with which velocity fields are stored becomes longer than a few days (e.g
459 Valdivieso Da Costa and Blanke, 2004; Qin et al., 2014).

460 3.2.2. *Time-implicit discrete integration schemes*

461 To determine volume transport pathways, the volume-preservation properties
462 of numerical integrators becomes an important consideration. Symplectic
463 time integration schemes are one method used to maintain volume conservation
464 for discrete methods. They can be mathematically shown to exactly
465 conserve area in divergence-free 2D fields, meaning that the area bounded
466 by a set of particles will stay constant over time in the absence of turbulent
467 diffusion¹⁰. Symplectic methods for Lagrangian particles in two dimensions
468 take the same form as symplectic integrators for systems of point vortices, but
469 now the velocity is prescribed (Marsden et al., 1999). The disadvantage of
470 these methods is that they are generally implicit in time. Hence, they require
471 iterative methods. For example, the implicit midpoint rule provides a sym-
472 plectic integrator for the Lagrangian trajectory equation in two dimensions
473 (McLachlan, 1999; Leimkuhler and Reich, 2004).

474 In three dimensions, the concept of symplectic integrators must be ex-
475 tended to Lie-Poisson integrators for 3D incompressible velocity fields (McLach-
476 lan, 1999; Leimkuhler and Reich, 2004). Few 3D symplectic integrators are
477 known, though the implicit midpoint rule is known to be such an integrator
478 and preserves volume in three dimensions.

479 3.2.3. *An analytical discrete streamtube method*

480 Another volume-preserving method to integrate the trajectory equation
481 (21) takes advantage of the discrete continuity equation. The resulting
482 virtual particle trajectories respect the volume conservation property of
483 an incompressible Boussinesq fluid, and thereby are particularly suited for
484 experiments where the focus is on the advective component of the flow. In
485 brief, this method analytically computes trajectories across grid cells by
486 making use of the gridded velocity field located on grid cell faces. This
487 approach approximates streamtubes through the use of volume conservation
488 constraints introduced in Section 2.4. While these methods have their origin
489 in applications with steady-state velocity fields, and the streamtube approach
490 is formally only applicable to these cases, there is a large community using
491 extended analytical discrete streamtube methods for time-varying flows too.

¹⁰See Hairer et al. (2006) for a comprehensive description of symplectic time integration schemes, and Leimkuhler and Reich (2004) for an introduction with applications targeted at scientists and engineers.

492 These applications typically achieve very similar results to the explicit time-
493 stepping schemes.

494 Algorithms following this approach calculate trajectories for a given steady-
495 state velocity field through analytic computation of three-dimensional stream-
496 tubes (Blanke and Raynaud, 1997). If the velocity fields are time-evolving, it
497 is possible to sub-sample them into piecewise steady fields, which are only
498 kept constant in time for a short time; this approach generally increases the
499 computational cost. Another method by de Vries and Döös (2001) allows
500 for analytical trajectories in a time-dependent case that accounts for flow
501 changes across time steps. Döös et al. (2017) showed that the time-dependent
502 trajectory solution is more accurate than the piecewise steady solution, espe-
503 cially in eddying regions, and only at a very small additional computational
504 cost (see also Appendix A.1.2).

505 The analytical calculations are on the scale of a model grid cell for which
506 components of the velocity field, or the volume transports, are typically
507 expressed on a staggered C grid (Mesinger and Arakawa, 1976), i.e., are
508 known over the six faces of the cell (see Figure 2).¹¹ The analytical method is
509 enabled by assuming that within a grid cell, the fluid velocity exhibits a linear
510 variation of each velocity component along each corresponding direction, so
511 that

$$\mathbf{v}_{\text{subgrid}} = (u(x), v(y), w(z)). \quad (22)$$

512 These subgrid scale velocity components $(u(x), v(y), w(z))$ are linear functions
513 of their arguments, with the precise form of these functions determined by the
514 known velocity components on the cell faces. This form of the subgrid scale
515 velocity then allows one to write analytical trajectory equations along the
516 three axes across the grid cell. Analytic time integration of these equations
517 binds each coordinate point (x, y, z) in a grid cell to time in the cell. Grid
518 cell crossing times in each of the three directions are evaluated independently
519 by imposing any of the six grid cell sides as a possible final position. The
520 minimum crossing time specifies the actual crossing time, and hence the
521 trajectory. This approach then allows for an accurate (within the confines of
522 the basic assumption of equation (22)) calculation of the final position of a

¹¹This method can also be used for A-grid or B-grid stencils, so long as these grids offer conservative volume transport components on tracer cell faces. The use of conservative flux-based transport schemes is a basic property of any finite volume ocean model, regardless the horizontal grid stencil.

523 particle on the relevant exit side of the grid cell.

524 This method for computing volume transport trajectories is both fast and
525 self-consistent. It is fast because it only calculates particle positions on the
526 edge of individual grid cells. It is self-consistent since it respects the local
527 three-dimensional non-divergence of the Boussinesq flow both at the subgrid
528 and the large scale. It therefore provides a judicious method to map volume
529 transport pathways by realizing a discrete implementation of streamtubes
530 introduced in Section 2.4.

531 Streamtube-based volume transport is reversible, so that backward inte-
532 grations can be performed to track the origin of a given volume. It is for these
533 reasons that practitioners of discrete streamtube methods generally do *not*
534 introduce diffusion (or stochastic noise) when computing particle trajectories.
535 Rather, the method is focused on determining volume transport pathways
536 defined from the resolved or the residual mean flow.

537 *3.3. Computing stochastic trajectories to simulate diffusion and unresolved*
538 *physics*

539 As noted above, streamtubes track water volume in a steady-state flow.
540 However, in many applications in oceanography, one is interested in tracking
541 tracers such as heat, salt, or nutrients and how they are affected by subgrid
542 scale diffusion and unresolved physics such as mixed layer processes and deep
543 convection (e.g. van Sebille et al., 2013). Tracer concentrations can directly be
544 computed from the spreading of a cloud of particles described by Stochastic
545 Differential Equations (SDEs, see Section 2.5.2), where unresolved physics
546 are represented by stochastic noise.

547 Two main approaches can be distinguished in efforts to add diffusion to
548 trajectories. One is to start with the tracer equation (16), where the eddy
549 transport is parameterized in terms of the eddy-induced velocity and the
550 appropriate form of the diffusivity tensor in order to derive the SDE for
551 particle trajectories (Section 3.3.1). The second approach (Section 3.3.2) is to
552 use an ‘ad hoc’ SDE where a Markov model is fit to observations from surface
553 drifter trajectories or virtual particles in a much finer resolution velocity field.

554 It remains an active area of research under which circumstances (e.g.
555 underlying research question, spatial and temporal model data resolutions)
556 and how exactly stochastic noise representing subgrid scale diffusion should
557 be implemented (see also section 3.3.3).

558 3.3.1. *Stochastic trajectories using the Fokker-Planck equation*

559 Here, we provide a brief introduction to the implementation of stochastic
 560 terms through the use of a Fokker-Planck Equation. The discussion here
 561 makes use of the more thorough discussions provided in the textbooks by
 562 Gardiner (1985), Jazwinski (1970), and Kloeden and Platen (1992), as well
 563 as the oceanographic review by Visser (2008). Advantages of this Lagrangian
 564 SDE approach over Eulerian tracer computations are that it can deal with
 565 steep concentration gradients and that tracer concentration can never become
 566 negative.

567 A stochastic differential equation (SDE) for a general trajectory $\mathbf{X}(t)$ is
 568 given by

$$dX_i(t) = a_i(t, \mathbf{X}) dt + \sigma_{ik}(t, \mathbf{X}) dW_k(t), \quad \mathbf{X}(t_0) = \mathbf{X}_0. \quad (23)$$

569 In this equation, $X_i(t)$ are components of the tracer trajectory vector $\mathbf{X}(t)$,
 570 and $dX_i(t) = X_i(t+dt) - X_i(t)$ is the stochastic particle displacement during
 571 the time interval $[t, t+dt]$. The term $a_i(t, \mathbf{X})$ is a deterministic drift, whereas
 572 $\sigma_{ik}(t, \mathbf{X})$ is related to a tracer diffusion tensor (see equations (25) and (26)
 573 below). Finally, $W_k(t)$ is a Wiener process, or Brownian motion, modelling
 574 stochastic fluctuations that represent unresolved motions like eddies, waves
 575 or small-scale turbulence. The increment $dW_k(t) = W_k(t+dt) - W_k(t)$ is
 576 a Gaussian variable with zero mean and variance dt , with non-overlapping
 577 increments independent of each other. The stochastic model (23) is Markovian,
 578 which means that information on the probability density of the trajectory
 579 $\mathbf{X}(t)$ at time t is sufficient to make predictions at later times. Non-Markovian
 580 models require information at earlier times, which is generally impractical.
 581 The presence of the Wiener process means that integrating the equation using
 582 deterministic calculus does not produce a unique solution. We make use
 583 of ideas proposed by Itô, who developed a stochastic calculus to produce a
 584 unique solution of the SDE (23) ¹².

¹²The Itô calculus used here is but one mathematical approach for realizing a unique solution to a SDE (e.g., Gardiner, 1985). Stratonovich and Itô-backward approaches offer alternative stochastic integration methods, and they can also be used to derive stochastic particle models (Gräwe et al., 2012; Shah et al., 2011; Spivakovskaya et al., 2007a,b). We focus on the Itô calculus as it is well known to physicists, as is the corresponding Fokker-Planck equation. Furthermore, the drift, $a_i(t, \mathbf{X})$, of an Itô SDE represents the mean of the stochastic particle tracks. Finally, the well known Euler scheme (see equation (28) below) is a straightforward numerical approximation of the Itô SDE, whereas this

585 A cloud of particles will estimate the probability density $P(t, \mathbf{x})$ for the
 586 stochastic tracer trajectories. Use of an Itô stochastic process $\mathbf{X}(t)$ ensures
 587 that the probability density function evolves according to the following Itô
 588 form of the Fokker-Planck or forward Kolmogorov equation

$$\frac{\partial P}{\partial t} = \partial_i(a_i P) + \partial_{ij}(b_{ij} P) \quad (24)$$

$$P(t_0, \mathbf{x}) = P_0(\mathbf{x}),$$

589 with

$$2 b_{ij} = \sigma_{ik} \sigma_{jk}. \quad (25)$$

590 We can relate the Fokker-Planck equation (24) to the Boussinesq form of the
 591 tracer equation (16), so that¹³

$$\begin{aligned} b_{ij} &= K_{ij} \\ a_i &= v_i^\dagger + \partial_j K_{ij} \\ P &= C. \end{aligned} \quad (26)$$

592 The corresponding SDE for the trajectory is given by

$$\begin{aligned} dX_i(t) &= \left(v_i^\dagger + \frac{\partial K_{ij}}{\partial x_j} \right) dt + \sigma_{ik}(t, \mathbf{X}) dW_k(t), \\ \mathbf{X}(t_0) &= \mathbf{X}_0. \end{aligned} \quad (27)$$

593 It is through this connection that we can derive a stochastic Lagrangian
 594 model for any advection-diffusion tracer equation.

595 Stochastic tracer trajectories can be generated numerically through discrete
 596 approximations to the Itô stochastic differential equation (Kloeden and Platen,
 597 1992). Discretizing the continuous stochastic differential equation (27) using
 598 the Euler scheme leads to

$$\begin{aligned} X_i(t + \Delta t) &= X_i(t) + (v_i^\dagger + \partial_j K_{ij}) \Delta t + \sigma_{ik}(t, \mathbf{X}) \Delta W_k(t) \\ \mathbf{X}(t_0) &= \mathbf{X}_0. \end{aligned} \quad (28)$$

scheme cannot be used to discretize a Stratonovich or an Itô-backward SDE.

¹³The tensor elements $\sigma_{ik}(t, \mathbf{X})$ are not uniquely determined by the diffusion tensor \mathbf{K} . However, all choices consistent with the relation $2 K_{ij} = \sigma_{ik} \sigma_{jk}$ result in statistically identical diffusion processes.

599 In this equation, $\Delta W_k(t)$ is a Gaussian random variable with zero mean
600 and variance Δt , generated via a random generator. The accuracy of the
601 Euler scheme is $\mathcal{O}(\Delta t^{1/2})$ in the strong sense; i.e., for approximating the
602 individual particle trajectories. When used to generate many trajectories
603 in order to approximate the probability distribution, or equivalently the
604 tracer concentration, then the Euler scheme is $\mathcal{O}(\Delta t)$ accurate; i.e. the Euler
605 scheme is $\mathcal{O}(\Delta t)$ in the weak sense. More accurate numerical schemes have
606 been developed, such as in Gräwe et al. (2012); Shah et al. (2011, 2013);
607 Spivakovskaya et al. (2005, 2007a,b).

608 There are methods to compute trajectories directly from a SDE for many
609 applications (e.g., Kloeden and Platen, 1992). Trajectory computation di-
610 rectly from SDEs is less mature in large-scale oceanography where it is often
611 difficult to include a realistic diffusion tensor for subgrid scale tracer transport.
612 Appendix B offers an example of tracer trajectories in the presence of an
613 isopycnal diffusion tensor with a time-constant diffusivity. This application is
614 nontrivial and a major advance in the Lagrangian tracer trajectory method.
615 Unfortunately, it is not fully representative of modern parametrisations for
616 global models, whereby the diffusivity is a function of space and time (Aber-
617 nathey et al., 2013), and the diffusivity tensor may be anisotropic in the
618 lateral directions as well as between lateral and vertical (Fox-Kemper et al.,
619 2013).

620 Even with a constant isopycnal diffusivity, sampling components of the
621 3×3 diffusion tensor for offline analysis is a nontrivial computational task,
622 particularly in the presence of realistic temporal variability. Additional
623 difficulty arises from time variations in the diapycnal diffusivity used for
624 planetary boundary layer schemes. Consequently, the current generation
625 of explicit SDEs for tracer trajectories are generally restricted to relatively
626 coarse resolution models with rudimentary subgrid scale parametrisations
627 (e.g., Shah et al., 2017), although efforts are underway to improve this.

628 3.3.2. A hierarchy of Markov models for stochastic trajectories

629 The second approach to adding the effects of diffusion and unresolved
630 physics to particles is to ‘ad hoc’ find an SDE that matches the statistics - e.g.
631 eddy decorrelation time scales and diffusivity - of the stochastic trajectories
632 with either observations or particles simulated in finer-resolution models. This
633 approach has been developed by Griffa (1996) and further by Berloff and
634 McWilliams (2003) in the context of ocean models. See also Vallis (2006,
635 sect 10.2) and LaCasce (2008) for discussion, and Veneziani et al. (2004) and

636 Koszalka et al. (2013a) for implementations.

637 A hierarchy of Markov models is considered, whereby the stochastic
 638 term is added to either particle displacement (zeroth-order Markov model,
 639 corresponding to uncorrelated eddy velocity field), the particle velocity (first-
 640 order model, accounting for correlations of the velocity) or the particle
 641 accelerations. In most cases, the first-order model is found to best approximate
 642 the oceanic mesoscale turbulence introduced by coherent eddies.

643 In the first-order Markov model (multiplicative noise), stochastic noise
 644 is used to modify the present position of a particle when updating to a new
 645 position, in which case the trajectory equation (21) can be written as

$$\mathbf{X}(t + \Delta t) = \mathbf{X}(t) + (1 + \epsilon) \int_t^{t+\Delta t} \mathbf{v}(\mathbf{x}, \tau) d\tau, \quad (29)$$

646 where ϵ is a random number. Notably, the application of noise in this manner
 647 does not ensure that $\mathbf{X}(t + \Delta t)$ results from time stepping a divergence-free
 648 velocity. For that purpose, we consider an alternative approach, whereby we
 649 introduce a stochastic divergence-free velocity

$$\mathbf{X}(t + \Delta t) = \mathbf{X}(t) + \int_t^{t+\Delta t} [\mathbf{v}(\mathbf{x}, \tau) + \mathbf{v}_{\text{noise}}(\mathbf{x}, \tau)] d\tau. \quad (30)$$

650 We can ensure $\nabla \cdot \mathbf{v}_{\text{noise}} = 0$ by introducing a stochastic vector streamfunction,
 651 so that for each each grid cell we have

$$\mathbf{v}_{\text{noise}}(\mathbf{x}) = \nabla \wedge \Psi_{\text{noise}}(\mathbf{x}). \quad (31)$$

652 Since the stochastic velocity remains non-divergent, this approach offers a
 653 realisation of stochastic streamtubes in steady-state flows. The choice of
 654 either equation (29) or equation (30) depends on the application and will be
 655 further discussed in Section 3.3.3.

656 In the zeroth-order Markov model (additive, or *random walk*, noise), the
 657 stochastic noise is added to the particle positions, which is often applied in a
 658 rather simple form, by adding an extra term to the trajectory equation (21):

$$\mathbf{X}(t + \Delta t) = \mathbf{X}(t) + \int_t^{t+\Delta t} \mathbf{v}(\mathbf{x}, \tau) d\tau + R\sqrt{2K\Delta t}. \quad (32)$$

659 In this equation, $R = N(0, 1)$ is a random number taken from the normal
660 distribution with zero mean and unit variance, and K is a constant tracer
661 diffusivity. A major limitation of this model is that, if the drift term is omitted,
662 equation (32) will lead to artificial accumulation of particles in regions of
663 low diffusivity, requiring an enhancement of the random walk model (Hunter
664 et al., 1993; Visser, 1997; Ross and Sharples, 2004; Berloff and McWilliams,
665 2002)

666 A myriad of behaviours can be added to a random walk model for capturing
667 the biological characteristic of Lagrangian particles. Examples include diurnal
668 vertical migration, temperature dependent planktonic larval duration and time
669 to settling competency. While it must be noted that enhanced complexity does
670 not necessarily imply enhanced accuracy, studies have shown that even modest
671 vertical migration velocities can significantly alter the dispersal patterns of
672 propagules. For example a recirculation in the Western Irish Sea of northwest
673 Europe, associated with summer stratification, retains surface drifters but
674 does not retain vertically migrating organisms (Phelps et al., 2015).

675 *3.3.3. When and how to add stochastic terms?*

676 In the above, we have described a few methods to incorporate mixing
677 through stochastic terms. However, exactly when and how to implement these
678 terms is an open question. It will likely depend on the temporal and spatial
679 resolution of the velocity fields, as well as the unresolved processes that the
680 added stochastic components are intended to reproduce. In particular, the
681 consideration should be whether mesoscale coherent eddies and attendant
682 nonlocal transport properties (velocity correlations and steep Eulerian ve-
683 locity spectra) are resolved by the ocean model velocity field underlying the
684 Lagrangian simulations.

685 If a velocity field is available at sufficiently high spatial and temporal
686 resolution, adding a stochastic component may be unnecessary and high
687 numbers of particles may suffice (Koszalka et al., 2013b). If the available
688 velocity field does not resolve important eddy processes, a first-order or second-
689 order Markov model may need to be used to account for a velocity correlations
690 induced by the mesoscale eddy field (Griffa, 1996; Berloff and McWilliams,
691 2002; LaCasce, 2008). The applicability of the stochastic simulations should
692 in any case be verified against existing observations (Koszalka et al., 2013a)
693 or high resolution model simulations, if available.

694 It is also still open how the Fokker-Plank Equation approach (Section
695 3.3.1) and the ad-hoc Markov model approach (Section 3.3.2) can be combined.

696 While the first approach is more mathematically rigorous, the second provides
697 an insight into the properties of observed or simulated oceanic turbulence
698 on different scales and in different regions, and may be useful in building
699 future parameterizations of eddy induced transport in terms of Lagrangian
700 stochastic parameterizations.

701 We leave this discussion of diffusivity here, as the research and understand-
702 ing of this issue is rapidly evolving, and strongly encourage the community to
703 gain a better understanding in how best to implement diffusion and unresolved
704 physics for Lagrangian particles.

705 *3.4. Spatial interpolation*

706 The trajectory equation (21) is defined on continuous velocity fields.
707 However, all ocean models work with discretized grids, where velocities
708 are only known on either vertices or edges of the grid cells (Griffies et al.,
709 2000). Therefore, computing Lagrangian trajectories from ocean model
710 data requires reconstruction of the continuous velocity field inside grid cells.
711 Bilinear, trilinear, or spline interpolation are viable choices on structured
712 grids. Interpolation on unstructured grids can be accomplished via methods
713 derived from particle-based approaches, e.g., inverse-distance weighting or
714 kernel-based convolutions, or unstructured extension of grid-based spatial
715 interpolation, e.g., Wachspress interpolation (Gillette et al., 2012).

716 On grids where velocities are defined on the corners of grids (e.g., Arakawa
717 A and B), the reconstruction choices include weak-form reconstruction (Perot,
718 2000), radial basis functions (Baudisch et al., 2006), or reconstruction via
719 finite-element basis functions (Wang et al., 2011). On grids where velocities
720 are known on the edges of grid cells (e.g., Arakawa C), this reconstruction is
721 often done using simple linear interpolation, although more work needs to be
722 done investigating what the errors are that arise from this.

723 Horizontal interpolation on arbitrary simplexes from vertex-data is pro-
724 vided by Wachspress interpolation (Gillette et al., 2012), which is a super-
725 linear interpolation scheme for arbitrary simplexes. For triangles, Wachspress
726 interpolation is equivalent to barycentric interpolation, which is commonly
727 used on triangular meshes and readily available in scientific packages (e.g.,
728 python-matplotlib). A primary benefit of this approach is that it provides a
729 continuous interpolant, e.g., \mathcal{C}^0 continuous. Options for higher-order interpo-
730 lation to obtain \mathcal{C}^n (for $n > 1$) continuity are more complex and less common,
731 particularly on arbitrary unstructured meshes.

732 Horizontal interpolation via Wachspress naturally keeps particles within
733 the domain for no-slip conditions where the velocity is zero for boundary points
734 on simplexes. Particles can be constrained to remain within the domain by
735 maintaining $CFL < 1$, where CFL is the Courant-Friedrichs-Lowy condition
736 (e.g., Durran, 1999). This implementation is intrinsically free of if-statements.
737 However, free-slip boundary conditions require further adaptation.

738 Vertical interpolation choices include linear and spline interpolants. Linear
739 interpolation is a standard approach and is consistent within model accuracy,
740 particularly for fine vertical resolution. Spline interpolation, however, allows
741 representation of vertical curvature, but at the potential cost of artificial
742 maxima and minima.

743 Particle tracking can employ a spatially-decoupled advection strategy by
744 splitting horizontal and vertical integration steps into sequential operations.
745 The benefit of this approach is that it decouples unstructured interpolants
746 in the horizontal from one-dimensional interpolation in the vertical and
747 allows different particle behaviours to be employed. For example, vertical
748 interpolation of velocities to specific potential density surfaces allows particles
749 to be advected isopycnally and avoid diapycnal mixing that can occur with
750 neutrally buoyant particle advection (Wolfram et al., 2015).

751 3.5. Available tools

752 As discussed throughout this section, it is in principle straightforward
753 to compute Lagrangian particle trajectories by time stepping the trajectory
754 equation (21). One merely needs to save the velocity field and update
755 the trajectories using available software like Matlab or Python, invoking
756 either rudimentary schemes or built-in functions such as the Matlab `ode`
757 suite. Several research groups have developed their own virtual particle codes
758 tailored to specific model output format, model grid and boundary conditions.
759 Examples include a 3D Lagrangian Matlab code for the MITgcm used by
760 Koszalka et al. (2013b) and von Appen et al. (2014) and a 2D Matlab code
761 of The Nonlinear Dynamical Systems Group at ETH Zurich (Farazmand and
762 Haller, 2012, <http://georgehaller.com/software/software.html>).

763 However, significantly more effort is required to develop an analysis code
764 that features a user-friendly interface and thus can be utilized across the mod-
765 elling communities. Further work is needed to ensure that the code is efficient
766 on data Input/Output. The suite of available tools can roughly be separated
767 into two sets. First, there are large community based Lagrangian codes such
768 as Ariane, TRACMASS, the Connectivity Modelling System (CMS), and

769 the new Parcels code. These are model-independent, run offline (i.e., on
770 stored velocity data) and provide extensive control on particle behaviour. The
771 second set includes Lagrangian codes tied to (and sometimes distributed with)
772 specific models, such as MITgcm, HYCOM, NEMO, ROMS and MPAS-O.
773 These model-specific codes can be run online (i.e., during the computation of
774 the velocity data).

775 Examples from both types of codes are discussed in appendix A. These
776 codes are also summarised in Table 1 and 2. Notably, all of these codes
777 employ either explicit or implicit time integration of volume transports and
778 while some can incorporate additional random terms (Section 3.3.2), there
779 are no community codes available for computing tracer trajectories through
780 the SDE-based methods of section 3.3.1.

781 4. Applications of Lagrangian particle trajectories

782 For most applications, the raw particle trajectories output by Lagrangian
783 analysis codes need to be further processed to help answer scientific questions.
784 In this section, we overview ways in which Lagrangian particle trajectories
785 can be used and analysed to improve our understanding of ocean circulation
786 and dynamics.

787 4.1. Dispersion and diffusivity

788 The ensemble particle dispersion and its rate of change, the diffusivity,
789 are the fundamental Lagrangian diagnostics of use for understanding tracer
790 transport in oceanic flows. Particle trajectories can be used to diagnose eddy
791 diffusivity via single, pair, and cluster techniques. The detailed theoretical
792 and practical underpinnings of these techniques in the context of oceanic
793 flows are summarized by LaCasce (2008); here we reiterate the main points.

794 The single-particle diffusivity stems from the seminal work of Taylor
795 (1921). It quantifies the ensemble-mean rate of particle dispersion from an
796 initial location, so that we have

$$797 \kappa(t) \equiv \frac{1}{2} \frac{d}{dt} \langle \mathbf{X}^2(t) \rangle = \langle \mathbf{V}(t) \cdot \mathbf{X}(t) \rangle = \int_0^t \langle \mathbf{V}(t) \cdot \mathbf{V}(\tau) \rangle d\tau. \quad (33)$$

798 In this equation, $\mathbf{X}(t)$ is the Lagrangian virtual particle trajectory, and
 $\mathbf{V}(t) = d\mathbf{X}(t)/dt$ is the Lagrangian particle velocity.

Code name	Ariane	TRACMASS	Octopus	LAMTA	CMS	Parcels
Website	www.univ-brest.fr/lpo/ariane	tracmass.org	github.com/jinbow/Octopus	bitbucket.org/f_nencio/spasso/overview	github.com/beatrixparks/connectivity-modeling-system	oceamparcel.org
License	CeCILL (http://www.cecill.info)	open source	MIT	GNU General Public License	GNU GPL v3	MIT
Key citation	Blanke and Raynaud (1997); Blanke et al. (1999)	Döös et al. (2017)	Wang et al. (2016a)	d'Ovidio et al. (2015)	Paris et al. (2013b)	Lange and van Sebille (2017)
OGCMs supported	NEMO/OPA, ROMS, Symphonie and any C-grid	NEMO, IFS (AGCM); MICOM, POM, HYCOM	MITgcm; any C-grid	AVISO satellite velocities; any velocity field on A-grids (euclidean or spherical)	HYCOM, OFES, NEMO, SOSE, MOM, MITgcm	NEMO, OFES, GlobCur- rent; customizable to any OGCM with NetCDF data format
Language(s)	Fortran 90/95; Matlab (IDL on request) for visualisation	Fortran	Fortran	GNU/Octave and C++	Fortran	Python user interface, auto-generated C++
Primary use	Offline calculation of 3D streamlines in the velocity field at any scale (regional, basin, global); volume transport calculations	3D water mass pathways, particle/tracer dispersion	3D watermass pathway, particle/tracer dispersion, cross-frontal transport, Argo float simulation	Compute satellite based Lagrangian diagnostics to optimize sampling strategy of mesoscale-based field campaign and support interpretation of in-situ observations	Dispersion, connectivity, fate of pollutants; Individual Based Modelling	Large scale oceanography; Individual Based Modelling; teaching (via customizable interface)
Advection method	Analytic	Analytic	RK4	RK4	RK4	RK4, RK45, Explicit Euler; extensible interface for custom advection methods
Diffusion method	No diffusion (purely kinematic method)	Brownian motion for background diffusion with random displacement or randomly added velocities	Brownian motion for background diffusion, random displacement within the mixed layer	Random walk optional	Brownian motion for background diffusion, random displacement within the mixed layer	Extensible interface for Random Walk and custom behaviour
Grids supported	Arakawa C, also tested with Arakawa B interpolated on C-grid; partial cells supported	Arakawa A, B, C. Spatially and temporally varying vertical grids supported (partial cells, z*, sigma, hybrid), including those for AGCMs	Arakawa C	Arakawa A	Orthogonal (rectangular) Arakawa A, B and C	Arakawa A, B and C; unstructured meshes planned
Key strengths	Almost 25 years of experience with core of the code; easy-to-install; easy-to-use; fast analytical solution; no coast crash; qualitative mode (full details of selected trajectories) and quantitative mode (volume transport calculations); compatible with the conservation laws of the OGCM	Volume conserving, fast analytical solutions without intermediate time steps; works with both OGCMs and AGCMs	Fast using Fortran, supports openMP	Designed to work out-of-the-box with AVISO surface geostrophic velocities. Already configured to compute a broad range of Lagrangian diagnostics (i.e. Finite Time/Size Lyapunov Exponents; longitudinal and latitudinal origin of particles; time of particle retention within mesoscale eddies etc.)	Modular, fast, parallel; Multi-grid support; Used in a wide variety of contexts, from marine ecology to physical oceanography	Easy-to-use, customizable extension interface and automated performance optimization
Shortcomings	No parallel mode; trajectory scheme is somewhat crude beyond the context of 3D water mass tracing	Need of improving the diffusion method	Non-scalable parallelization, not very efficient in reading large model output	Particle advection only 2D; cannot be run in parallel.	No support for non-orthogonal grids; parallel implementation is heavy on I/O	Not yet parallel; support for unstructured meshes in progress

Table 1: Summary of the specifications of the offline Lagrangian codes discussed appendix A

Code name	LIGHT in MPAS-O	NEMO online floats and icebergs	MITgcm	HYCOM	ROMS
Website	mpas-dev.github.io	nemo-ocean.eu/About-NEMO/Reference-manuals	mitgcm.org	hycom.org	myroms.org/wiki/floats.in
License	Copyright (c) 2013, Los Alamos National Security, LLC (LANS) and the University Corporation for Atmospheric Research (UCAR).	CeCILL (http://www.cecill.info)	None	None	Open source MIT/X
Key citation	Wolfram et al. (2015)	Madec and NEMO team (2016) for floats; Marshall et al. (2015) for icebergs	Marshall et al. (1997a)	Hallwell and Garraffo (2002); Garraffo et al. (2001a,b)	Piñones et al. (2011); Narvaez et al. (2012b)
OGCMs supported	Model for Prediction Across Scales Ocean (MPAS-O) (Ringler et al., 2013)	NEMO	MITgcm	Hybrid Coordinate Ocean Model (HYCOM) (Bleck, 2002; Chassignet et al., 2003, 2006)	ROMS
Language(s)	Fortran (post-processing in python)	Fortran	Fortran	Fortran	Fortran
Primary use	Large scale oceanography, diagnosing ocean mixing	Floats: large-scale, eddying ocean circulation. Icebergs: coupling of iceberg fluxes with ocean physics and dynamics and sea ice, via heat, freshwater and momentum fluxes; evaluating/forecasting iceberg hazard	Ocean modelling at all scales, offline advection	Large scale and coastal oceanography, biology	Coastal and mesoscale oceanography. Individual Based modeling for biophysical applications
Advection method	Sub-stepped generalized RK for time integration; Wachspress and RBF horizontal interpolation; linear vertical and temporal interpolation	Floats: Ariane method or RK4 RK4. Icebergs: RK4	RK4	Brownian motion optional	Vertical random walk optional
Diffusion method	None	None	None	Arakawa C	Arakawa C
Grids supported	Unstructured C-grid	Arakawa C	Arakawa C	Stable and relatively easy to use and understand	Reliable since trajectories are coherent with ocean circulation, parallel, easy to set up
Key strengths	Fast (minimal cost to OGCM), high temporal and spatial fidelity, computes isopycnal advection by construction, extensible within Fortran framework	Floats: Analytical advection on model timestep resolution. Icebergs: freshwater flux due to melting icebergs	Works well with archived MITgcm velocity fields, scales to very large sizes using MPI and domain tiling	No parallel mode	Computationally expensive since no offline model is available; Large output files for long runs or many particles.
Shortcomings	Currently no explicit offline mode, tied to MPAS framework and presently embedded in MPAS-O	Floats: limited use/publications to date. Icebergs: physics and dynamics subject to several uncertain parameters; giant tabular icebergs not yet represented; interactions with sea ice currently limited	Complicated to set up		

Table 2: Summary of the specifications of the online Lagrangian codes discussed appendix A

799 The Taylor formulation pertains to homogeneous, stationary and isotropic
 800 flows, and is non-trivial to apply in practice. Different approaches to esti-
 801 mation of single-particle statistics for particles deployed in stationary and
 802 homogeneous Eulerian flows, with cautious notes on particle deployment
 803 strategies and transient behavior, are discussed by Davis (1982) in the context
 804 of numerical simulations. For modelled ocean flows of realistic complexity,
 805 the estimation of single-particle statistics must be further refined to account
 806 for non-stationarity and inhomogeneities of the underlying Eulerian field
 807 (Davis, 1983, 1985, 1987, 1991). Under the assumption that the velocity field
 808 is slowly-varying with respect to the time increment dt (in practice, dt can
 809 be the time step of a Lagrangian model) this assumption can be satisfied by
 810 segmentation of trajectories over a relevant time scale (e.g., seasonal cycle,
 811 the velocity decorrelation time scale), and segregation in space into locally
 812 homogeneous regions (Davis, 1991; Koszalka and LaCasce, 2010, see also sect.
 813 4.3).

814 If the focus is on the transport by mesoscale turbulent flows ('eddy
 815 diffusivity'), an appropriate technique for 'the mean (or slowly-varying) flow
 816 removal' must be applied to the Lagrangian velocity in equation (33) (e.g.,
 817 Berloff et al., 2002; Rypina et al., 2012; Lumpkin and Johnson, 2013). The
 818 Lagrangian transport anisotropy can be quantified by using the concept
 819 of tensor diffusivity (where equation (33) applies to the different velocity
 820 vector components) and projection of the flow in the along- and across-flow
 821 directions of maximum dispersion (Rypina et al., 2011, 2012; Fox-Kemper
 822 et al., 2013; Kamenkovich et al., 2015; Wolfram et al., 2015). In general,
 823 anisotropy of the Lagrangian transport arises from spatio-temporal patterns
 824 and velocity correlations due to eddies. A significant challenge is that the
 825 observed Lagrangian particle dispersion is often non-diffusive on long time
 826 scales (e.g., Rypina et al., 2012) due to persistent Lagrangian flow correlations.

827 Double-particle statistics builds upon the works of Batchelor (1952) and
 828 Bennett (1987). The relative diffusivity (the time rate of the mean square
 829 pair separation) is

$$\kappa_R(t) \equiv \frac{1}{2} \frac{d}{dt} \langle r^2(t) \rangle = \frac{1}{2} \frac{d}{dt} \left\langle \sum_{m \neq n} [\mathbf{X}^{(m)}(t) - \mathbf{X}^{(n)}(t)]^2 \right\rangle, \quad (34)$$

830 where the sum is over all pairs of particles (m, n) . At times longer than
 831 the velocity decorrelation time scale, the pair particles move independently
 832 from one another, and the relative diffusivity is constant at twice the single

833 particle diffusivity (LaCasce, 2008). Using the relative diffusivity rectifies
834 the problem of the time-mean flow removal by measuring particle relative
835 separation, though it will still be influenced by the mean flow shear. In
836 practice, double-particle statistics are often implemented in terms of cluster
837 or moment methods which are equivalent to double-particle statistics on the
838 plane (LaCasce, 2008).

839 The single- and double-particle diagnostics derived from simulated trajec-
840 tories may be used for the following.

- 841 • Quantifying the advection by the turbulent mesoscale flows (eddy dif-
842 fusivity) in eddying models as a function of time and separation, for
843 example for parameterisations of diffusive processes in models that do
844 not resolve eddies (Poje et al., 2010).
- 845 • Eddy diffusivity maps obtained by binning (see Section 4.3) quantify
846 regional variability in eddy diffusivity and other derived statistics (eddy
847 length, time scales; e.g., LaCasce et al., 2014; Griesel et al., 2014, 2015).
- 848 • Investigating the nature of the oceanic turbulent transport. The relative
849 diffusivity as a function of particle separation is related to the Eulerian
850 kinetic energy spectra. Together with the FSLEs (see Section 4.2), the
851 relative velocity diagnostics and the pair displacement PDFs can be
852 used to check for consistency with quasigeostrophic turbulence, chaotic
853 advection, and mean shear (LaCasce, 2008; Koszalka et al., 2009).

854 *4.2. Lagrangian Coherent Structures*

855 The ocean is full of eddies, jets and other coherent structures, which
856 are visible in ocean tracers such as temperature or chlorophyll. The field
857 of Lagrangian Coherent Structures (LCS) aims to identify the kinematic
858 skeleton of such objects based on the Lagrangian trajectories of the fluid and
859 to study the role of these structures in transport. Here we provide a very
860 brief introduction and overview of the field and refer the interested reader to
861 the more comprehensive review articles on the topic (e.g. Peacock and Dabiri,
862 2010; Peacock and Haller, 2013; Haller, 2015).

863 The most developed branch of LCS theory is concerned with identifying
864 distinguished material surfaces which serve as the boundaries of coherent
865 regions in unsteady flows. According to Haller (2015), a method for identifying
866 such surfaces must (a) be objective (i.e. gives the same result in all observer

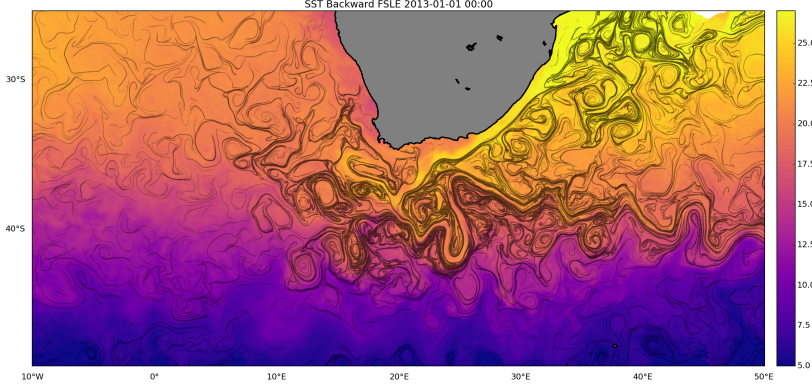


Figure 3: Backward Finite Size Lyapunov Exponents for January 1 2013 computed as in d’Ovidio et al. (2004), with initial separation distance of 0.01° and final separation distance of 1° . The FSLE have been computed using surface absolute geostrophic velocities produced by Ssalto/Duacs and distributed by AVISO, with support from CNES (delayed time, all satellite merged product). Ridges of FSLE (≥ 0.3) are overlaid on Multi-scale Ultra-high Resolution (MUR) Sea Surface Temperature (<http://mur.jpl.nasa.gov/>), showing good correspondence between the Lagrangian coherent structures and the distribution of the surface tracer advected by the Agulhas current, the Agulhas retroreflection and their associated mesoscale activity.

reference frames), (b) be applicable over a finite time interval, (c) describe an actual material surface, and (d) converge with respect to spatial resolution.

Many different LCS diagnostics have been developed to detect different types of structures. A starting point in many LCS identification methods, however, is the finite-time flow map $F_{t_0}^t(\mathbf{x}_0)$, which gives the positions at time t of particles initially located at \mathbf{x}_0 at time t_0 . The flow map can only be calculated by numerically advecting a large ensemble of closely spaced Lagrangian particles. From this flow map, one can compute the Cauchy Green Strain Tensor $C(\mathbf{x}_0) = [\nabla F_{t_0}^t(\mathbf{x}_0)]^T \nabla F_{t_0}^t(\mathbf{x}_0)$, which measures the magnitude of the growth in separation of infinitesimal perturbations in the initial position space. C is characterised by its eigenvalues λ and corresponding eigenvectors.

The original diagnostic of LCSs is the Finite Time Lyapunov Exponent (FTLE). The FTLE is a measure of the exponential rate of separation of trajectories of infinitesimally close initial points over a finite-time interval and is given by

$$FTLE(\mathbf{x}_0, t_0, \tau) = \frac{1}{\tau} \ln \sqrt{\lambda_{max}} \quad (35)$$

with λ_{max} the maximum eigenvalue of C over the chosen finite integration

time $\tau = t - t_0$. Early applications of the FTLE were to distinguish regions of high and low predictability in chaotic flows (FTLE; Pierrehumbert and Yang, 1993; Artale et al., 1997). Later, FTLE fields were applied to the identification of attracting and repelling transport barriers (Haller and Yuan, 2000; Lapeyre, 2002). The ridges (i.e. curves of local maxima) of the FTLE field correspond with repelling LCS positions at t_0 ; as regions of extreme local stretching, these structures represent material barriers which remain coherent under advection (unlike general material lines). Attracting LCSs, which represent the Lagrangian skeleton of tracer filaments, can similarly be obtained as ridges of the FTLE field calculated from a *backward* time integration. Haller and Sapsis (2011) review different strategies for calculating attracting and repelling LCSs from forward- and backward-time FTLEs. A related diagnostic is the Finite Size Lyapunov Exponent (FSLE; Aurell et al., 1997), which represents the *time* required for particle separation to reach a specified size (Figure 3). FSLEs have also been used widely for LCS identification and can be related to the statistics of turbulent dispersion (LaCasce, 2008). However, Karrasch and Haller (2013) proved that FSLE and FTLE ridges do not coincide in general and argued that FSLEs were less reliable for the identification of LCSs.

The statistics of FTLE and FSLE based on flow maps constructed from Lagrangian particle trajectories have been applied to characterize regimes of dispersion and regional differences in mixing (Drijfhout et al., 2003; Waugh and Abraham, 2008; Haza et al., 2010; Lumpkin and Eliot, 2010; Schroeder et al., 2011; Poje et al., 2014). Instantaneous maps of FTLE and FSLE derived from satellite altimetric velocities have also been used to identify LCS positions in the ocean (d’Ovidio et al., 2004; Olascoaga et al., 2006; Lehahn et al., 2007; Beron Vera et al., 2008). Attracting LCS represent transport barriers, and indeed several studies have confirmed the tight correlation between the detected structures and fronts of advected tracers including sea surface temperature (Abraham and Bowen, 2002; d’Ovidio et al., 2009), chlorophyll concentrations (Lehahn et al., 2007), oxygen (Bettencourt et al., 2015), oil spills (Mezić et al., 2010), and even different dominant phytoplanktonic types (d’Ovidio et al., 2010).

Not all coherent structures relevant for transport can reliably be deduced from the FTLE or FSLE fields. Over the past decade, LCS detection methods have developed increasing precision at discriminating different flavours of structure geometry, resulting in a proliferation of techniques (Haller, 2015). Haller and Beron-Vera (2012) used a variational approach to find the least-stretching material lines in the forward and backward flow maps; the initial

921 positions of these lines (called hyperbolic LCSs) can be identified as the
922 geodesic curves of a Riemannian metric related to the Cauchy-Green strain
923 tensor. Definitions of parabolic and elliptic LCSs, corresponding to jet cores
924 and vortex boundaries, can similarly be made using the tools of differential
925 geometry (Haller and Beron-Vera, 2013; Haller, 2015). Additional methods for
926 vortex identification based on dynamic polar decomposition and Lagrangian-
927 averaged vorticity deviation have recently been proposed (Haller, 2016; Haller
928 et al., 2016), while yet a different class of methods identifies LCS based on a
929 probabilistic transfer function (Froyland et al., 2007). A much needed critical
930 comparison of different methods and their performance in different test cases
931 was recently undertaken by Hadjighasem et al. (2017), which provides valuable
932 practical advice for researchers wishing to implement these techniques.

933 A central preoccupation of LCS techniques is the identification of coherent
934 mesoscale eddies. Beron-Vera et al. (2013) used the elliptic LCS framework to
935 identify materially coherent Agulhas rings, emphasizing the advantages over
936 Eulerian eddy-identification methods, while Froyland et al. (2012) applied
937 the transfer function method to the same region. Wang et al. (2016b) and
938 Froyland et al. (2015) used the identified structures to study the transport,
939 origin, and decay of Agulhas ring waters. Abernathey and Haller (2017) used
940 the Lagrangian-averaged vorticity deviation method of Haller et al. (2016)
941 to identify eddies in the eastern Pacific and quantify their role in meridional
942 dispersion. These studies illustrate the value of LCS methods for questions of
943 long-range material transport.

944 4.3. Probability distributions

945 A common way to visualize trajectory data is to bin particle positions into
946 histograms. The result is a map of particle density which, when normalised by
947 the total number of particle positions, yields a probability map. Alternatively
948 we can produce probability maps by counting the visit of a particular particle
949 only once per bin and then normalizing by the total number of particles
950 (instead of the total number of particle positions, e.g., van Sebille et al., 2012;
951 von Appen et al., 2014). Both methods offer a useful means to identify flow
952 structure through particle pathways from a set of release points.

953 Figure 4 illustrates the use of both methods for studying the flow re-
954 sponsible for the spreading of particles originating in the Agulhas Current.
955 Figure 4a shows the probability derived from the procedure described at
956 first. Obviously, bins located within the areas of the Agulhas Current (AC),
957 the Agulhas Return Current (ARC), and the Agulhas Ring corridor show

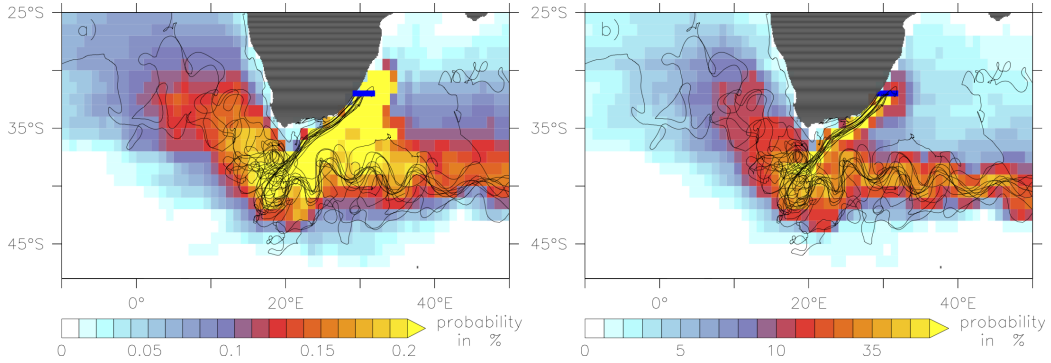


Figure 4: Lagrangian modelling approach to determine pathways of particles released in the Agulhas Current at 32°S (blue line extending east from Southeast Africa), based on a set of 5-year long trajectories initialized in the year 2000 (some examples visualized as black lines): a) Probability with that a $1^\circ \times 1^\circ$ bin spanning the whole depth range is occupied by a particle during the considered time span. The probability for each bin has been obtained by counting the number of particles occupying this bin at each time step, summing up this particle counts over the whole integration period and then dividing it by the total number of recorded particle counts for all bins. Thus, the sum of the probabilities of all bins yields 100%; b) Probability that a particle occupies a particular bin at least once during the considered time span. In this case the probability for each bin has been obtained by counting the number of different particles occupying this bin and dividing by the total number of particles. Thus, the probability for each bin can range between 0 and 100%. The Lagrangian analysis was performed with the ARIANE tool using the 3D 5day-mean velocity fields from the high-resolution model INALT01 (Durgadoo et al., 2013).

958 the highest probabilities, highlighting the most probable spreading pathways
959 along the major currents and via mesoscale eddies. But even between the
960 AC and ARC there is a region with comparable particle position counts.
961 Figure 4b reveals that this is not due to a particularly strong circulation
962 feature transporting many particles, but rather due to the recirculation of
963 fewer particles.

964 One consideration in the choice of bin resolution is aliasing. If either the
965 grid resolution is too fine or the period of particle position updates is too long,
966 trajectories may pass through more than one histogram bin within a given
967 output time step and thus may not be adequately accounted for. The density
968 maps from binning can also be scaled to account for the residence time in
969 bins and the time step of the Lagrangian simulation. One practice is to scale
970 the particle density maps by the time step dt to obtain the density maps in
971 units of days (e.g., Koszalka et al., 2011). Another is to scale the particle
972 densities in bins with the integral Lagrangian time scale, T_L , yielding particle
973 distributions in bins in terms of the ‘number of independent observations’:
974 $N_{ind} = N/\sqrt{T/T_L}$, where T is the total time (e.g., Koszalka and LaCasce,
975 2010).

976 Apart from using particle density maps to assess the water mass path-
977 ways and connectivity, binning of particle positions and their corresponding
978 properties allows the investigation of mean properties (temperature, density)
979 and their changes along simulated trajectories (e.g., van Sebille et al., 2014).
980 Binning Lagrangian velocities to test the Gaussianity of their distributions
981 and other velocity statistics is yet another application (LaCasce, 2005). The
982 binning is also used to construct maps of eddy diffusivity from particle sim-
983 ulations in high resolution models (e.g., LaCasce et al., 2014; Griesel et al.,
984 2014, 2015). Using binning to estimate spatially-dependent eddy diffusivities
985 (‘pseudo-Eulerian eddy diffusivity maps’) and other parameters (maps of eddy
986 time and length scales) has been widely used in observational Lagrangian
987 analysis (Bauer et al., 2002; Koszalka et al., 2011; Rypina et al., 2012; Lump-
988 kin and Johnson, 2013; Zhurbas, 2004), as well as in particle simulations in
989 eddy-resolving models (e.g., Berloff et al., 2002; LaCasce et al., 2014; Griesel
990 et al., 2014, 2015)

991 Binning can be used to verify the spreading of Lagrangian particles by
992 comparing the ensemble particle movement with large-scale distributions of
993 either conserved quantities, such as potential vorticity, or a tracer field whose
994 evolution is explicitly computed online in the OGCM (e.g., Gary et al., 2012)).
995 Such evaluations can be statistically formalised using pointwise correlation

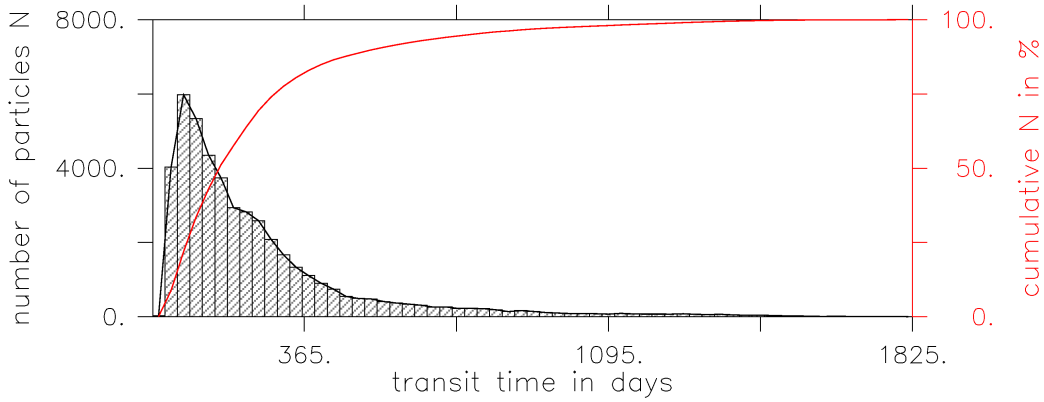


Figure 5: Example transit time distribution for particles released in the Agulhas Current at 32°S (blue lines in Figures 4 and 6, extending east from Southeast Africa) in the year 2000 and traced towards the GoodHope line (red line in Figure 6). The Lagrangian analysis was performed with the ARIANE tool using the 3D 5day-mean velocity fields from the high-resolution model INALT01 (Durgadoo et al., 2013).

996 between the binned histogram and the online tracer (Simons et al., 2013).
 997 Binning is not limited to spatial boxes as particles can be binned by
 998 virtually any variable that can be determined along a particle's path: for
 999 example depth, time, density, temperature, salinity, etc. This sort of binning
 1000 can be useful to highlight along-pathway water mass transformations (e.g.,
 1001 Koszalka et al., 2013b; Iudicone et al., 2011; Gary et al., 2014; van Sebille
 1002 et al., 2014). Particles can also be binned by the distance from the deployment
 1003 site. Such a distance metric can be redefined to account for the topographic
 1004 steering (Davis, 1998). Finally, an alternative to binning was proposed by
 1005 Koszalka and LaCasce (2010). Rather than grouping the Lagrangian data in
 1006 bins of fixed size, they grouped a fixed number of nearest-neighbor particle
 1007 positions together using a clustering algorithm.

1008 4.4. Water mass ages and transit times

1009 The 'age' of ocean water, or the time taken for water to transit between
 1010 defined regions or reservoirs, is a property of the flow that provides useful
 1011 understanding of the ocean circulation (Deleersnijder et al., 2001). Such a
 1012 metric can be easily derived from Lagrangian calculations by determining the
 1013 transit time of particles. Since the age of water can also be recovered from

1014 float trajectories or observations of chemical tracers (Fine et al., 2002; Waugh
1015 et al., 2004), there is the possibility to use the age to evaluate model results
1016 in comparison to observations. However, this comparison requires careful
1017 interpretation (Khatiwala et al., 2001) and has been rare (e.g. Haines et al.,
1018 1999).

1019 The age of a parcel of ocean water, described by numerous particle trajec-
1020 tories, is not unique, since different particles may transit between two regions
1021 by distinct pathways, travelling for different lengths of time (Phelps et al.,
1022 2013). As such, the age of ocean water is in fact a probability distribution:
1023 the transit time distribution (TTD) that an individual particle might take to
1024 travel between the two regions (Holzer and Hall, 2000; Deleersnijder et al.,
1025 2001; Haine and Hall, 2002). Given a sufficient number of Lagrangian tra-
1026 jectories, a TTD between two regions can be formed from a histogram of
1027 the particle ages (see Figure 5 for an example in the Agulhas region). In
1028 Lagrangian ocean analysis, the range, maximum or variance of this TTD is
1029 used to understand the inherent timescales of the circulation (e.g. Rühs et al.,
1030 2013). However, transit time distributions are highly sensitive to the spatial
1031 scales resolved by the numerical model from which Lagrangian trajectories
1032 are determined.

1033 In Lagrangian analyses, the ‘age’ can be evaluated as the time since a
1034 particle was last within the surface ocean (the ventilation timescale), in
1035 which case it reveals the timescales on which the ocean interacts with the
1036 atmosphere, and influences global climate. This method has been considered
1037 for the global ocean (Blanke and Speich, 2002) as well as specific water
1038 masses (Koch-Larrouy et al., 2010). In regional seas (with riverine forcing) an
1039 analogue to ventilation with the atmosphere is freshwater age (Phelps et al.,
1040 2013). One difficulty is that the ventilation timescale of deep ocean flows
1041 (which can be on the order of thousands of years) often exceeds the length of
1042 available OGCM output such that the velocity fields must to be ‘looped’ to
1043 calculate the full TTD (see also section 3.2).

1044 By considering the entry and exit of particles from an enclosed region,
1045 transit times can be interpreted as a residence timescale. For a marginal sea
1046 with one point of exchange, such as the Baltic Sea, this has been used as an
1047 alternative to the classic box model approach (Döös et al., 2004; Jönsson et al.,
1048 2004). Where there are multiple points of exchange, such as the Arctic Ocean,
1049 the approach determines the timescales on which these gateways interact
1050 (Lique et al., 2010).

1051 Lagrangian transit times are also used to evaluate the timescales on

which anomalies in a certain region would influence the flow downstream (e.g., Speich et al., 2001; van Sebille et al., 2011; Rühs et al., 2013), or to determine time-integrated properties of specific flows, such as the average speed (Koszalka et al., 2013c) or the most rapid pathways (Gary et al., 2012).

4.5. Volume transport and Lagrangian streamfunctions

Among the first uses of basin-scale Lagrangian particle tracking was to assess seawater volume transports between chosen sites in the ocean, resulting in an effective way of quantifying Lagrangian connectivity. In these applications, each particle is ‘tagged’ with a transport upon release, and that transport is then conserved along the trajectory as per the streamtube discussion in Section 2.4. We can construct volume transport pathways by summing the transports of particles that connect two regions (see Figure 6 for an illustrative example).

Just like in the Eulerian framework, the concept of volume conservation (as in a Boussinesq fluid discussed in Section 2.4) can be used to ‘collapse’ the full three-dimensional transport into a two-dimensional streamfunction. The unique feature in Lagrangian streamfunctions is that they can be constructed for only that part of the flow that connects the section where particles are released and where they are received. This concept has been applied to study for example the cold and warm water routes into the Atlantic (Speich et al., 2001, 2002; Drijfhout et al., 2003), Agulhas leakage (Durgadoo et al., 2017), the Pacific-to-Indian Ocean connectivity (van Sebille et al., 2014), the Lagrangian decomposition of the Deacon Cell (Döös et al., 2008), and the Atlantic MOC (Thomas et al., 2015b).

The concept of Lagrangian streamfunctions was introduced by Blanke et al. (1999) and is closely tied to the analytical integration method (Section 3.2.3). Consider a domain with open boundaries, such as the Agulhas region around South Africa. Trajectories are initialized along the boundaries of a control volume (box in Figure 6), and traced until they again reach the boundaries. Each trajectory is associated with a volume transport, and the volume transport is recorded at each grid-wall crossing of a trajectory. This method results in a non-divergent field of volume fluxes through all grid walls that can be integrated to Lagrangian streamfunctions. It is to be noted that this streamfunction represents the mean flow during the whole integration period, i.e. ideally until all trajectories have left the box.

Both Döös et al. (2008) and Kjellsson and Döös (2012a) showed that the total Lagrangian streamfunction is almost identical to the Eulerian stream-

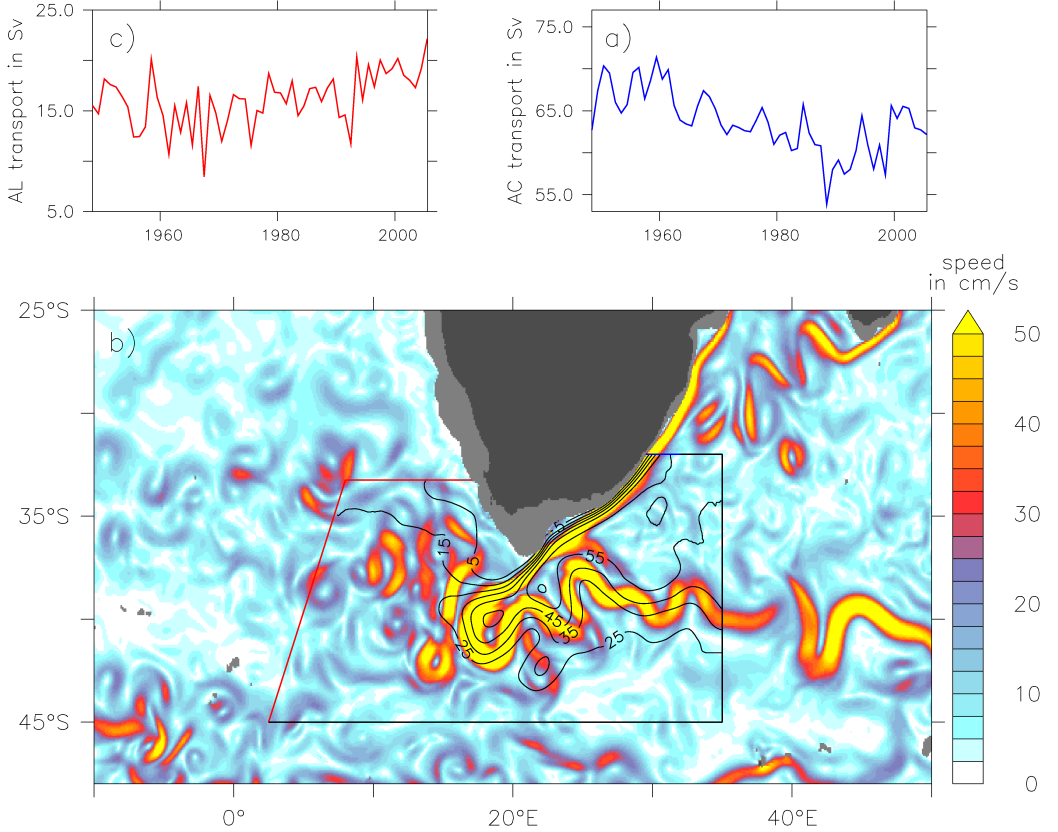


Figure 6: Quantitative Lagrangian modelling approach to determine Agulhas Leakage: a) Time series of the annual Agulhas Current (AC) transport at 32°S, where particles were released continuously proportional to the current volume transport, each particle associated with a fraction of this transport; b) Snapshot (18-Apr-2000) of current speed at 450m depth in the Agulhas region (colour shading, in cm/s), as well as the horizontal Lagrangian streamfunction (contours, in Sv) for all trajectories initialized in the year 2000 and traced along 3D streamlines towards the control sections (black and red lines); c) Time series of annual Agulhas Leakage (AL) transport, obtained by considering for each release year only the transports of those trajectories, that cross the approximated GoodHope section (red lines) within 5 years. The Lagrangian analysis was performed with the ARIANE tool using the 3D 5day-mean velocity fields from the high-resolution model INALT01 (Durgadoo et al., 2013).

1089 function. One of the main differences is that the Lagrangian streamfunction
1090 is based on trajectories with varying residence times ranging from hours
1091 to months or even years, while Eulerian streamfunctions are snapshots or
1092 time-averages.

1093 *4.6. Biological connectivity*

1094 Lagrangian particle trajectories can be used to study how water moves
1095 around in the ocean. Additionally, Lagrangian particles can be interpreted as
1096 passively drifting (biological) particulates. Many marine organisms reproduce
1097 with larvae that are dispersed at the whim of the currents. Hydrodynamic
1098 connectivity therefore has important implications for population dynamics
1099 (e.g., Kool et al., 2013; Thomas et al., 2014). In particular, this connectivity
1100 generally allows for longer dispersal and more rapid range expansion than is
1101 observed in terrestrial species (Kinlan and Gaines, 2003), as well as directly
1102 creating range limits (Gaylord and Gaines, 2000). Understanding these
1103 processes and their implications is important for a range of management
1104 objectives.

1105 Transport models have provided insights in varied contexts including
1106 the creation of robust networks of Marine Protected Areas (Gaines et al.,
1107 2003; Berglund et al., 2012; Burgess et al., 2014), conservation of coral reefs
1108 (Tremel et al., 2008; Wood et al., 2013), sustainability of fisheries (Gilbert
1109 et al., 2010), competition between biophysical and hydrodynamical controls on
1110 larvae retention (Phelps et al., 2015), and spread of invasive species. Similar
1111 models are frequently applied in coastal scenarios to understand the spread of
1112 aquaculture parasites (Salama and Rabe, 2013) and invasive benthic organisms
1113 (Brandt et al., 2008). It is important to note that horizontal resolution and
1114 subgrid scale diffusivity of the underlying Eulerian flow field can be a key
1115 for the distribution and time scales, as it was the case for the dispersion of
1116 European glass eels (Blanke et al., 2012; Baltazar-Soares et al., 2014).

1117 How these larvae interact with the water column depends on a range of
1118 characteristics such as size, development rate and behaviour (McManus and
1119 Woodson, 2012). Models investigating biological connectivity must therefore
1120 account for these characteristics and many others (e.g., Visser, 2008; Paris
1121 et al., 2013b), in addition to physical processes. ‘Behaviour’ such as orientation
1122 and swimming in response to scent plumes released from suitable habitat
1123 (Holstein et al., 2014; Staaterman and Paris, 2013) is often documented, as is
1124 vertical migration (Lampert, 1989).

1125 Observations of microchemical markers, genetic microsatellite markers
1126 and single nucleotide polymorphisms can provide information on realised
1127 connectivity between spatially separated populations. They can provide a
1128 direct comparison for Lagrangian tracking predictions (e.g., Pujolar et al.,
1129 2013; Wilkins et al., 2013; Teske et al., 2015) in terms of population similarity,
1130 and can provide evidence of biogeographic barriers (for example coral species
1131 in the Gulf of Mexico; Sammarco et al., 2012). Recent work hints at the
1132 possibility of applying such techniques to understand population connectivity
1133 and evaluate predicted patterns at a global scale (e.g., Hellweger et al., 2014;
1134 Villar et al., 2015; Jonsson and Watson, 2016).

1135 **5. Outlook**

1136 Lagrangian analysis provides a powerful tool to help interpret output from
1137 OGCMs. This power will only increase as OGCMs enter ‘peta-scale’ territory.
1138 In this final section, we offer outlooks on where we see new and exciting
1139 opportunities and possibilities for the Lagrangian analysis of OGCMs.

1140 *5.1. The next generation of particle tools*

1141 A major challenge with particle tracking is obtaining performance for a
1142 large number (order of billions) of particles. For small velocity data sets,
1143 offline parallel particle tracking can be employed via a Single Instruction
1144 Multiple Data (SIMD) approach, e.g., openMP or GPU-based implementa-
1145 tions. However, Input/Output will remain a bottle-neck, with most codes
1146 simply reading in the entire velocity field, even if the particles occupy only
1147 a subregion of the domain. Recent advances in the NetCDF library toolkit,
1148 however, mean that it is now feasible to read in only those parts of the grid
1149 where there are particles, so that the number of Input/Output operations
1150 could potentially be reduced by orders of magnitude. Implementation of these
1151 new libraries, in combination with better memory management and efficient
1152 use of tiered cache levels, will lead to vastly faster codes that also have smaller
1153 memory footprints.

1154 Nevertheless, for petabyte-scale velocity data sets such as those from grand
1155 challenge climate simulations, online particle tracking is necessary to avoid
1156 the unsustainable storage costs associated with offline particle tracking. The
1157 challenge in this arena, however, is utilization of heterogeneous computer ar-
1158 chitectures. Message-passing (MPI) between computational nodes is essential
1159 and a hybrid approach utilising on-node openMP, GPU, or MIC threading

1160 will be required on next-generation architectures to obtain peak performance.
1161 Task-based parallelism, if implemented for OGCMs, may provide at least
1162 a partial solution. However, at present, no definitive framework or “best
1163 practice” has been adopted.

1164 Several OGCMs already have on-line particle diagnostics (see section A.2),
1165 yet no general library for coupled Lagrangian particle tracking exists so far. As
1166 a result, development efforts are disjoint and functionalities are often model-
1167 specific. On the other hand, run-time integration with OGCMs requires close
1168 coupling with grid data in order to reduce performance overheads, while the
1169 variety of grid types makes finding a general abstraction difficult. Moreover,
1170 such a library needs to provide parallel performance and scalability, as well
1171 as an easily accessible API that allows it to be integrated with different types
1172 of ocean models.

1173 *5.2. A case for standard tests of particle tools*

1174 Most of the Lagrangian particle tracking tools described in section 3.5 have
1175 never been compared against each other, which makes it hard to assess their
1176 skill and fidelity. While most codes are designed for very different purposes,
1177 we propose to develop a set of test cases that we suggest code developers
1178 to use when debugging codes. This set of test cases would then also serve
1179 to highlight differences in explicit versus analytical time stepping codes, for
1180 example, or differences between particle tracking on A, B and C grids. While
1181 we envision the set to grow over time, the following would be a minimum
1182 requirement.

1183 A first set of tests to consider are those where analytical expressions are
1184 known for trajectories.

- 1185 1. Radial rotation with known period. This setup tests particle trajectories
1186 in the simplest-possible flow, without time evolution.
- 1187 2. Longitudinal shear dispersion flow in a pipe (e.g., Fischer et al., 2013)
1188 to ensure that shear dispersion effects are properly represented.
- 1189 3. Effective lateral diffusion due to an oscillating vertical shear flow (Bow-
1190 den, 1965) to test particle trajectories in a time-evolving flow.
- 1191 4. Steady-state flow around a peninsula (Ådlandsvik et al., 2009). This
1192 setup tests particle trajectories in a domain with an obstacle, and can
1193 be used to test how codes behave near land boundaries.

- 1194 5. Steady-state flow in a Stommel gyre and western boundary current
 1195 (Fabbroni, 2009) to test particle trajectories in a domain with large
 1196 gradients in flow speed.
- 1197 6. Damped inertial oscillation on a geostrophic flow (Fabbroni, 2009; Döös
 1198 et al., 2013) to appropriately quantify sub-inertial motion, e.g., loopers.
- 1199 7. For codes that include diffusivity, a simulation of Brownian motion with
 1200 a given K_h and K_v to test for sub-grid parameterizations of diffusivity.
- 1201 A second set of tests can be considered that do not have an analytical solution,
 1202 but that test for speed and efficiency of the code in more realistic idealized
 1203 test cases corresponding to eddy resolving simulations, e.g., as are becoming
 1204 standard in modern climate models.
- 1205 8. Zonally-periodic baroclinic channel (Ilicak et al., 2012; Berloff et al.,
 1206 2009; Abernathey et al., 2013; Ringler et al., 2016; Wolfram and Ringler,
 1207 2017a,b) to explore unconstrained eddy and mean flow interactions, e.g.,
 1208 in an idealized Antarctic Circumpolar Current.
- 1209 9. Eddying double-gyre flow (Shevchenko and Berloff, 2015; Wolfram et al.,
 1210 2015) to explore idealized eddying flows constrained within an ocean
 1211 basin.
- 1212 Looking forward, a list such as this one might form the basis of a La-
 1213 grangian Model Intercomparison Project (LMIP), similar to that used in the
 1214 climate modelling community through the Coupled Model Intercomparison
 1215 Project (Eyring et al., 2015) or the Ocean Model Intercomparison Project
 1216 (Griffies et al., 2016). An LMIP could host the velocity fields and analytical
 1217 solutions of the set of test cases needed by particle model developers for
 1218 debugging purposes. To allow for use across a broad suite of analysis software,
 1219 we encourage developers of tools to make the trajectory data CF-compliant,
 1220 as stated at <http://cfconventions.org/Data/cf-conventions/cf-conventions-1.6/build/cf-conventions.html#discrete-sampling-geometries>.

1222 *5.3. Whole-Earth System and Water Cycle Modelling*

1223 Beyond quantifying the pathways of seawater in the ocean, it is tantalis-
 1224 ing to consider whether Lagrangian methods could be used to track water
 1225 throughout the entire climate system. Such analysis could be used to quan-
 1226 tify coupled thermodynamic cycles (Laliberte et al., 2015; Kjellsson et al.,

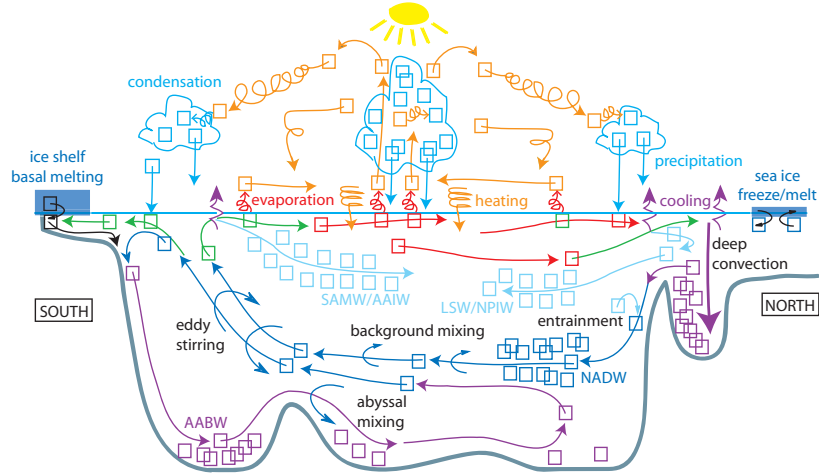


Figure 7: Illustrating how water particles follow the water cycle in the Earth System. We emphasize here the global ocean conveyor circulation in a pole-to-pole, meridional-vertical plane, coupled to selected and idealized atmospheric circulation in the same plane, omitting land for convenience [terrestrial processes such as evapo-transpiration, storage and runoff are also part of the full water cycle]. Individual water particles are represented by color-coded boxes, advected quickly/chaotically through the atmosphere, and slowly/steadily through the ocean. Particles are stored on a wide range of timescales: in clouds (hours-days); in sea ice (seasons-years); in the ocean (years-centuries); in ice sheets/shelves (centuries-millennia). In the ocean, colour coding identifies selected water masses and advection thereof: Antarctic Bottom Water (AABW); North Atlantic Deep Water (NADW); Labrador Sea Water (LSW); Antarctic Intermediate Water (AAIW); North Pacific Intermediate Water (NPIW); Subantarctic Mode Water (SAMW). In the atmosphere, colour-coding distinguishes vapor and liquid phases. Highlighted processes involve phase change or ocean-atmosphere exchange: ocean surface heating/cooling; evaporation; condensation; precipitation; sea ice freezing/melting; ice shelf basal melting. Highlighted processes internal to the ocean transform water particle density: deep convection; entrainment; enhanced abyssal mixing; eddy stirring; weak background mixing.

1227 2014; Zika et al., 2012; Döös et al., 2012), geographical connectivity (Gimeno
1228 et al., 2010), and the transport, dilution and fractionation of salt, nutrients
1229 and oxygen (Figure 7). Here we will discuss such prospects including basic
1230 requirements and challenges of such analysis.

1231 One important reason for modelling the water cycle is the intensification
1232 evident over recent decades in ocean salinity (Hosoda et al., 2009; Helm et al.,
1233 2010; Durack et al., 2012). Central to this intensification are changes to moist
1234 processes in the atmosphere (Held and Soden, 2006). However, based on
1235 observed salinity and in CMIP5 simulations, the hydrological cycle intensifies
1236 at around half the rate predicted from moist thermodynamics alone (Skliris
1237 et al., 2016), while observations are currently inadequate for an accurate
1238 quantification of changes in key processes (Hegerl et al., 2015), including
1239 precipitation and evaporation over the oceans (Skliris et al., 2014). With a
1240 Lagrangian description of the global water cycle in coupled climate models, it
1241 will be possible to fully explore the full range of atmospheric processes that
1242 are driving and retarding the observed intensification.

1243 Another motivation is the possibility of tracing stable water isotopes
1244 through the Earth system. Stable water isotopes are a cornerstone in paleo-
1245 climate reconstructions, since their concentrations can be used to infer the
1246 source of the water. For example, water vapour that has evaporated from the
1247 ocean has low concentrations of heavy isotopes. Likewise, ice on Antarctica
1248 also has very low concentrations of heavy isotopes, so it is likely that the ice
1249 originates from evaporated water that precipitated over the continent (Gat,
1250 1996). Hence, an observed decrease in heavy isotope concentrations in the
1251 ocean could be due to either less evaporation, or advection of meltwater from
1252 ice sheets or land (Roche, 2013). If we could trace the isotopic composition
1253 of water as it moves between oceans, atmosphere, land and ice we could
1254 reconstruct the hydrological cycles of past climates.

1255 In general, if a Lagrangian code is to exchange particles between ocean and
1256 other components of the earth system, it must first deal appropriately with
1257 sources and sinks of water within the ocean itself. It is now common for ocean
1258 models to have explicit water fluxes at the sea-surface due to evaporation,
1259 precipitation and river run-off (Griffies et al., 2000). These sources and sinks
1260 of water in the ocean should be accounted for in any Lagrangian framework
1261 (e.g., with sources and sinks of particles) regardless of whether water is being
1262 traced between components.

1263 Secondly, for water to be consistently traced between components of the
1264 climate system, water must be conserved between them. This is for example

1265 the case in some sea-ice and iceberg models which are integrated into ocean
1266 modelling systems (Martin and Adcroft, 2010; Marsh et al., 2015, some of
1267 which incidentally use a Lagrangian framework). However, challenges remain
1268 in conserving water consistently between the ocean, atmosphere, terrestrial
1269 hydrological systems (e.g. lakes, soil moisture, groundwater and irrigation)
1270 and ice-sheets.

1271 Tracking water within each component of the earth system other than
1272 the ocean presents its own challenges. There is, for example, a rich history of
1273 Lagrangian methods in meteorology (Stohl, 1998), some having evolved from
1274 the oceanographic community (e.g. TRACMASS, see Kjellsson and Döös,
1275 2012a). It is common for such methods to track air masses rather than water
1276 itself. Water in the atmosphere comes in three phases: vapour, liquid and
1277 ice, making the tracking of water challenging. However, robust methods are
1278 in common use (see for example the FLEXPART model; Stohl and James,
1279 2005; Gimeno et al., 2010).

1280 Simulating the movement of water as Lagrangian particles between differ-
1281 ent components of the earth system is further complicated by vast contrasts
1282 in scale both in storage and transport rates between them. The atmosphere
1283 for example holds 0.001% of all the water in the climate system while the
1284 ocean holds 97%. In contrast, the cycle of evaporation and precipitation over
1285 the globe amounts to approximately 16 Sv (i.e. multiplying global mean
1286 precipitation of 2.7mm/day, Trenberth, 1998, by the area of the earth). So
1287 while storage of water in the atmosphere is small relative to the ocean its
1288 transport of water is equivalent to that of major ocean currents. Differences
1289 in scales of motion and numerical description of these systems present great
1290 technical challenges beyond the scope of this review.

1291 6. Concluding remarks

1292 In this review article, we have presented an extensive overview of the
1293 state of the art in Lagrangian particle analysis. We focused on the use of
1294 particles determined by integral curves of the velocity field and large-scale
1295 open ocean applications. Based on the collective knowledge of the authors, we
1296 have identified opportunities and issues for improvements of these methods as
1297 we move towards a petascale age of computing. We hope that the guidance
1298 provided here can provide a starting point for new users, as well as an impetus
1299 for experienced users and developers of these codes.

1300 **Acknowledgements**

1301 This review paper is the result of very fruitful discussions during the
1302 “Future of Lagrangian Ocean Modelling” workshop, held at Imperial College
1303 London, UK, in September 2015. Funding for this workshop was provided
1304 through an EPSRC Institutional Sponsorship grant to EvS under reference
1305 number EP/N50869X/1. EvS has received funding from the European Re-
1306 search Council (ERC) under the European Unions Horizon 2020 research
1307 and innovation programme (grant agreement No 715386). This research for
1308 PJW was supported as part of the Energy Exascale Earth System Model
1309 (E3SM) project, funded by the U.S. Department of Energy, Office of Science,
1310 Office of Biological and Environmental Research. Funding for Henri Drake
1311 was provided by Grant No. DE-SC0012457 from the US Department of
1312 Energy. SFG is supported by NERC National Capability funding through the
1313 Extended Ellett Line Programme. ED is an honorary Research Associate with
1314 the Belgian Fund for Scientific Research (F.R.S.-FNRS). We thank Sergey
1315 Danilov (editor), Andrew Shao, François Primeau, Nathaniel Tarshish, and
1316 five anonymous reviewers for very helpful comments.

1317 We also wish to thank all the scientists, researchers and programmers who
1318 built the Ocean General Circulation and Lagrangian tracking models over the
1319 past decades.

1320 **A. Community tools for Lagrangian Ocean Analysis**

1321 In this appendix, we provide further background to the different community
1322 codes, both for offline and online particle tracking, listed in Tables 1 and 2.

1323 *A.1. Community-based offline 3D Lagrangian codes*

1324 *A.1.1. Ariane*

1325 Ariane is a numerical diagnostic tool developed at the Laboratoire de
1326 Physique des Océans (Brest, France). It is dedicated to the off-line computa-
1327 tion of the advective component of 3D trajectories and subsequent volume
1328 transport analyses in given velocity and tracer fields, most often obtained
1329 from the numerical integration of an ocean general circulation model.

1330 The trajectory integration scheme at the core of the Ariane calculations
1331 (Blanke and Raynaud, 1997) dates back to 1992 (Speich, 1992). It takes full
1332 advantage of the volume continuity equation expressed on a C-grid (Mesinger
1333 and Arakawa, 1976). There are several advantages to the analytical calculation

1334 of streamlines on the model grid for successive time intervals, over which the
1335 velocity is assumed to be steady-state (see section 3.2.3). The method only
1336 calculates particle positions on the edge of grid cells, and it respects the local
1337 three-dimensional non-divergence of the flow. Doing so makes the method
1338 both fast and accurate in terms of truncation error relative to an RK4 code.
1339 It offers flexibility too, in which backward integrations can be performed to
1340 track the origin of a given volume. A trajectory scheme that respects the
1341 continuity equation shows excellent capability for volume tracing, following
1342 the streamtube perspective discussed in Section 2.4.

1343 Following the methodology proposed by Döös (1995) and taken up by
1344 Blanke and Raynaud (1997) to take advantage of such a scheme, water volume
1345 transfers between selected control sections can be assessed with great accuracy.
1346 They can be portrayed by means of Lagrangian streamfunctions, defined either
1347 on a geographic plane (Blanke et al., 1999) or on other sets of coordinates
1348 that include the model physical tracers (Blanke et al., 2006).

1349 *A.1.2. TRACMASS*

1350 The TRACMASS Lagrangian trajectory code was originally developed by
1351 Döös (1995) and a thorough documentation was given by Döös et al. (2013)
1352 and Döös et al. (2017). TRACMASS has been used to calculate trajectories
1353 using velocity and tracer fields from a variety of ocean models. TRACMASS
1354 has also been used to study the atmospheric Hadley and Ferrell Cells using
1355 ERA-Interim as input (Kjellsson and Döös, 2012a). Hence, TRACMASS can
1356 handle a wide variety of vertical grids and data formats.

1357 TRACMASS solves the path of a trajectory through a grid box analytically
1358 (see section 3.2.3) Trajectories are thus unique and if a trajectory is calculated
1359 forward and then backward the solution will be the same up to numerical
1360 noise due to round-off errors. There are two algorithms for calculating the
1361 trajectories. The original from Döös (1995) uses velocities and tracers for
1362 trajectory calculations that are assumed piecewise constant in time. Another
1363 algorithm was developed by de Vries and Döös (2001) where time-dependence
1364 was taken into account by linearly interpolating the velocities in both time
1365 and space. Döös et al. (2017) showed that the time-interpolating scheme
1366 resulted in much more accurate calculations than the piecewise time-constant
1367 scheme.

1368 TRACMASS trajectories have also been used to simulate the behaviour of
1369 surface drifters (Kjellsson and Döös, 2012b; Nilsson et al., 2013). Comparing
1370 the simulated drifter trajectories with observed surface-drifter trajectories

1371 has showed that coarse-resolution ocean models lack variability in the surface
1372 currents, which is very likely due to the omission of stochastic noise to mimic
1373 subgrid scale diffusion.

1374 *A.1.3. Octopus*

1375 Octopus is an offline particle tracking code first written to conduct offline
1376 particle simulation using the Southern Ocean State Estimation (Mazloff et al.,
1377 2010), which makes use of the MITgcm. The code was used to study tracer
1378 evolution (Wang et al., 2016a) observed during the Diapycnal and Isopycnal
1379 Mixing Experiment in the Southern Ocean (DIMES; Gille et al., 2007; Ledwell
1380 et al., 2011). It was later used in simulating Argo floats as a component of
1381 observational system planning for the Southern Ocean Carbon and Climate
1382 Observations and Modeling project (SOCCOM, <http://soccom.princeton.edu>)
1383 and in studies of watermass pathways in the Southern Ocean.

1384 The interpolation scheme is linear in time and trilinear in space. The
1385 RK4 scheme is used for time integration. The boundary condition is reflective
1386 at the surface and solid walls. The model is currently written in Fortran
1387 for structured C-grids. OpenMP is implemented for shared-memory parallel
1388 calculation.

1389 *A.1.4. LAMTA software package*

1390 The LAgrangian Manifolds and Trajectories Analyser (LAMTA) consists
1391 of a set of functions developed for gnu-octave and intended for the analysis
1392 of two-dimensional velocity fields, in particular for oceanic current datasets.
1393 The source code is freely available and distributed under a GPL license upon
1394 direct request to the authors (d'Ovidio and Nencioli).

1395 The package provides routines to compute particle trajectories and La-
1396 grangian diagnostics based on user defined velocity fields (which include
1397 analytical test cases, numerical model results and altimetry-based surface
1398 geostrophic currents). The trajectories are computed using a Runge-Kutta
1399 fourth order advection scheme (section 3.2.1). Particle advection can be
1400 performed either forward or backward in time. The scheme applies bi-linear
1401 interpolation of velocities in space and, if necessary, linear interpolation in
1402 time. Lagrangian diagnostics include Finite Time/Size Lyapunov Exponents,
1403 eddy retention, origin of water particles, age of a water particles from a given
1404 bathymetry.

1405 The package has been applied to investigate the relationship between
1406 satellite-based Lagrangian coherent structures and ocean surface tracers in

1407 the open ocean (d’Ovidio et al., 2004; Lehahn et al., 2007; d’Ovidio et al.,
1408 2009), the retention of mesoscale structures (Smetacek et al., 2012; Martin
1409 et al., 2013), the impact of horizontal advection in structuring ecological
1410 niches (d’Ovidio et al., 2010) up to top predators (Cotté et al., 2011; De Monte
1411 et al., 2012; Bon et al., 2015; Cotté et al., 2015) and for contextualizing
1412 biodiversity genomic data Sunagawa et al. (2015). LAMTA has been recently
1413 included in the SPASSO (Software Package for an Adaptive Satellite-based
1414 Sampling for Ocean campaigns) software package¹⁴ developed to guide the
1415 in-situ sampling strategy as well as the interpretation of collected observations
1416 from (sub)mesoscale oriented field experiments. The package has been used
1417 to support experiments in the NW Mediterranean (LATEX, e.g. Nencioli
1418 et al., 2011, 2013), tropical North Atlantic (STRASSE, Reverdin et al., 2015)
1419 and Southern Indian ocean: KEOPS2 (d’Ovidio et al., 2015) and LOHAFEX
1420 (Martin et al., 2013). The code has also been integrated in the package used
1421 by Cnes/AVISO to produce global maps of Lyapunov exponents and vectors
1422 from altimetry data.

1423 *A.1.5. The Connectivity Modeling System (CMS)*

1424 The Connectivity Modelling System (CMS Paris et al., 2013b) is an open-
1425 source Fortran toolbox, created at the University of Miami, for the multi-scale
1426 tracking of biotic and abiotic particles in the ocean. The tool is inherently
1427 multiscale, allowing for the seamless moving of particles between grids at
1428 different resolutions.

1429 The CMS has been used on velocity fields from OFES, HYCOM, NEMO,
1430 MITgcm, UVic, ECCO2, SOSE, MOM and many other ocean models to
1431 compute dispersion, connectivity and fate in applications including large scale
1432 oceanography, marine reserve planning, and movement of marine biota all
1433 across the world.

1434 The CMS uses RK4 timestepping and tricubic interpolation and is designed
1435 to be modular and probabilistic, meaning that it is relatively easy to add
1436 additional ‘behaviours’ to the particles, with attributed randomly assigned
1437 for a distribution of traits. Modules distributed with the code include random
1438 walk diffusion, mortality, vertical migration, mixed layer mixing, and a
1439 seascape module designed to generate a connectivity matrix output from the
1440 source to the final destination of the particles.

¹⁴<http://www.mio.univ-amu.fr/doglioli/spasso.htm>

1441 *A.1.6. Other Biotic-particle models*

1442 While the CMS discussed above is also used for physical oceanogra-
1443 phy applications, the code has been developed as a so-called Individual
1444 Based Model (IBM), which serve predominantly biophysical applications.
1445 Another widely-used example of an IBM is ICHTYOP (Lett et al., 2008,
1446 <http://www.ichthyop.org/>). We will not cover IBMs in this discussion, as a
1447 very good recent overview can be found in Lynch et al. (2014).

1448 *A.1.7. Parcels*

1449 Parcels is an experimental prototype code aimed at exploring novel ap-
1450 proaches for Lagrangian tracking of virtual ocean tracer particles in the
1451 petascale age. Parcels, which is currently under development, is designed
1452 from the ground up to be efficient and fast for the next generation of ocean
1453 circulation models. These ocean models are so big and massively parallel,
1454 and they produce so much data, that in a few years we may face a situation
1455 where many of the Lagrangian frameworks cannot be used on the latest data
1456 any more (see also section 5.1).

1457 The user interface of Parcels is written in python, while the computational
1458 intensive integration is Just-In-Time (JIT) compiled into C. The code is formed
1459 around a flexible and customisable API that allows rapid model development,
1460 based on discrete time-stepping algorithms (section 3.2.1). It has a high-level
1461 abstraction that hides complexities from the user (field sampling, efficient
1462 loop scheduling, file I/O, etc.). This allows computer architecture experts to
1463 optimise underlying methods without changing the high-level description of
1464 the model.

1465 *A.2. Online tools within OGCMs*

1466 *A.2.1. LIGHT within MPAS-O*

1467 The Los Alamos National Laboratory Model for Prediction Across Scales
1468 Ocean (MPAS-O) (Ringler et al., 2013) is a fully unstructured C-grid ocean
1469 model capable of multiscale ocean simulation that is part of the Energy Exas-
1470 cale Earth System Model (E3SM), formerly known as Accelerated Climate
1471 model for Energy (ACME). MPAS-O uses an online diagnostic particle track-
1472 ing technique called LIGHT (Wolfram et al., 2015), for Lagrangian, in Situ,
1473 Global, High-performance particle Tracking, which is integrated within the
1474 MPAS framework and uses different particle advection modes corresponding
1475 to different vertical interpolation schemes. For example, particles can be
1476 advected along isopycnally-constrained trajectories. Time advancement uses a

1477 generalized Runge-Kutta sub-stepping scheme. Horizontal interpolation with
1478 Wachspress interpolation (Gillette et al., 2012) occurs following reconstruction
1479 of the full velocity vector via an inverse multi-quadratic radial basis function
1480 approach (Baudisch et al., 2006). Particles are implemented in linked-lists on
1481 each processor to conserve memory for large particle simulations and paral-
1482 lelism is via MPI. Parallel communication occurs during the computational
1483 step between spatially-adjacent processors for particles advecting from one
1484 processor to another and global parallel communication is reserved for Input
1485 and Output (I/O) tasks. Processor exchange lists for I/O may either be incre-
1486 mentally updated or globally computed to minimize communication overhead
1487 in different particle tracking configurations. LIGHT provides the capability
1488 to advect the same number of particles as cells to obtain a complementary
1489 Lagrangian description of the flow computed by the Eulerian prognostic solver
1490 in MPAS-O. A version of MPAS-O that includes LIGHT will be available via
1491 the public release of the U.S. Department of Energy’s Energy Exascale Earth
1492 System Model (E3SM).

1493 *A.2.2. NEMO*

1494 NEMO (the Nucleus for European Modelling of the Ocean) model (Madec
1495 and NEMO team, 2016) includes both Lagrangian floats (Madec, 2008) and
1496 interactive icebergs, module ICB (both RK4). In addition to the online
1497 icebergs option (NEMO-ICB; Marsh et al., 2015), icebergs can be forced in
1498 offline mode (for tracking purposes) using the Stand-Alone Surface forced
1499 (SAS) option, as SAS-ICB. In both NEMO-ICB and SAS-ICB, implementation
1500 exploits available MPI parallelism.

1501 *A.2.3. MITgcm*

1502 The Massachusetts Institute of Technology General Circulation model
1503 (MITgcm Marshall et al., 1997b,c) is a generalized level coordinate ocean
1504 model with a wide range of configuration possibilities. The MITgcm in-
1505 cludes a package for Lagrangian particle advection. The Lagrangian package,
1506 named `f1t`, is however poorly documented and not described in the liter-
1507 ature. Nevertheless, this package provides a convenient way to integrate
1508 Lagrangian analysis into existing MITgcm setups, thereby taking advantage
1509 of the MPI parallelism of the model. Numerically, floats are advected using
1510 RK4. A fixed memory buffer is allocated for floats on each tile, implying
1511 that memory is wasted for sparse particle ensembles. Because of MITgcm’s
1512 “offline mode” (Adcroft et al., 2014), which enables loading of velocity fields

1513 from files, MITgcm can be effectively used as a general-purpose Lagrangian
1514 model. Numerous studies have employed this configuration for simulating
1515 Lagrangian trajectories from satellite-derived geostrophic velocities (Klocker
1516 et al., 2012b,a; Klocker and Abernathey, 2014) and three-dimensional model
1517 output (Abernathey et al., 2013).

1518 *A.2.4. HYCOM*

1519 HYCOM (the HYbrid Coordinate Ocean Model) is a generalized (hybrid)
1520 vertical coordinate ocean model (isopycnal, terrain following, and/or pressure).
1521 It is isopycnal in the open stratified ocean, but reverts smoothly to a terrain-
1522 following coordinate in shallow coastal regions, and to pressure coordinates
1523 near the surface in the mixed layer (Bleck, 2002; Chassignet et al., 2003,
1524 2006). HYCOM includes online code designed to follow numerical particles
1525 during model run time (Halliwell and Garraffo, 2002; Wallcraft et al., 2009).
1526 In addition to the ability to follow a fluid particle in three dimensions, one
1527 can also release both isobaric and isopycnic floats. Isobaric floats remain at
1528 prescribed pressure levels while isopycnic floats remain on prescribed density
1529 surfaces.

1530 Because of the generalized (or hybrid) vertical coordinate of HYCOM,
1531 one has to be especially attentive when performing vertical and horizontal
1532 interpolations/advections. The horizontal, vertical, and temporal interpola-
1533 tion schemes used in HYCOM to advect the floats are adapted from Garraffo
1534 et al. (2001a,b). Horizontal interpolation is performed using a sixteen-point
1535 grid box surrounding the float when a sufficient number of good grid points
1536 are available (bilinear interpolation otherwise). Vertical interpolation first
1537 locates the bounding pressure interfaces and all properties are then linearly
1538 interpolated to the float location. Temporal interpolation is performed using
1539 RK4. Since the vertical velocity is not a prognostic variable in HYCOM, it is
1540 diagnosed using the continuity equation (see Halliwell and Garraffo (2002)
1541 and Wallcraft et al. (2009) for details on the implementation).

1542 *A.2.5. ROMS*

1543 ROMS (Regional Ocean Model System, <https://www.myroms.org/>) is
1544 a free surface, hydrostatic primitive equations ocean model with terrain-
1545 following vertical coordinates that allow differential stretching (Shchepetkin
1546 and McWilliams, 2005; Haidvogel et al., 2008). It is an open source parallel
1547 Fortran code coupled to several models including biogeochemistry, waves,
1548 sediments, bio-optical and sea ice. It offers great flexibility for configura-

tion and is widely used by the scientific community for a diverse range of
 1549 applications. ROMS includes a module called **floats**, which allows the
 1550 release and tracking of numerical particles during model run time. Passive
 1551 floats can be of 3 different types: neutral density 3D Lagrangian, isobaric
 1552 (remain at prescribed pressure level) or geopotential (remain at prescribed
 1553 depth). The numerical scheme used to time-step simulated floats trajectories
 1554 is a fourth-order Milne predictor and fourth-order Hamming corrector. It
 1555 is possible to add a random walk to the floats to simulate subgrid scale
 1556 vertical diffusion. The random walk component is implemented considering
 1557 spatially variable diffusivity following Hunter et al. (1993). Floats can either
 1558 reflect or ‘stick’ when they hit the surface/bottom boundaries. Clusters of
 1559 floats with user defined distributions can be released at specified locations.
 1560 It is possible to release particles multiple times, at defined time intervals
 1561 throughout the run. Recently new subroutines have been implemented to
 1562 allow for ‘biological floats’ that behave according to user defined parameters.
 1563 The complex biology of oyster larvae, including variable growth rates and
 1564 vertical swimming dependent on food, salinity, temperature and turbidity has
 1565 been implemented (Narvaez et al., 2012a,b), and is available with the latest
 1566 ROMS release.
 1567

1568 **B. Tracer trajectories with isopycnal diffusion**

1569 We here illustrate the stochastic differential equation discussion from
 1570 Section 3.3.1. We consider the calculation of Lagrangian tracer trajectories in
 1571 a 3D benchmark for diffusive tracer transport from Shah et al. (2011, 2013).
 1572 Note that in two dimensions, the approach is slightly different (see Appendix
 1573 C). For this purpose, let x and y denote the horizontal coordinates, while
 1574 z denotes the vertical coordinate and assume zero diapycnal diffusion. If
 1575 ρ is the potential density field (assume linear equation of state), then the
 1576 isopycnal diffusion tensor (Redi, 1982) reads

$$\mathbf{K} = \frac{K_I}{\rho_x^2 + \rho_y^2 + \rho_z^2} \begin{pmatrix} \rho_y^2 + \rho_z^2 & -\rho_x \rho_y & -\rho_x \rho_z \\ -\rho_y \rho_x & \rho_x^2 + \rho_z^2 & -\rho_y \rho_z \\ -\rho_z \rho_x & -\rho_z \rho_y & \rho_x^2 + \rho_y^2 \end{pmatrix}. \quad (36)$$

1577 Here K_I represents the isopycnal diffusion coefficient and ρ is given by

$$\rho(x, y, z) = \rho_0 \left[1 - \frac{N^2 z}{g} + \alpha_x \sin(\kappa_x x) + \alpha_y \sin(\kappa_y y) \right]. \quad (37)$$

1578 Note that the vertical density gradient is assumed to be constant, but the
 1579 horizontal one is not, so that the isopycnal surfaces are not flat.

1580 The concentration satisfies the following initial value problem:

$$\frac{\partial C}{\partial t} = \frac{\partial}{\partial x_i} \left(K_{ij} \frac{\partial C}{\partial x_j} \right), \quad t_0 \leq t \leq T \quad (38)$$

$$C(\mathbf{x}, t) = C_0(\mathbf{x}).$$

1581 To solve this problem with the stochastic model given by equation (27), one
 1582 needs to decompose the diffusion tensor \mathbf{K} in the form $2K_{ij} = \sigma_{ik}\sigma_{jk}$. Using
 1583 a Cholesky decomposition method, the components of the matrix σ can be
 1584 determined. This decomposition leads to the following stochastic differential
 1585 equations describing the behaviour of the individual particles (note that due
 1586 to the use of Cholesky decomposition, the components σ_{xy} , σ_{xz} and σ_{yz} of
 1587 the matrix σ are zero)

$$\begin{aligned} dX(t) &= a_x dt + \sqrt{2}\sigma_{xx}dW_x(t), \\ dY(t) &= a_y dt + \sqrt{2}\sigma_{yx}dW_x(t) + \sqrt{2}\sigma_{yy}dW_y(t), \\ dZ(t) &= a_z dt + \sqrt{2}\sigma_{zx}dW_x(t) + \sqrt{2}\sigma_{zy}dW_y(t), \\ X(t_0) &= X_0, \quad Y(t_0) = Y_0, \quad Z(t_0) = Z_0, \end{aligned} \quad (39)$$

1588 where the drift coefficients a_x , a_y and a_z are given by

$$a_x = \frac{\partial K_{xx}}{\partial x} + \frac{\partial K_{xy}}{\partial y}, \quad a_y = \frac{\partial K_{yx}}{\partial x} + \frac{\partial K_{yy}}{\partial y} \quad \text{and} \quad a_z = \frac{\partial K_{zx}}{\partial x} + \frac{\partial K_{zy}}{\partial y}. \quad (40)$$

1589 In Figure 8a results of a simulation are shown for parameter values that
 1590 are relevant for ocean transport problems (Shah et al., 2011, 2013). Here
 1591 the particles have been released at the origin $(x, y, z) = (0, 0, 0)$, a point that
 1592 belongs to the isopycnal surface. The position vector $[x_j(t), y_j(t), z_j(t)]$, $j =$
 1593 $1, 2 \dots J$, of each particles is simulated by means of a Lagrangian scheme.
 1594 Because the diapycnal diffusion is zero, the particles should not leave the
 1595 isopycnal surface. However, numerical errors are unavoidable and their
 1596 magnitude can be estimated by means of a spurious diapycnal diffusivity. The
 1597 results presented in Figure 8b show that the higher order Milstein scheme
 1598 performs better than the Euler scheme.

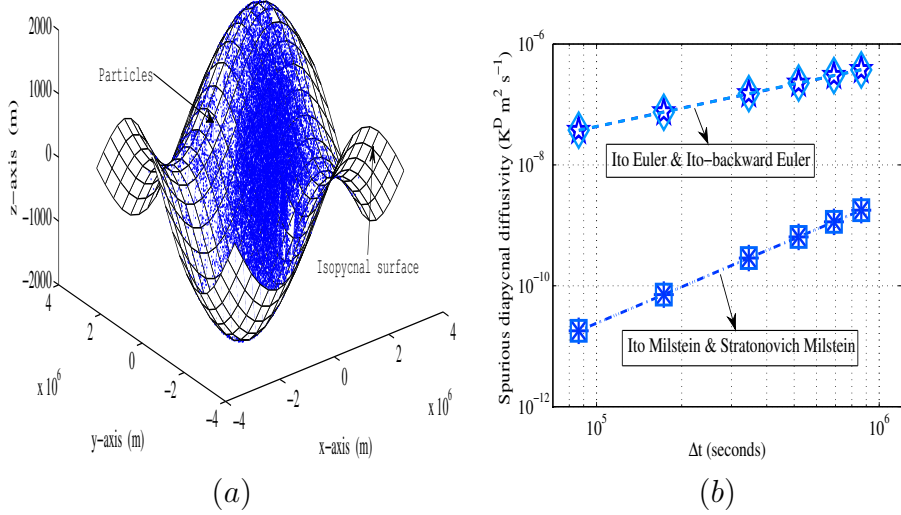


Figure 8: (a) Simulated position of Lagrangian particles at a certain time on the non-flat isopycnal surface and (b) the spurious diapycnal diffusivity for different Lagrangian schemes.

1599 **C. Diffusion in two-dimensional models and associated Lagrangian
1600 tracer trajectories**

1601 This review article deals with Lagrangian methods for large-scale open-
1602 ocean applications in oceanography. This is why the theoretical developments
1603 and the flows dealt with are essentially three-dimensional. There are, however,
1604 difficulties inherent in one- or two-dimensional transport models, which cannot
1605 be regarded as an idealisation or simplification of three-dimensional models.
1606 Some aspect thereof are outlined below.

1607 Let $H, u_i (i = 1, 2)$ and C be functions of the time and horizontal co-
1608 ordinates representing the height of the water column, the depth-averaged
1609 horizontal velocity and the depth-averaged concentration of a passive tracer,
1610 respectively. Then, the continuity equation is

$$\partial_t H + \partial_i (H u_i) = 0 \quad (41)$$

1611 and the equation obeyed by the concentration reads (e.g. Vanderborght et al.,
1612 2007)

$$\partial_t (H C) + \partial_i (H C u_i) = \partial_i (H K_{ij} \partial_j C) \quad (42)$$

1613 where the diffusivity tensor K_{ij} is symmetric and positive definite. The
 1614 latter partial differential equation may be transformed into a Fokker-Planck
 1615 equation in which HC (rather than C) should be viewed as the unknown:

$$\partial_t(HC) + \partial_i(HC u_i^{\text{drift}}) = \partial_i \partial_j(K_{ij} HC) \quad (43)$$

1616 where the drift velocity is (Heemink, 1990)

$$u_i^{\text{drift}} = u_i + H^{-1} \partial_j(H K_{ij}) = u_i + \partial_i(K_{ij}) + K_{ij} H^{-1} \partial_j H. \quad (44)$$

1617 The first two terms on the right-hand-side of equation (44) are equivalent
 1618 to those used in three-dimensional models, whilst the last one is specific to
 1619 depth-integrated models.

1620 If the last term in (44) is not taken into account in a Lagrangian model,
 1621 then particles might tend to concentrate into the shallowest areas, which clearly
 1622 is unphysical and may lead to erroneous conclusions (e.g. Spagnol et al., 2002).
 1623 A test case was designed by Deleersnijder (2015) that includes an analytical
 1624 solution for diffusion in a depth-varying domain, and implemented numerically
 1625 by Thomas et al. (2015a). This exact solution exhibits a somewhat counter-
 1626 intuitive behaviour, with the location of the maximum of the concentration
 1627 and the tracer patch centre of mass moving in opposite directions.

Somewhat similar developments are made when designing a one-dimensional, cross section-averaged transport model. Such models are often used to simulate transport processes in elongated domains such as rivers or estuaries (e.g. Everbecq et al., 2001; Hofmann et al., 2008). In this case all the variables and parameters depend on time and the along-flow coordinate x . If S , u and C denote the cross-sectional area, the cross-section-averaged velocity and the cross-section-averaged concentration, respectively, then the one-dimensional counterparts to equations (41)-(44) are

$$\partial_t S + \partial_x(Su) = 0 \quad (45a)$$

$$\partial_t(SC) + \partial_x(SCu) = \partial_x(SK \partial_x C) \quad (45b)$$

$$\partial_t(SC) + \partial_x(SCu^{\text{drift}}) = \partial_x \partial_x(KSC) \quad (45c)$$

1628 where

$$u^{\text{drift}} = u + S^{-1} \partial_x(SK) = u + \partial_x K + K S^{-1} \partial_x S \quad (46)$$

1629 is the drift velocity, and K is the along-flow diffusivity.

1630 In depth- and section-averaged models, the diffusion term is rarely meant
 1631 to represent turbulent diffusion per se. Instead, it is essentially the effect of

shear dispersion (e.g. Young and Jones, 1991) that is to be parameterized, i.e. the impact on the resolved (reduced-dimension) processes of the combined effect of sheared-advection and turbulent diffusion in the transversal direction. As a consequence, the diffusivity coefficients are often significantly larger than those that would be used in a three-dimensional model of the same domain.

References

- Abernathay, R., Ferreira, D., and Klocker, A. (2013). Diagnostics of isopycnal mixing in a circumpolar channel. *Ocean Modelling*, 72:1 – 16.
- Abernathay, R. and Haller, G. (2017). Transport by lagrangian vortices in the eastern pacific. In revision at J. Phys. Oceanogr.
- Abraham, E. R. and Bowen, M. M. (2002). Chaotic stirring by a mesoscale surface-ocean flow. *Chaos*, 12(2):373–381.
- Adcroft, A., Campin, J., Dutkiewicz, S., Evangelinos, C., Ferreira, D., Forget, G., Fox-Kemper, B., Heimbach, P., Hill, C., Hill, E., et al. (2014). Mitgcm user manual.
- Ådlandsvik, B., Bartsch, J., Brickman, D., Browman, H. I., Edwards, K., Fiksen, Ø., Gallego, A., Hermann, A. J., Hinckley, S., Houde, E., Huret, M., Irisson, J.-O., Lacroix, G., Leis, J. M., McCloghrie, P., Megrey, B. A., Miller, T., Van der Molen, J., Mullon, C., North, E. W., Parada, C., Paris, C. B., Pepin, P., Petitgas, P., Rose, K., Thygesen, U. H., and Werner, C. (2009). Manual of recommended practices for modelling physical – biological interactions during fish early life. Technical report, IFREMER, Dépt. EMH BP 21105 FR-44311 Nantes, Cedex 03, France.
- Aris, R. (1962). *Vectors, Tensors and the Basic Equations of Fluid Mechanics*. Dover Publishing, New York.
- Artale, V., Boffetta, G., Celani, A., Cencini, M., and Vulpiani, A. (1997). Dispersion of passive tracers in closed basins: Beyond the diffusion coefficient. *Physics of Fluids (1994-present)*, 9(11):3162–3171.
- Aurell, E., Boffetta, G., Crisanti, A., Paladin, G., and Vulpiani, A. (1997). Predictability in the large: an extension of the concept of Lyapunov exponent. *J. Phys. A*, 30(1):1.

- 1663 Awaji, T., Imasato, N., and Kunishi, H. (1980). Tidal exchange through a
1664 strait: A numerical experiment using a simple model basin. *Journal of*
1665 *Physical Oceanography*, 10(10):1499–1508.
- 1666 Baltazar-Soares, M., Biastoch, A., Harrod, C., Hanel, R., Marohn, L., Prigge,
1667 E., Evans, D., Bodles, K., Behrens, E., and Böning, C. W. (2014). Recruitment
1668 collapse and population structure of the European eel shaped by local
1669 ocean current dynamics. *Current Biology*, 24(1):104–108.
- 1670 Batchelor, G. (1952). Diffusion in a field of homogeneous turbulence. In
1671 *Mathematical Proceedings of the Cambridge Philosophical Society*, volume
1672 48–02, pages 345–362. Cambridge Univ Press.
- 1673 Batchelor, G. K. (1967). *An Introduction to Fluid Dynamics*. Cambridge
1674 University Press, Cambridge, England.
- 1675 Bates, M. L., Griffies, S. M., and England, M. H. (2012). A dynamic,
1676 embedded Lagrangian model for ocean climate models. Part I: Theory and
1677 implementation. *Ocean Modelling*, 59–60(C):41–59.
- 1678 Baudisch, J., Bonaventura, L., Iske, A., and Miglio, E. (2006). Matrix valued
1679 radial basis functions for local vector field reconstruction: applications to
1680 computational fluid dynamic models. *MOX Report*, 75.
- 1681 Bauer, S., Swenson, M. S., and Griffa, A. (2002). Eddy mean flow decomposi-
1682 tion and eddy diffusivity estimates in the tropical Pacific Ocean: 2. Results.
1683 *J. Geophys. Res.*, 107(C10):3154.
- 1684 Bennett, A. F. (1987). A lagrangian analysis of turbulent diffusion. *Reviews*
1685 *of Geophysics*, 25(4):799–822.
- 1686 Bennett, A. F. (2006). *Lagrangian Fluid Dynamics*. Cambridge University
1687 Press, Cambridge.
- 1688 Berglund, M., Nilsson Jacobi, M., and Jonsson, P. R. (2012). Optimal
1689 selection of marine protected areas based on connectivity and habitat
1690 quality. *Ecological Modelling*, 240:105–112.
- 1691 Berloff, P., Kamenkovich, I., and Pedlosky, J. (2009). A model of multiple
1692 zonal jets in the oceans: Dynamical and kinematical analysis. *Journal of*
1693 *Physical Oceanography*, 39(11):2711–2734.

- 1694 Berloff, P. and McWilliams, J. (2003). Material transport in oceanic gyres.
1695 part iii. randomized stochastic models. *Journal of Physical Oceanography*,
1696 33:1416–1445.
- 1697 Berloff, P., McWilliams, J., and Bracco, A. (2002). Material transport in
1698 oceanic gyres. part i. phenomenology. *Journal of Physical Oceanography*,
1699 32:764–796.
- 1700 Berloff, P. S. and McWilliams, J. C. (2002). Material transport in oceanic gyres.
1701 part ii: Hierarchy of stochastic models. *Journal of Physical Oceanography*,
1702 32(3):797–830.
- 1703 Beron-Vera, F. J. and LaCasce, J. H. (2016). Statistics of simulated and
1704 observed pair separations in the Gulf of Mexico. *Journal of Physical
1705 Oceanography*, 46(7):2183–2199.
- 1706 Beron Vera, F. J., Olascoaga, M. J., and Goni, G. J. (2008). Oceanic mesoscale
1707 eddies as revealed by Lagrangian coherent structures. *Geophys. Res. Lett.*,
1708 35(12).
- 1709 Beron-Vera, F. J., Wang, Y., Olascoaga, M. J., Goni, G. J., and Haller, G.
1710 (2013). Objective Detection of Oceanic Eddies and the Agulhas Leakage.
1711 *Journal of Physical Oceanography*, 43(7):1426–1438.
- 1712 Bettencourt, J. a. H., López, C., Hernández-García, E., Montes, I., Sudre,
1713 J., Dewitte, B., Paulmier, A., and Garcon, V. (2015). Boundaries of the
1714 peruvian oxygen minimum zone shaped by coherent mesoscale dynamics.
1715 *Nature Geoscience*.
- 1716 Blanke, B., Arhan, M., Madec, G., and Roche, S. (1999). Warm water paths
1717 in the equatorial Atlantic as diagnosed with a general circulation model.
1718 *Journal of Physical Oceanography*, 29:2753–2768.
- 1719 Blanke, B., Arhan, M., and Speich, S. (2006). Salinity changes along the
1720 upper limb of the Atlantic thermohaline circulation. *Geophysical Research
1721 Letters*, 33:L06609.
- 1722 Blanke, B., Bonhommeau, S., Grima, N., and Drillet, Y. (2012). Sensitivity of
1723 advective transfer times across the North Atlantic Ocean to the temporal
1724 and spatial resolution of model velocity data: Implication for European eel
1725 larval transport. *Dyn. Atmos. Ocean.*, 55-56:22–44.

- 1726 Blanke, B. and Raynaud, S. (1997). Kinematics of the Pacific Equatorial
1727 Undercurrent: An Eulerian and Lagrangian approach from GCM results.
1728 *Journal of Physical Oceanography*, 27(6):1038–1053.
- 1729 Blanke, B. and Speich, S. (2002). A global diagnostic of interior ocean
1730 ventilation. *Geophysical research Letters*, 29(8):1–4.
- 1731 Bleck, R. (2002). An oceanic general circulation model framed in hybrid
1732 isopycnic-Cartesian coordinates. *Ocean Modelling*, 4(1):55–88.
- 1733 Bon, C., Della Penna, A., dOvidio, F., Arnould, J. Y., Poupart, T., and Bost,
1734 C.-A. (2015). Influence of oceanographic structures on foraging strategies:
1735 Macaroni penguins at crozet islands. *Movement ecology*, 3(1):1–11.
- 1736 Böning, C. W. and Cox, M. D. (1988). Particle dispersion and mixing of
1737 conservative properties in an eddy-resolving model. *Journal of Physical
1738 Oceanography*, 18.
- 1739 Bowden, K. F. (1965). Horizontal mixing in the sea due to a shearing current.
1740 *J. Fluid Mech.*, 21(2):83–95.
- 1741 Bower, A. S., Lozier, M. S., Gary, S. F., and Böning, C. W. (2009). Interior
1742 pathways of the North Atlantic meridional overturning circulation. *Nature*,
1743 459:243–248.
- 1744 Brandt, G., Wehrmann, A., and Wirtz, K. W. (2008). Rapid invasion of
1745 Crassostrea gigas into the German Wadden Sea dominated by larval supply.
1746 *Journal of Sea Research*, 59(4):279–296.
- 1747 Burgess, S. C., Nickols, K. J., Griesemer, C. D., Barnett, L. A. K., Dedrick,
1748 A. G., Satterthwaite, E. V., Yamane, L., Morgan, S. G., White, J. W., and
1749 Botsford, L. W. (2014). Beyond connectivity: how empirical methods can
1750 quantify population persistence to improve marine protected-area design.
1751 *Ecological Applications: A Publication of the Ecological Society of America*,
1752 24(2):257–270.
- 1753 Butcher, J. C. (2016). *Numerical methods for ordinary differential equations*.
1754 John Wiley & Sons.
- 1755 Cetina-Heredia, P., Roughan, M., van Sebille, E., Feng, M., and Coleman,
1756 M. A. (2015). Strengthened currents override the effect of warming on
1757 lobster larval dispersal & survival. *Global Change Biology*, 21:4377–4386.

- 1758 Chassignet, E., Smith, L. T., Halliwell, G., and Bleck, R. (2003). North
1759 Atlantic simulations with the Hybrid Coordinate Ocean Model (HYCOM):
1760 Impact of the vertical coordinate choice, reference pressure, and thermo-
1761 baricity. *Journal of Physical Oceanography*, 33(12):2504–2526.
- 1762 Chassignet, E. P., Hurlburt, H., Smedstad, O. M., Halliwell, G., Wallcraft,
1763 A. J., Metzger, E. J., Blanton, B., Lozano, C., Rao, D., Hogan, P., and
1764 Srinivasan, A. (2006). Generalized Vertical Coordinates for Eddy-Resolving
1765 Global and Coastal Ocean Forecasts. *Oceanography*, 19(1):118–129.
- 1766 Chenillat, F., Blanke, B., Grima, N., Franks, P. J. S., Capet, X., and Rivière,
1767 P. (2015). Quantifying tracer dynamics in moving fluids: a combined
1768 Eulerian-Lagrangian approach. *Frontiers in Environmental Science*, 3:1–15.
- 1769 Chu, P. C. and Fan, C. (2014). Accuracy Progressive Calculation of Lagrangian
1770 Trajectories from a Gridded Velocity Field. *Journal of Atmospheric and*
1771 *Oceanic Technology*, 31(7):1615–1627.
- 1772 Cotté, C., d’Ovidio, F., Chaigneau, A., Lévy, M., Taupier Letage, I., Mate,
1773 B., and Guinet, C. (2011). Scale-dependent interactions of Mediterranean
1774 whales with marine dynamics. *Limnol. Oceanogr.*, 106(20):219–232.
- 1775 Cotté, C., d’Ovidio, F., Dragon, A.-C., Guinet, C., and Lévy, M. (2015).
1776 Flexible preference of southern elephant seals for distinct mesoscale features
1777 within the antarctic circumpolar current. *Progress in Oceanography*, 131:46–
1778 58.
- 1779 Cowen, R. K., Paris, C. B., and Srinivasan, A. (2006). Scaling of connectivity
1780 in marine populations. *Science*, 311:522–527.
- 1781 Cummins, S. J., Sylvester, T. B., and Cleary, P. W. (2012). Three-dimensional
1782 wave impact on a rigid structure using smoothed particle hydrodynamics.
1783 *Int. J. Numer. Methods Fluids*, 68(12):1471–1496.
- 1784 Danabasoglu, G. (2004). A comparison of global ocean general circulation
1785 model solutions obtained with synchronous and accelerated integration
1786 methods. *Ocean Modelling*, 7:323–341.
- 1787 Davis, R. E. (1982). On relating eulerian and lagrangian velocity statistics:
1788 single particles in homogeneous flows. *Journal of Fluid Mechanics*, 114:1–26.

- 1789 Davis, R. E. (1983). Oceanic property transport, lagrangian particle statistics,
1790 and their prediction. *Journal of Marine Research*, 41:163–194.
- 1791 Davis, R. E. (1985). Drifter observations of coastal surface currents during
1792 code: The statistical and dynamical views. *Journal of Geophysical Research*,
1793 90(C3):4756–4772.
- 1794 Davis, R. E. (1987). Modeling eddy transport of passive tracers. *Journal of*
1795 *Marine Research*, 45(3):635–666.
- 1796 Davis, R. E. (1991). Observing the general circulation with floats. *Deep Sea*
1797 *Res.*, 38:531–571.
- 1798 Davis, R. E. (1998). Preliminary results from directly measuring mid-depth
1799 circulation in the Tropical and South Pacific. *J. Geophys. Res.*, 103:24619–
1800 24639.
- 1801 Dawson, M. N., Sen Gupta, A., and England, M. H. (2005). Coupled
1802 biophysical global ocean model and molecular genetic analyses identify
1803 multiple introductions of cryptogenic species. *Proceedings of the National*
1804 *Academy of Sciences*, 102(34):11968–11973.
- 1805 De Monte, S., Cotté, C., d’Ovidio, F., Lévy, M., Le Corre, M., and Weimer-
1806 skirch, H. (2012). Frigatebird behaviour at the ocean–atmosphere interface:
1807 integrating animal behaviour with multi-satellite data. *Journal of The*
1808 *Royal Society Interface*, 9(77):3351–3358.
- 1809 de Vries, P. and Döös, K. (2001). Calculating lagrangian trajectories using
1810 time-dependent velocity fields. *J. Atmos. Oceanic Technology.*, 18(6):1092–
1811 1101.
- 1812 DeGroot, S. R. and Mazur, P. (1984). *Non-Equilibrium Thermodynamics*.
1813 Dover Publications, New York. 510 pp.
- 1814 Deleersnijder, E. (2015). A depth-integrated diffusion problem
1815 in a depth-varying, unbounded domain for assessing Lagrangian
1816 schemes. Technical report, Université Catholique de Louvain;
1817 <http://hdl.handle.net/2078.1/160980>.
- 1818 Deleersnijder, E., Campin, J. M., and Delhez, E. J. M. (2001). The concept of
1819 age in marine modelling I. Theory and preliminary model results. *Journal*
1820 *of Marine Systems*, 28:229–267.

- 1821 Döös, K. (1995). Inter-ocean exchange of water masses. *Journal of Geophysical*
1822 *Research: Oceans*, 100:13499–13514.
- 1823 Döös, K., Jönsson, B., and Kjellsson, J. (2017). Evaluation of oceanic and
1824 atmospheric trajectory schemes in the TRACMASS trajectory model v6.0.
1825 *Geoscientific Model Development*, 10(4):1733–1749.
- 1826 Döös, K., Kjellsson, J., and Jönsson, B. (2013). TRACMASS—A Lagrangian
1827 Trajectory Model. In *Preventive Methods for Coastal Protection*, pages
1828 225–249. Springer International Publishing, Heidelberg.
- 1829 Döös, K., Meier, H. E. M., and Döscher, R. (2004). The Baltic haline conveyor
1830 belt or the overturning circulation and mixing in the Baltic. *Ambio*, 33(4–
1831 5):261–266.
- 1832 Döös, K., Nilsson, J., Nycander, J., Brodeau, L., and Ballarotta, M. (2012).
1833 The World Ocean Thermohaline Circulation. *Journal of Physical Oceanog-
1834 raphy*, 42(9):1445–1460.
- 1835 Döös, K., Nycander, J., and Coward, A. C. (2008). Lagrangian decomposition
1836 of the Deacon Cell. *J. Geophys. Res. Ocean.*, 113(C7):C07028.
- 1837 Dormand, J. and Prince, P. (1980). A family of embedded runge-kutta
1838 formulae. *Journal of Computational and Applied Mathematics*, 6(1):19 –
1839 26.
- 1840 d’Ovidio, F., De Monte, S., Alvain, S., Dandonneau, Y., and Lévy, M. (2010).
1841 Fluid dynamical niches of phytoplankton types. *Proceedings of the National
1842 Academy of Sciences*, 107(43):18366–18370.
- 1843 d’Ovidio, F., Della Penna, A., Trull, T. W., Nencioli, F., Pujol, M.-I., Rio,
1844 M.-H., Park, Y.-H., Cotté, C., Zhou, M., and Blain, S. (2015). The bioge-
1845 chemical structuring role of horizontal stirring: Lagrangian perspectives
1846 on iron delivery downstream of the Kerguelen Plateau. *Biogeosciences*,
1847 12(19):5567–5581.
- 1848 d’Ovidio, F., Fernández, V., Hernández García, E., and López, C. (2004).
1849 Mixing structures in the Mediterranean Sea from finite-size Lyapunov
1850 exponents. *Geophys. Res. Lett.*, 31:L17203.

- 1851 d'Ovidio, F., Isern Fontanet, J., López, C., Hernández García, E., and García
1852 Ladona, E. (2009). Comparison between Eulerian diagnostics and finite-size
1853 Lyapunov exponents computed from altimetry in the Algerian basin. *Deep*
1854 *Sea Res.* *I*, 56(1):15–31.
- 1855 Drijfhout, S., de Vries, P., Döös, K., and Coward, A. (2003). Impact of eddy-
1856 induced transport on the lagrangian structure of the upper branch of the
1857 thermohaline circulation. *Journal of Physical Oceanography*, 24:2141–2155.
- 1858 Drijfhout, S. S., Maier-Reimer, E., and Mikolajewicz, U. (1996). Tracing
1859 the conveyor belt in the Hamburg large-scale geostrophic ocean general
1860 circulation model. *Journal of Geophysical Research: Oceans*, 101:22563–
1861 22575.
- 1862 Durack, P. J., Wijffels, S. E., and Matear, R. J. (2012). Ocean Salinities
1863 Reveal Strong Global Water Cycle Intensification During 1950 to 2000.
1864 *Science*, 336(6080):455–458.
- 1865 Durgadoo, J. V., Loveday, B. R., Reason, C. J. C., Penven, P., and Biastoch,
1866 A. (2013). Agulhas Leakage Predominantly Responds to the Southern
1867 Hemisphere Westerlies. *J. Phys. Oceanogr.*, 43(10):2113–2131.
- 1868 Durgadoo, J. V., Rühs, S., Biastoch, A., and Böning, C. W. B. (2017). Indian
1869 ocean sources of agulhas leakage. *Journal of Geophysical Research: Oceans*,
1870 122:3481–3499.
- 1871 Durran, D. R. (1999). *Numerical Methods for Wave Equations in Geophysical*
1872 *Fluid Dynamics*. Springer Verlag, Berlin. 470 pp.
- 1873 Eckart, C. (1948). An analysis of the stirring and mixing processes in
1874 incompressible fluids. *Journal of Marine Research*, 7:265–275.
- 1875 England, M. (1995). The Age of Water and Ventilation Timescales in a Global
1876 Ocean Model. *Journal of Physical Oceanography*, 25:2756–2777.
- 1877 Everbecq, E., Gosselain, V., Viroux, L., and Descy, J. P. (2001). Potamon: A
1878 dynamic model for predicting phytoplankton composition and biomass in
1879 lowland rivers. *Water Research*, 35(4):901–912.
- 1880 Eyring, V., Bony, S., Meehl, J., Senior, C., Stevens, B., Stouffer, R., and
1881 Taylor, K. (2015). Overview of the coupled model intercomparison project

- 1882 phase 6 (cmip6) experimental design and organisation. *Geoscientific Model*
1883 *Development Discussions*, 2015:10539–10583.
- 1884 Fabbroni, N. (2009). *Numerical simulations of passive tracers dispersion in*
1885 *the sea*. PhD thesis, Universita di Bologna.
- 1886 Farazmand, M. M. and Haller, G. (2012). Computing lagrangian coherent
1887 structures from their variational theory. *Chaos*, 22.
- 1888 Fine, R. A., Rhein, M., and Andrié, C. (2002). Using a CFC effective age to
1889 estimate propagation and storage of climate anomalies in the deep western
1890 North Atlantic Ocean. *Geophysical Research Letters*, 29(24):80–1.
- 1891 Fischer, H. B., List, J. E., Koh, C. R., Imberger, J., and Brooks, N. H. (2013).
1892 *Mixing in inland and coastal waters*. Elsevier.
- 1893 Fox-Kemper, B., Lumpkin, R., and Bryan, F. (2013). Lateral transport in
1894 the ocean interior. In Siedler, G., Griffies, S. M., Gould, J., and Church,
1895 J., editors, *Ocean Circulation and Climate, 2nd Edition: A 21st Century*
1896 *Perspective*, volume 103 of *International Geophysics Series*, pages 185–209.
1897 Academic Press.
- 1898 Froyland, G., Horenkamp, C., Rossi, V., Santitissadeekorn, N., and Sen Gupta,
1899 A. (2012). Three-dimensional characterization and tracking of an Agulhas
1900 Ring. *Ocean Modelling*, 52-53:69–75.
- 1901 Froyland, G., Horenkamp, C., Rossi, V., and van Sebille, E. (2015). Studying
1902 an Agulhas ring’s long-term pathway and decay with finite-time coherent
1903 sets. *Chaos*, 25(8):083119.
- 1904 Froyland, G., Padberg-Gehle, K., England, M. H., and Treguier, A.-M. (2007).
1905 Detection of coherent oceanic structures via transfer operators. *Physical*
1906 *Review Letters*, 98(22):224503.
- 1907 Fujio, S. and Imasato, N. (1991). Diagnostic calculation for circulation and
1908 water mass movement in the deep pacific. *Journal of Geophysical Research: Oceans*, 96(C1):759–774.
- 1909
- 1910 Fujio, S., Kadowaki, T., and Imasato, N. (1992). World ocean circulation
1911 diagnostically derived from hydrographic and wind stress fields: 2. the water
1912 movement. *Journal of Geophysical Research: Oceans*, 97(C9):14439–14452.

- 1913 Gaines, S. D., Gaylord, B., and Largier, J. L. (2003). Avoiding current
1914 oversights in marine reserve design. *Ecological Applications*, 13(sp1):32–46.
- 1915 Gardiner, C. W. (1985). *Handbook of stochastic models*, 2nd ed. Springer,
1916 Heidelberg.
- 1917 Garraffo, Z. D., Griffa, A., Mariano, A. J., and Chassignet, E. P. (2001a).
1918 Lagrangian data in a high-resolution numerical simulation of the North
1919 Atlantic II. On the pseudo-Eulerian averaging of Lagrangian data. *Journal
1920 of Marine Systems*, 29(1-4):177–200.
- 1921 Garraffo, Z. D., Mariano, A. J., Griffa, A., Veneziani, C., and Chassignet,
1922 E. P. (2001b). Lagrangian data in a high-resolution numerical simulation
1923 of the North Atlantic I. Comparison with in situ drifter data. *Journal of
1924 Marine Systems*, 29(1-4):157–176.
- 1925 Gary, S. F., Lozier, M. S., Biastoch, A., and Bning, C. W. (2012). Reconciling
1926 tracer and float observations of the export pathways of Labrador Sea Water.
1927 *Geophysical Research Letters*, 39(November):1–5.
- 1928 Gary, S. F., Lozier, M. S., Kwon, Y.-O., and J., P. J. (2014). The fate of north
1929 atlantic subtropical mode water in the flame model. *Journal of Physical
1930 Oceanography*, 44(5).
- 1931 Gat, J. R. (1996). Oxygen and hydrogen isotopes in the hydrologic cycle.
1932 *Annual Review of Earth and Planetary Sciences*, 24:225–262.
- 1933 Gaylord, B. and Gaines, S. D. (2000). Temperature or transport? range
1934 limits in marine species mediated solely by flow. *The American Naturalist*,
1935 155(6):769–789.
- 1936 Gilbert, C. S., Gentleman, W. C., Johnson, C. L., DiBacco, C., Pringle,
1937 J. M., and Chen, C. (2010). Modelling dispersal of sea scallop (*Placopecten
1938 magellanicus*) larvae on Georges Bank: The influence of depth-distribution,
1939 planktonic duration and spawning seasonality. *Progress in Oceanography*,
1940 87(1-4):37–48.
- 1941 Gille, S. T., Speer, K., Ledwell, J. R., and Garabato, A. C. N. (2007).
1942 Mixing and Stirring in the Southern Ocean. *Eos, Transactions American
1943 Geophysical Union*, 88:382.

- 1944 Gillette, A., Rand, A., and Bajaj, C. (2012). Error estimates for generalized barycentric interpolation. *Advances in computational mathematics*, 37(3):417–439.
- 1947 Gimeno, L., Drumond, A., Nieto, R., Trigo, R. M., and Stohl, A. (2010).
1948 On the origin of continental precipitation. *Geophysical Research Letters*, 37(13):n/a–n/a.
- 1950 Graham, F. and McDougall, T. (2013). Quantifying the nonconservative production of Conservative Temperature, potential temperature, and entropy.
1951 *Journal of Physical Oceanography*, 43:838–862.
- 1953 Gräwe, U., Deleersnijder, E., Shah, S. H. A. M., and Heemink, A. W. (2012).
1954 Why the euler-scheme in particle-tracking is not enough: the shallow sea
1955 test case. *Ocean Dynamics*, 62(4):501–514.
- 1956 Griesel, A., Eden, C., Koopmann, N., and Yulaeva, E. (2015). Comparing
1957 isopycnal eddy diffusivities in the southern ocean with predictions from
1958 linear theory. *Ocean Modelling*, 94:33–45.
- 1959 Griesel, A., McClean, J., Gille, S., Sprintall, J., and Eden, C. (2014). Eulerian
1960 and lagrangian isopycnal eddy diffusivities in the southern ocean of an
1961 eddying model. *J. Phys. Oceanogr*, 44:644–661.
- 1962 Griffa, A. (1996). Applications of stochastic particle models to oceanographic
1963 problems. In *Stochastic modelling in physical oceanography*, pages 113–140.
1964 Springer.
- 1965 Griffies, S. M. (1998). The Gent-McWilliams skew-flux. *Journal of Physical
1966 Oceanography*, 28:831–841.
- 1967 Griffies, S. M., Böning, C. W., Bryan, F. O., Chassignet, E. P., Gerdes,
1968 R., Hasumi, H., Hirst, A. C., Treguier, A.-M., and Webb, D. J. (2000).
1969 Developments in ocean climate modelling. *Ocean Modelling*, 2:123–192.
- 1970 Griffies, S. M., Danabasoglu, G., Durack, P. J., Adcroft, A. J., Balaji, V.,
1971 Böning, C. W., Chassignet, E. P., Curchitser, E., Deshayes, J., Drange,
1972 H., Fox-Kemper, B., Gleckler, P., Gregory, J., Haak, H., Hallberg, R.,
1973 Heimbach, P., Hewitt, H., Holland, D., Ilyina, T., Jungclaus, J., Komuro,
1974 Y., Krasting, J., Large, W., Marsland, S., Masina, S., McDougall, T.,
1975 Nurser, A. G., Orr, J., Pirani, A., Qiao, F., Stouffer, R., Taylor, K.,

- 1976 Treguier, A. M., Tsujino, H., Uotila, P., Valdivieso, M., Wang, Q., Winton,
1977 M., and Yeager, S. (2016). Omip contribution to cmip6: experimental
1978 and diagnostic protocol for the physical component of the ocean model
1979 intercomparison project. *Geoscientific Model Development*, 9:3231–3296.
- 1980 Hadjighasem, A., Farazmand, M., Blazevski, D., Froyland, G., and Haller, G.
1981 (2017). A critical comparison of lagrangian methods for coherent structure
1982 detection. *Chaos: An Interdisciplinary Journal of Nonlinear Science*,
1983 27(5):053104.
- 1984 Haertel, P. T. and Fedorov, A. (2012). The Ventilated Ocean. *Journal of
1985 Physical Oceanography*, 42(1):141–164.
- 1986 Haertel, P. T. and Randall, D. A. (2002). Could a pile of slippery sacks
1987 behave like an ocean? *Monthly Weather Review*, 130(12):2975–2988.
- 1988 Haidvogel, D., Arango, H., Budgell, W., Cornuelle, B., Curchitser, E., Lorenzo,
1989 E. D., Fennel, K., Geyer, W., Hermann, A., Lanerolle, L., Levin, J.,
1990 McWilliams, J., Miller, A., Moore, A., Powell, T., Shchepetkin, A., Sher-
1991 wood, C., Signell, R., Warner, J., and Wilkin, J. (2008). Ocean forecast-
1992 ing in terrain-following coordinates: Formulation and skill assessment of
1993 the regional ocean modeling system. *Journal of Computational Physics*,
1994 227(7):3595 – 3624. Predicting weather, climate and extreme events.
- 1995 Haine, T. W. and Hall, T. M. (2002). A generalized transport theory: Water-
1996 mass composition and age. *Journal of physical oceanography*, 32(6):1932–
1997 1946.
- 1998 Haines, M. A., Fine, R. A., Luther, M. E., and Ji, Z. (1999). Particle
1999 trajectories in an Indian Ocean model and sensitivity to seasonal forcing.
2000 *Journal of Physical Oceanography*, 29(4):584–598.
- 2001 Hairer, E., Lubich, C., and Wanner, G. (2006). *Geometric numerical inte-
2002 gration: structure-preserving algorithms for ordinary differential equations*,
2003 volume 31. Springer Science & Business Media.
- 2004 Haller, G. (2015). Lagrangian Coherent Structures. *Annual Review of Fluid
2005 Mechanics*, 47(1):137–162.
- 2006 Haller, G. (2016). Dynamic rotation and stretch tensors from a dynamic polar
2007 decomposition. *Journal of the Mechanics and Physics of Solids*, 86:70–93.

- 2008 Haller, G. and Beron-Vera, F. J. (2012). Geodesic theory of transport barriers
2009 in two-dimensional flows. *Physica D: Nonlinear Phenomena*, 241(20):1680–
2010 1702.
- 2011 Haller, G. and Beron-Vera, F. J. (2013). Coherent Lagrangian vortices: the
2012 black holes of turbulence. *Journal of Fluid Mechanics*, 731:69–10.
- 2013 Haller, G., Hadjighasem, A., Farazmand, M., and Huhn, F. (2016). Defining
2014 coherent vortices objectively from the vorticity. *Journal of Fluid Mechanics*,
2015 795:136–173.
- 2016 Haller, G. and Sapsis, T. (2011). Lagrangian coherent structures and the
2017 smallest finite-time lyapunov exponent. *Chaos: An Interdisciplinary Journal
2018 of Nonlinear Science*, 21(2):023115.
- 2019 Haller, G. and Yuan, G. (2000). Lagrangian coherent structures and mixing
2020 in two-dimensional turbulence. *Physica D*, 147(3-4):352 – 370.
- 2021 Halliwell, G. and Garraffo, Z. D. (2002). Synthetic Floats, Drifters, and
2022 Moorings in HYCOM. Technical report, HYCOM Consortium.
- 2023 Haza, A., Özgökmen, T., and Hogan, P. (2016). Impact of submesoscales on
2024 surface material distribution in a gulf of mexico mesoscale eddy. *Ocean
2025 Modelling*, 107:28 – 47.
- 2026 Haza, A. C., Özgökmen, T. M., Griffa, A., Molcard, A., Poulain, P.-M.,
2027 and Peggion, G. (2010). Transport properties in small-scale coastal flows:
2028 relative dispersion from VHF radar measurements in the Gulf of La Spezia.
2029 *Ocean Dyn.*, 60(4):861–882.
- 2030 Heemink, A. W. (1990). Stochastic Modeling of Dispersion in Shallow-Water.
2031 *Stochastic Hydrology and Hydraulics*, 4(2):161–174.
- 2032 Hegerl, G. C., Black, E., Allan, R. P., Ingram, W. J., Polson, D., Trenberth,
2033 K. E., Chadwick, R. S., Arkin, P. A., Sarojini, B. B., Becker, A., Dai, A.,
2034 Durack, P. J., Easterling, D., Fowler, H. J., Kendon, E. J., Huffman, G. J.,
2035 Liu, C., Marsh, R., New, M., Osborn, T. J., Skliris, N., Stott, P. A., Vidale,
2036 P.-L., Wijffels, S. E., Wilcox, L. J., Willett, K. M., and Zhang, X. (2015).
2037 Challenges in Quantifying Changes in the Global Water Cycle. *Bulletin of
2038 the American Meteorological Society*, 96(7):1097–1115.

- 2039 Held, I. M. and Soden, B. J. (2006). Robust responses of the hydrological
2040 cycle to global warming. *Journal of Climate*, 19(21):5686–5699.
- 2041 Hellweger, F. L., van Sebille, E., and Fredrick, N. D. (2014). Biogeographic
2042 patterns in ocean microbes emerge in a neutral agent-based model. *Science*,
2043 345:1346–1349.
- 2044 Helm, K. P., Bindoff, N. L., and Church, J. A. (2010). Changes in the
2045 global hydrological-cycle inferred from ocean salinity. *Geophysical Research
Letters*, 37.
- 2047 Hofmann, A. F., Soetaert, K., and Middelburg, J. J. (2008). Present nitrogen
2048 and carbon dynamics in the Scheldt estuary using a novel 1-D model.
2049 *Biogeosciences*, 5(4):981–1006.
- 2050 Holstein, D. M., Paris, C. B., and Mumby, P. M. (2014). Consistency and
2051 inconsistency in multispecies population network dynamics of coral reef
2052 ecosystems. *Marine Ecology Progress Series*, 499:1–18.
- 2053 Holzer, M. and Hall, T. M. (2000). Transit-Time and Tracer-Age Distributions
2054 in Geophysical Flows. *Journal of the Atmospheric Sciences*, 57(21):3539–
2055 3558.
- 2056 Hosoda, S., Suga, T., Shikama, N., and Mizuno, K. (2009). Global Surface
2057 Layer Salinity Change Detected by Argo and Its Implication for Hydrological
2058 Cycle Intensification. *Journal of Oceanography*, 65(4):579–586.
- 2059 Hunter, J., Craig, P., and Phillips, H. (1993). On the use of random walk
2060 models with spatially variable diffusivity. *Journal of Computational Physics*,
2061 106(2):366–376.
- 2062 Ilicak, M., Adcroft, A. J., Griffies, S. M., and Hallberg, R. W. (2012). Spurious
2063 dianeutral mixing and the role of momentum closure. *Ocean Modelling*,
2064 45:37–58.
- 2065 Imasato, N., Awaji, T., and Kunishi, H. (1980). Tidal exchange through
2066 naruto, akashi and kitani straits. *Journal of the Oceanographical Society of
2067 Japan*, 36(3):151–162.
- 2068 Imasato, N. and Qiu, B. (1987). An event in water exchange between
2069 continental shelf and the kuroshio off southern japan: Lagrangian tracking of

- 2070 a low-salinity water mass on the kuroshio. *Journal of physical oceanography*,
2071 17(7):953–968.
- 2072 Iudicone, D., Rodgers, K., Stendardo, I., Aumont, O., Madec, G., Bopp, L.,
2073 Mangoin, O., and d'Alcala, M. R. (2011). Water masses as a unifying frame-
2074 work for understanding the Southern Ocean Carbon Cycle. *Biogeosciences*,
2075 8:1031–1052.
- 2076 Jazwinski, A. H. (1970). *Stochastic Processes and Filtering Theory*. Academic
2077 Press, New York.
- 2078 Jones, B. T., Solow, A., and Ji, R. (2016). Resource allocation for lagrangian
2079 tracking. *Journal of Atmospheric and Oceanic Technology*, 33(6):1225–1235.
- 2080 Jönsson, B. F., Lundberg, P. a., and Döös, K. (2004). Baltic sub-basin
2081 turnover times examined using the Rossby Centre Ocean model. *Ambio*,
2082 33(4-5):257–60.
- 2083 Jönsson, B. F., Salisbury, J. E., and Mahadevan, A. (2011). Large variability
2084 in continental shelf production of phytoplankton carbon revealed by satellite.
2085 *Biogeosciences*, 8(5):1213–1223.
- 2086 Jonsson, B. F. and Watson, J. R. (2016). The timescales of global surface-
2087 ocean connectivity. *Nature Communications*, 7:1–6.
- 2088 Jutzeler, M., Marsh, R., Carey, R. J., White, J. D. L., Talling, P. J., and
2089 Karlstrom, L. (2014). On the fate of pumice rafts formed during the 2012
2090 Havre submarine eruption. *Nature Communications*, 5:3660.
- 2091 Kamenkovich, I., Rypina, I. I., and Berloff, P. (2015). Properties and origins
2092 of the anisotropic eddy-induced transport in the north atlantic. *Journal of
2093 Physical Oceanography*, 45(3):778–791.
- 2094 Karrasch, D. and Haller, G. (2013). Do finite-size lyapunov exponents detect
2095 coherent structures? *Chaos: An Interdisciplinary Journal of Nonlinear
2096 Science*, 23(4):043126.
- 2097 Khatiwala, S., Visbeck, M., and Schlosser, P. (2001). Age tracers in an
2098 ocean GCM. *Deep-Sea Research Part I: Oceanographic Research Papers*,
2099 48(6):1423–1441.

- 2100 Kinlan, B. and Gaines, S. (2003). Propagule dispersal in marine and terrestrial
2101 environments: a community perspective. *Ecology*, 84(8):2007–2020.
- 2102 Kjellsson, J. and Döös, K. (2012a). Lagrangian decomposition of the hadley
2103 and ferrel cells. *Geophys. Res. Lett.*, 39:L15807.
- 2104 Kjellsson, J. and Döös, K. (2012b). Surface drifters and model trajectories in
2105 the baltic sea. *Boreal Environment Research*, 17:447–459.
- 2106 Kjellsson, J., Doos, K., Laliberte, F. B., and Zika, J. D. (2014). The Atmo-
2107 spheric General Circulation in Thermodynamical Coordinates. *Journal of*
2108 *the Atmospheric Sciences*, 71(3):916–928.
- 2109 Klocker, A. and Abernathey, R. (2014). Global patterns of mesoscale eddy
2110 properties and diffusivities. *J. Phys. Oceanogr.*, 44:1030–1047.
- 2111 Klocker, A., Ferrari, R., and LaCasce, J. H. (2012a). Estimating suppression
2112 of eddy mixing by mean flow. *J. Phys. Oceanogr.*, 9:1566–1576.
- 2113 Klocker, A., Ferrari, R., LaCasce, J. H., and Merrifield, S. T. (2012b). Recon-
2114 ciling float-based and tracer-based estimates of lateral diffusivities. *Journal*
2115 *of Marine Research*, 70(4):569–602.
- 2116 Kloeden, P. E. and Platen, E. (1992). *Numerical solutions of Stochastic*
2117 *Differential equations. Application of Mathematics, Stochastic Modelling*
2118 *and applied probability*. Springer-Verlag, Berlin Heidelberg.
- 2119 Koch-Larrouy, A., Morrow, R., Penduff, T., and Juza, M. (2010). Origin and
2120 mechanism of Subantarctic Mode Water formation and transformation in
2121 the Southern Indian Ocean. *Ocean Dynamics*, 60(3):563–583.
- 2122 Kool, J. T., Moilanen, A., and Treml, E. A. (2013). Population connectivity:
2123 recent advances and new perspectives. *Landscape Ecology*, 28(2):165–185.
- 2124 Koszalka, I. and LaCasce, J. H. (2010). Lagrangian analysis by clustering.
2125 *Ocean Dynamics*, 60(4):957–972.
- 2126 Koszalka, I., LaCasce, J. H., Andersson, M., Orvik, K. A., and Mauritzen, C.
2127 (2011). Surface circulation in the Nordic Seas from clustered drifters. *Deep*
2128 *Sea Res. I*, 58(4):468–485.

- 2129 Koszalka, I., LaCasce, J. H., and Mauritzen, C. (2013a). In pursuit of
2130 anomalies - analyzing the poleward transport of Atlantic Water with
2131 surface drifters. *Deep Sea Res. II*, 85:96–108.
- 2132 Koszalka, I., LaCasce, J. H., and Orvik, K. A. (2009). Relative dispersion in
2133 the Nordic Seas. *J. Mar. Res.*, 67:411–433.
- 2134 Koszalka, I. M., Haine, T. W. N., and Magaldi, M. G. (2013b). Fates and
2135 travel times of Denmark Strait Overflow Water in the Irminger Basin. *J.
2136 Phys. Oceanogr.*, 43(12):2611–2628.
- 2137 Koszalka, I. M., Haine, T. W. N., and Magaldi, M. G. (2013c). Fates and
2138 Travel Times of Denmark Strait Overflow Water in the Irminger Basin.
2139 *Journal of Physical Oceanography*, 43(12):2611–2628.
- 2140 Kruggel-Emden, H., Sturm, M., Wirtz, S., and Scherer, V. (2008). Selection
2141 of an appropriate time integration scheme for the discrete element method
2142 (DEM). *Comput. Chem. Eng.*, 32(10):2263–2279.
- 2143 Kundu, P. K., Cohen, I. M., and Dowling, D. R. (2012). Chapter 3 - kinematics.
2144 In *Fluid Mechanics*, pages 65 – 93. Academic Press, Boston, fifth edition.
- 2145 LaCasce, J. (2008). Statistics from lagrangian observations. *Progress in
2146 Oceanography*, 77(1):1–29.
- 2147 LaCasce, J. H. (2005). Eulerian and Lagrangian velocity distributions in the
2148 North Atlantic. *Journal of Physical Oceanography*, 35(12):2327–2336.
- 2149 LaCasce, J. H., Ferrari, R., Marshall, J., Tulloch, R., Balwada, D., and Speer,
2150 K. (2014). Float-Derived Isopycnal Diffusivities in the DIMES Experiment.
2151 *Journal of Physical Oceanography*, 44(2):764–780.
- 2152 Laliberte, F., Zika, J. D., Mudryk, L., Kushner, P. J., Kjellsson, J., and Döös,
2153 K. (2015). Constrained work output of the moist atmospheric heat engine
2154 in a warming climate. *Science*, 347(6221):540–543.
- 2155 Lampert, W. (1989). The adaptive significance of diel vertical migration of
2156 zooplankton. *Functional Ecology*, 3(1):21–27.
- 2157 Lange, M. and van Sebille, E. (2017). Parcels v0.9: prototyping a lagrangian
2158 ocean analysis tool for the petascale age. *Geoscientific Model Development
2159 Discussions*, in review.

- 2160 Lapeyre, G. (2002). Characterization of finite-time lyapunov exponents and
2161 vectors in two-dimensional turbulence. *Chaos: An Interdisciplinary Journal*
2162 of Nonlinear Science, 12(3):688–698.
- 2163 Lebedev, K. V., Yoshinari, H., Maximenko, N. A., and Hacker, P. (2007).
2164 YoMaHa'05: Velocity data derived from trajectories of Argo floats at
2165 parking level and at the sea surface. Technical report, IPRC Technical
2166 Note.
- 2167 Lebreton, L. C. M., Greer, S. D., and Borerro, J. C. (2012). Numerical
2168 modelling of floating debris in the world's oceans. *Marine Pollution Bulletin*,
2169 64:653–661.
- 2170 Ledwell, J. R., St. Laurent, L. C., Girton, J. B., and Toole, J. M. (2011).
2171 Diapycnal Mixing in the Antarctic Circumpolar Current. *Journal of Physical*
2172 *Oceanography*, 41(1):241–246.
- 2173 Lehahn, Y., d'Ovidio, F., Levy, M., and Heifetz, E. (2007). Stirring of
2174 the northeast Atlantic spring bloom: A Lagrangian analysis based on
2175 multisatellite data. *J. Geophys. Res.*, 112(C8):C08005.
- 2176 Leimkuhler, B. and Reich, S. (2004). *Simulating Hamiltonian dynamics*,
2177 volume 14. Cambridge University Press.
- 2178 Lett, C., Verley, P., and Mullon C, e. (2008). A lagrangian tool for modelling
2179 ichthyoplankton dynamics. *Environ. Model Softw.*, 23:1210–1214.
- 2180 Lique, C., Treguier, A. M., Blanke, B., and Grima, N. (2010). On the origins
2181 of water masses exported along both sides of Greenland: A Lagrangian
2182 model analysis. *Journal of Geophysical Research*, 115(C5):C05019.
- 2183 Liu, G. and Chua, V. P. (2016). A SUNTANS-based unstructured grid local
2184 exact particle tracking model. *Ocean Dynamics*, pages 1–11.
- 2185 Lumpkin, R. and Eliot, S. (2010). Surface drifter pair spreading in the North
2186 Atlantic. *J. Geophys. Res.*, 115.
- 2187 Lumpkin, R. and Johnson, G. C. (2013). Global ocean surface velocities from
2188 drifters: Mean, variance, enso response, and sea- sonal cycle. *J. Geophys.*
2189 *Res. Oceans*, 118:2992–3006.

- 2190 Lumpkin, R. and Pazos, M. (2007). Measuring surface currents with surface
2191 velocity program drifters: the instrument, its data, and some recent results.
2192 In Griffa, A., Kirwan, Jr, A. D., Mariano, A. J., and Rossby, H. T.,
2193 editors, *Lagrangian Analysis and Prediction of Coastal and Ocean Dynamics*.
2194 Cambridge University Press.
- 2195 Lynch, D. R., Greenberg, D. A., Bilgili, A., McGillicuddy Jr, D. J., Manning,
2196 J. P., and Aretxabaleta, A. L. (2014). Individual-based models – biotic
2197 particles. In *Particles in the Coastal Ocean Theory and Applications*.
2198 Cambridge University Press.
- 2199 Madec, G. (2008). Nemo ocean engine. Technical report, Note du Pole de
2200 modlisation de l'Institut Pierre-Simon No 27, ISSN no.
- 2201 Madec, G. and NEMO team (2016). NEMO Ocean Engine. Technical report,
2202 Institut Pierre-Simon Laplace (IPSL).
- 2203 Marsden, J. E., Pekarsky, S., and Shkoller, S. (1999). Stability of relative
2204 equilibria of point vortices on a sphere and symplectic integrators. *Nuovo
2205 cimento della Società italiana di fisica. C*, 22(6):793–802.
- 2206 Marsh, R., Ivchenko, V. O., Skliris, N., Alderson, S., Bigg, G. R., Madec,
2207 G., Blaker, A. T., Aksenov, Y., Sinha, B., Coward, A. C., Le Sommer, J.,
2208 Merino, N., and Zalesny, V. B. (2015). NEMO-ICB (v1.0): interactive
2209 icebergs in the NEMO ocean model globally configured at eddy-permitting
2210 resolution. *Geoscientific Model Development*, 8(5):1547–1562.
- 2211 Marshall, J., Adcroft, A., Hill, C., Perelman, L., and Heisey, C. (1997a).
2212 A finite-volume, incompressible Navier Stokes model for studies of the
2213 ocean on parallel computers. *Journal of Geophysical Research-Oceans*,
2214 102(C3):5753–5766.
- 2215 Marshall, J., Adcroft, A., Hill, C., Perelman, L., and Heisey, C. (1997b). A
2216 finite-volume, incompressible navier stokes model for studies of the ocean
2217 on parallel computers. *J. Geophys. Res.*, 102:5753–5766.
- 2218 Marshall, J., Hill, C., Perelman, L., and Adcroft, A. (1997c). Hydrostatic,
2219 quasi-hydrostatic, and non-hydrostatic ocean modeling. *J. Geophys. Res.*,
2220 102:5733–5752.

- 2221 Martin, P., Loeff, M. R., Cassar, N., Vandromme, P., d’Ovidio, F., Stemmann,
2222 L., Rengarajan, R., Soares, M., González, H. E., Ebersbach, F., et al. (2013).
2223 Iron fertilization enhanced net community production but not downward
2224 particle flux during the southern ocean iron fertilization experiment lohafex.
2225 *Global Biogeochemical Cycles*, 27(3):871–881.
- 2226 Martin, T. and Adcroft, A. (2010). Parameterizing the fresh-water flux from
2227 land ice to ocean with interactive icebergs in a coupled climate model.
2228 *Ocean Modelling*, 34(3-4):111–124.
- 2229 Mazloff, M. R., Heimbach, P., and Wunsch, C. (2010). An Eddy-permitting
2230 southern ocean state estimate. *Journal of Physical Oceanography*, 40(5):880–
2231 899.
- 2232 McDougall, T. J. (2003). Potential enthalpy: a conservative oceanic vari-
2233 able for evaluating heat content and heat fluxes. *Journal of Physical*
2234 *Oceanography*, 33:945–963.
- 2235 McLachlan, R. I. (1999). Area preservation in computational fluid dynamics.
2236 *Physics Letters A*, 264(1):36–44.
- 2237 McManus, M. A. and Woodson, C. B. (2012). Plankton distribution and
2238 ocean dispersal. *The Journal of Experimental Biology*, 215(6):1008–1016.
- 2239 Mesinger, F. and Arakawa, A. (1976). *Numerical methods used in atmospheric*
2240 *models*. GARP Publications. World Meteorological Organization.
- 2241 Mezić, I., Loire, S., Fonoferov, V. A., and Hogan, P. (2010). A New Mixing
2242 Diagnostic and Gulf Oil Spill Movement. *Science*, 330(6003):486–489.
- 2243 Middleton, J. F. and Loder, J. W. (1989). Skew fluxes in polarized wave
2244 fields. *Journal of Physical Oceanography*, 19:68–76.
- 2245 Monaghan, J. J. (1992). Smoothed particle hydrodynamics. *Annu. Rev.*
2246 *Astron. Astrophys.*, 30:543–574.
- 2247 Mouchet, A., Cornaton, F., Deleersnijder, E., and Delhez, E. (2016). Partial
2248 ages: diagnosing transport processes by means of multiple clocks. *Ocean*
2249 *Dynamics*, 66:367–386.

- 2250 Narvaez, D. A., Klinck, J. M., Powell, E. N., Hofmann, E. E., Wilkin, J., and
2251 Haidvogel, D. B. (2012a). Circulation and behavior controls on dispersal of
2252 eastern oyster (*Crassostrea virginica*) larvae in Delaware Bay. *Journal of*
2253 *Marine Research*, 70(2-3):411–440.
- 2254 Narvaez, D. A., Klinck, J. M., Powell, E. N., Hofmann, E. E., Wilkin, J., and
2255 Haidvogel, D. B. (2012b). Modeling the dispersal of eastern oyster
2256 (*Crassostrea virginica*) larvae in Delaware Bay. *Journal of Marine Research*,
2257 70(2-3):381–409.
- 2258 Nencioli, F., d’Ovidio, F., Doglioli, A. M., and Petrenko, A. A. (2011). Surface
2259 coastal circulation patterns by in-situ detection of Lagrangian coherent
2260 structures. *Geophys. Res. Lett.*, 38(17):L17604.
- 2261 Nencioli, F., d’Ovidio, F., Doglioli, A. M., and Petrenko, A. A. (2013). In
2262 situ estimates of submesoscale horizontal eddy diffusivity across an ocean
2263 front. *Journal of Geophysical Research: Oceans*, 118(12):7066–7080.
- 2264 Nilsson, J. A. U., Döös, K., Ruti, P. M., Artale, V., Coward, A. C., and
2265 Brodeau, L. (2013). Observed and modeled global ocean turbulence regimes
2266 as deduced from surface trajectory data. *Journal of Physical Oceanography*,
2267 43:2249–2269.
- 2268 Olascoaga, M. J., Rypina, I. I., Brown, M. G., Beron Vera, F. J., Kocak, H.,
2269 Brand, L. E., Halliwell, G. R., and Shay, L. K. (2006). Persistent transport
2270 barrier on the West Florida Shelf. *Geophys. Res. Lett.*, 33(22).
- 2271 Ollitrault, M. and Rannou, J.-P. (2013). ANDRO: An Argo-Based Deep
2272 Displacement Dataset. *Journal of Atmospheric and Oceanic Technology*,
2273 30(4):759–788.
- 2274 Paris, C. B., Atema, J., Irisson, J.-O., Kingsford, M., Gerlach, G., and
2275 Guigand, C. M. (2013a). Reef Odor: A Wake Up Call for Navigation in
2276 Reef Fish Larvae. *PLOS One*, 8(8):e72808–8.
- 2277 Paris, C. B., Cowen, R. K., Claro, R., and Lindeman, K. C. (2005). Larval
2278 transport pathways from Cuban snapper (Lutjanidae) spawning aggregations
2279 based on biophysical modeling. *Marine Ecology-Progress Series*,
2280 296:93–106.

- 2281 Paris, C. B., Helgers, J., van Sebille, E., and Srinivasan, A. (2013b). Connec-
2282 tivity Modeling System: A probabilistic modeling tool for the multi-scale
2283 tracking of biotic and abiotic variability in the ocean. *Environmental*
2284 *Modelling & Software*, 42:47–54.
- 2285 Paris, C. B., Le Hénaff, M., Aman, Z. M., Subramaniam, A., Helgers, J.,
2286 Wang, D.-P., Kourafalou, V. H., and Srinivasan, A. (2012). Evolution of
2287 the Macondo Well Blowout: Simulating the Effects of the Circulation and
2288 Synthetic Dispersants on the Subsea Oil Transport. *Environmental Science*
2289 *& Technology*, page 121203084426001.
- 2290 Pavia, E. G. and Cushman-Roisin, B. (1988). Modeling of oceanic fronts using
2291 a particle method. *Journal of Geophysical Research: Oceans*, 93:3554–3562.
- 2292 Peacock, T. and Dabiri, J. (2010). Introduction to focus issue: Lagrangian
2293 coherent structures. *Chaos: An Interdisciplinary Journal of Nonlinear*
2294 *Science*, 20(1):017501.
- 2295 Peacock, T. and Haller, G. (2013). Lagrangian coherent structures: The
2296 hidden skeleton of fluid flows. *Physics today*, 66(2):41.
- 2297 Perot, B. (2000). Conservation properties of unstructured staggered mesh
2298 schemes. *Journal of Computational Physics*, 159(1):58–89.
- 2299 Phelps, J. J., Polton, J. A., Souza, A. J., and Robinson, L. A. (2013).
2300 Hydrodynamic timescales in a hyper-tidal region of freshwater influence.
2301 *Continental Shelf Research*, 63:13–22.
- 2302 Phelps, J. J. C., Polton, J. A., Souza, A. J., and Robinson, L. A. (2015).
2303 Behaviour influences larval dispersal in shelf sea gyres: Nephrops norvegicus
2304 in the Irish Sea. *Marine Ecology Progress Series*, 518:177–191.
- 2305 Piñones, A., Hofmann, E. E., Dinniman, M. S., and Klinck, J. M. (2011).
2306 Lagrangian simulation of transport pathways and residence times along the
2307 western Antarctic Peninsula. *Deep Sea Research Part II: Topical Studies*
2308 *in Oceanography*, 58(1316):1524–1539.
- 2309 Pierrehumbert, R. and Yang, H. (1993). Global chaotic mixing on isentropic
2310 surfaces. *Journal of the atmospheric sciences*, 50(15):2462–2480.

- 2311 Poje, A. C., Haza, A. C., Özgökmen, T. M., Magaldi, M. G., and Garraffo,
2312 Z. D. (2010). Resolution dependent relative dispersion statistics in a
2313 hierarchy of ocean models. *Ocean Modelling*, 31(1-2):36–50.
- 2314 Poje, A. C., Özgökmen, T. M., Lipphardt, B. L., Haus, B. K., Ryan, E. H.,
2315 Haza, A. C., Jacobs, G. A., Reniers, A. J. H. M., Olascoaga, M. J., Novelli,
2316 G., Griffa, A., Beron Vera, F. J., Chen, S. S., Coelho, E., Hogan, P. J.,
2317 Kirwan, A. D., Huntley, H. S., and Mariano, A. J. (2014). Submesoscale
2318 dispersion in the vicinity of the Deepwater Horizon spill. *Proceedings of
the National Academy of Sciences*, 111(35):12693–12698.
- 2319
- 2320 Pujolar, J. M., Schiavina, M., Di Franco, A., Melià, P., Guidetti, P., Gatto,
2321 M., De Leo, G. A., and Zane, L. (2013). Understanding the effectiveness of
2322 marine protected areas using genetic connectivity patterns and Lagrangian
2323 simulations. *Diversity and Distributions*, 19(12):1531–1542.
- 2324 Qin, X., van Sebille, E., and Gupta, A. S. (2014). Quantification of errors
2325 induced by temporal resolution on lagrangian particles in an eddy-resolving
2326 model. *Ocean Modelling*, 76:20–30.
- 2327 Redi, M. H. (1982). Oceanic isopycnal mixing by coordinate rotation. *Journal
of physical Oceanography*, 12(10):1154–1158.
- 2328
- 2329 Reverdin, G., Morisset, S., Marié, L., Bourras, D., Sutherland, G., Ward,
2330 B., Salvador, J., Font, J., Cuypers, Y., Centurioni, L., Hormann, V.,
2331 Koldziejczyk, N., Boutin, J., D’Ovidio, F., Nencioli, F., Martin, N., Diverres,
2332 D., Alory, G., and Lumpkin, R. (2015). Surface salinity in the North
2333 Atlantic subtropical gyre during the STRASSE/SPURS summer 2012
2334 cruise. *Oceanography*, 28:114–123.
- 2335 Ringler, T., Petersen, M., Higdon, R. L., Jacobsen, D., Jones, P. W., and
2336 Maltrud, M. (2013). A multi-resolution approach to global ocean modeling.
2337 *Ocean Modelling*, 69:211–232.
- 2338 Ringler, T. D., Saenz, J. A., Wolfram, P. J., and van Roekel, L. (2016).
2339 A thickness-weighted average perspective of force balance in an idealized
2340 circumpolar current. *Journal of Physical Oceanography*.
- 2341 Roche, D. M. (2013). $\delta^{18}\text{O}$ water isotope in the iloveclim model (version 1.0)
2342 part 1: Implementation and verification. *Geoscientific Model Development*,
2343 6(5):1481–1491.

- 2344 Ross, O. N. and Sharples, J. (2004). Recipe for 1-D Lagrangian particle
2345 tracking models in space-varying diffusivity. *Limnol. Oceanogr.: Methods*,
2346 pages 289–302.
- 2347 Rossi, V., van Sebille, E., Sen Gupta, A., Garçon, V., and England, M. H.
2348 (2013). Deep-Sea Research I. *Deep-Sea Research Part I-Oceanographic*
2349 *Research Papers*, 80(C):37–46.
- 2350 Rühs, S., Durgadoo, J. V., Behrens, E., and Biastoch, A. (2013). Advective
2351 timescales and pathways of Agulhas leakage. *Geophysical Research Letters*,
2352 40(15):3997–4000.
- 2353 Rypina, I., Kamenkovich, I., Berloff, P., and Pratt, L. (2012). Eddy-induced
2354 particle dispersion in the upper-ocean north atlantic. *Journal of Physical*
2355 *Oceanography*, 42:2206–2228.
- 2356 Rypina, I., Scott, S., Pratt, L., and Brown, M. (2011). Investigating the
2357 connection between complexity of isolated trajectories and lagrangian
2358 coherent structures. *Nonlinear Processes in Geophysics*, 18(6):977–987.
- 2359 Salama, N. K. G. and Rabe, B. (2013). Developing models for investigating
2360 the environmental transmission of disease-causing agents within open-cage
2361 salmon aquaculture. *Aquaculture Environment Interactions*, 4(2):91–115.
- 2362 Salmon, R. (1998). *Lectures on Geophysical Fluid Dynamics*. Oxford University
2363 Press, Oxford, England. 378 + xiii pp.
- 2364 Sammarco, P. W., Brazeau, D. A., and Sinclair, J. (2012). Genetic connectivity
2365 in scleractinian corals across the northern gulf of mexico: Oil/gas platforms,
2366 and relationship to the flower garden banks. *PLoS ONE*, 7(4):e30144.
- 2367 Schroeder, K., Haza, A. C., Griffa, A., Özgökmen, T. M., Poulain, P. M.,
2368 Gerin, R., Peggion, G., and Rixen, M. (2011). Relative dispersion in the
2369 Liguro-Provencal basin: From sub-mesoscale to mesoscale. *Deep Sea Res.*
2370 *I*, 58(3):209–228.
- 2371 Scott, R., Biastoch, A., Roder, C., Stiebens, V. A., and Eizaguirre, C. (2014).
2372 Nano-tags for neonates and ocean-mediated swimming behaviours linked
2373 to rapid dispersal of hatchling sea turtles. *Proceedings of the Royal Society*
2374 *B: Biological Sciences*, 281(1796):20141209–20141209.

- 2375 Shah, S., Primeau, F., Deleersnijder, E., and Heemink, A. (2017). Tracing
2376 the ventilation pathways of the deep North Pacific Ocean using Lagrangian
2377 particles and Eulerian tracers. *Journal of Physical Oceanography*, 47:1261–
2378 1280.
- 2379 Shah, S. H. A. M., Heemink, A. W., and Deleersnijder, E. (2011). Assessing
2380 lagrangian schemes for simulating diffusion on non-flat isopycnal surfaces.
2381 *Ocean Modelling*, 39(3–4):351–361.
- 2382 Shah, S. H. A. M., Heemink, A. W., Gräwe, U., and Deleersnijder, E. (2013).
2383 Adaptive time stepping algorithm for lagrangian transport models: Theory
2384 and idealised test cases. *Ocean Modelling*, 68:9–21.
- 2385 Shchepetkin, A. F. and McWilliams, J. C. (2005). The regional oceanic mod-
2386 eling system (ROMS): a split-explicit, free-surface, topography-following-
2387 coordinate oceanic model. *Ocean Modelling*, 9(4):347–404.
- 2388 Shevchenko, I. V. and Berloff, P. S. (2015). Multi-layer quasi-geostrophic
2389 ocean dynamics in Eddy-resolving regimes. *Ocean Modelling*, 94(C):1–14.
- 2390 Simons, R. D., Siegel, D. A., and Brown, K. S. (2013). Model sensitivity
2391 and robustness in the estimation of larval transport: a study of particle
2392 tracking parameters. *Journal of Marine Systems*, 119.
- 2393 Skliris, N., Marsh, R., Josey, S. A., Good, S. A., Liu, C., and Allan, R. P.
2394 (2014). Salinity changes in the World Ocean since 1950 in relation to
2395 changing surface freshwater fluxes. *Climate Dynamics*, 43(3–4):709–736.
- 2396 Skliris, N., Zika, J., Nurser, A., Josey, S. A., and Marsh, R. (2016). Global
2397 water cycle amplifying at less than the Clausius-Clapeyron rate. *Scientific
2398 Reports*, in press.
- 2399 Smetacek, V., Klaas, C., Strass, V. H., Assmy, P., Montresor, M., Cisewski,
2400 B., Savoye, N., Webb, A., d’Ovidio, F., Arrieta, J. M., Bathmann, U.,
2401 Bellerby, R., Berg, G. M., Croot, P., Gonzalez, S., Henjes, J., Herndl,
2402 G. J., Hoffmann, L. J., Leach, H., Losch, M., Mills, M. M., Neill, C.,
2403 Peeken, I., Rottgers, R., Sachs, O., Sauter, E., Schmidt, M. M., Schwarz, J.,
2404 Terbruggen, A., and Wolf Gladrow, D. (2012). Deep carbon export from a
2405 Southern Ocean iron-fertilized diatom bloom. *Nature*, 487(7407):313–319.

- 2406 Spagnol, S., Wolanski, E., Deleersnijder, E., Brinkman, R., McAllister, F.,
2407 Cushman-Roisin, B., and Hanert, E. (2002). An error frequently made
2408 in the evaluation of advective transport in two-dimensional Lagrangian
2409 models of advection-diffusion in coral reef waters. *Marine Ecology Progress Series*,
2410 235:299–302.
- 2411 Speich, S. (1992). *Etude du forçage de la circulation océanique par les détroits: cas de la Mer d'Alboran*. PhD thesis, Université de Paris 06.
- 2412 Speich, S., Blanke, B., de Vries, P., Drijfhout, S. S., Döös, K., Ganachaud, A.,
2413 and Marsh, R. (2002). Tasman leakage: A new route in the global ocean
2414 conveyor belt. *Geophysical Research Letters*, 29(10):1416.
- 2415 Speich, S., Blanke, B., and Madec, G. (2001). Warm and cold water routes of
2416 an OGCM thermohaline conveyor belt. *Geophys. Res. Lett.*, 28(2):311–314.
- 2417 Spivakovskaya, D., Heemink, A. W., and Deleersnijder, E. (2007a). The
2418 backward Ito method for the lagrangian simulation of transport processes
2419 with large space variations of the diffusivity. *Ocean Sciences*, 3:525–535.
- 2420 Spivakovskaya, D., Heemink, A. W., and Deleersnijder, E. (2007b). Lagrangian
2421 modelling of multidimensional advection-diffusion with space-varying diffu-
2422 sivities: theory and idealized test cases. *Ocean Dynamics*, 57(3):189–203.
- 2423 Spivakovskaya, D., Heemink, A. W., Milstein, G. N., and Schoenmakers,
2424 J. G. M. (2005). Simulation of the transport particles in coastal waters
2425 usinf forward and reverse time diffusion. *Advances in Water Resources*,
2426 28(9):927–938.
- 2427 Staaterman, E. and Paris, C. B. (2013). Modelling larval fish navigation: the
2428 way forward. *ICES Journal of Marine Science: Journal du Conseil*, page
2429 fst103.
- 2430 Stohl, A. (1998). Computation, accuracy and applications of trajectories: a
2431 review and bibliography. *Atmospheric Environment*, 32(6):947 – 966.
- 2432 Stohl, A. and James, P. (2005). A Lagrangian analysis of the atmospheric
2433 branch of the global water cycle. Part II: Moisture transports between
2434 earth's ocean basins and river catchments. *Journal of Hydrometeorology*,
2435 6(6):961–984.

- 2437 Stouffer, R. J. (2004). Time scales of climate response. *Journal of Climate*,
2438 17:209–217.
- 2439 Sunagawa, S., Coelho, L. P., Chaffron, S., Kultima, J. R., Labadie, K.,
2440 Salazar, G., Djahanschiri, B., Zeller, G., Mende, D. R., Alberti, A., et al.
2441 (2015). Structure and function of the global ocean microbiome. *Science*,
2442 348(6237):1261359.
- 2443 Swift, D. D. and Riser, S. C. (1994). RAFOS floats: Defining and targeting
2444 surfaces of neutral buoyancy. *Journal of atmospheric and Oceanic ...*,
2445 11(4):1079–1092.
- 2446 Taylor, G. I. (1921). Diffusion by continuous movements. *Proc. London Math.*
2447 *Soc.*, 20:196–212.
- 2448 Teske, P. R., Sandoval-Castillo, J., van Sebille, E., Waters, J., and Beheregaray,
2449 L. B. (2015). On-shelf larval retention limits population connectivity in a
2450 coastal broadcast spawner. *Marine Ecology-Progress Series*, 532:1–12.
- 2451 Thomas, C. et al. (2015a). *Modelling marine connectivity in the Great Barrier*
2452 *Reef and exploring its ecological implications*. PhD thesis, UCL.
- 2453 Thomas, C. J., Lambrechts, J., Wolanski, E., Traag, V. A., Blondel, V. D.,
2454 Deleersnijder, E., and Hanert, E. (2014). Numerical modelling and graph
2455 theory tools to study ecological connectivity in the Great Barrier Reef.
2456 *Ecological Modelling*, 272:160–174.
- 2457 Thomas, M. D., Trégouier, A.-M., Blanke, B., Deshayes, J., and Volodkoire,
2458 A. (2015b). A Lagrangian Method to Isolate the Impacts of Mixed Layer
2459 Subduction on the Meridional Overturning Circulation in a Numerical
2460 Model. *Journal of Climate*, 28:7503–7517.
- 2461 Trembl, E. A., Halpin, P. N., Urban, D. L., and Pratson, L. F. (2008). Modeling
2462 population connectivity by ocean currents, a graph-theoretic approach for
2463 marine conservation. *Landscape Ecology*, 23:19–36.
- 2464 Trenberth, K. E. (1998). Atmospheric moisture residence times and cy-
2465 cling: Implications for rainfall rates and climate change. *Climatic change*,
2466 39(4):667–694.

- 2467 Ullman, D. S., O'Donnell, J., Kohut, J., Facke, T., and Allen, A. (2006).
2468 Trajectory prediction using HF radar surface currents: Monte Carlo simula-
2469 tions of prediction uncertainties. *Journal of Geophysical Research: Oceans*,
2470 111(C12):C12005–14.
- 2471 Valdivieso Da Costa, M. and Blanke, B. (2004). Lagrangian methods for flow
2472 climatologies and trajectory error assessment. *Ocean Modelling*, 6(3-4):335–
2473 358.
- 2474 Vallis, G. K. (2006). *Atmospheric and Oceanic Fluid Dynamics: Fundamentals*
2475 and Large-scale Circulation
- . Cambridge University Press, Cambridge, 1st
-
- 2476 edition. 745 + xxv pp.
- 2477 van Sebille, E., Beal, L. M., and Johns, W. E. (2011). Advective time scales of
2478 Agulhas leakage to the North Atlantic in surface drifter observations and the
2479 3D OFES model. *Journal of Physical Oceanography*, 41(2002):1026–1034.
- 2480 van Sebille, E., Johns, W. E., and Beal, L. M. (2012). Does the vorticity flux
2481 from Agulhas rings control the zonal pathway of NADW across the South
2482 Atlantic? *Journal of Geophysical Research*, 29:2753–2768.
- 2483 van Sebille, E., Scussolini, P., Durgadoo, J. V., Peeters, F. J. C., Biastoch,
2484 A., Weijer, W., Turney, C. S. M., Paris, C. B., and Zahn, R. (2015). Ocean
2485 currents generate large footprints in marine palaeoclimate proxies. *Nature*
2486 *Communications*, 6:6521.
- 2487 van Sebille, E., Spence, P., Mazloff, M. R., England, M. H., Rintoul, S. R.,
2488 and Saenko, O. A. (2013). Abyssal connections of Antarctic Bottom Water
2489 in a Southern Ocean State Estimate. *Geophysical Research Letters*, 40.
- 2490 van Sebille, E., Sprintall, J., Schwarzkopf, F. U., Sen Gupta, A., Santoso, A.,
2491 England, M. H., Biastoch, A., and Böning, C. W. (2014). Pacific-to-Indian
2492 Ocean connectivity: Tasman leakage, Indonesian Throughflow, and the role
2493 of ENSO. *J. Geophys. Res. Ocean.*, 119(2):1365–1382.
- 2494 Vanderborght, J.-P., Folmer, I. M., Aguilera, D. R., Uhrenholdt, T., and
2495 Regnier, P. (2007). Reactive-transport modelling of C , N , and O_2 in a
2496 river-estuarine-coastal zone system: Application to the Scheldt estuary.
2497 *Marine Chemistry*, 106(1-2):92–110.

- 2498 Veneziani, M., Griffa, A., Reynolds, A. M., and Mariano, A. J. (2004). Oceanic
2499 turbulence and stochastic models from subsurface lagrangian data for the
2500 northwest atlantic ocean. *Journal of Physical Oceanography*, 34(8):1884–
2501 1906.
- 2502 Villar, E., Farrant, G. K., Follows, M., Garczarek, L., Speich, S., Audic, S.,
2503 Bittner, L., Blanke, B., Brum, J. R., Brunet, C., Casotti, R., Chase, A.,
2504 Dolan, J. R., d'Ortenzio, F., Gattuso, J.-P., Grima, N., Guidi, L., Hill, C. N.,
2505 Jahn, O., Jamet, J.-L., Le Goff, H., Lepoivre, C., Malviya, S., Pelletier, E.,
2506 Romagnan, J.-B., Roux, S., Santini, S., Scalco, E., Schwenck, S. M., Tanaka,
2507 A., Testor, P., Vannier, T., Vincent, F., Zingone, A., Dimier, C., Picheral,
2508 M., Searson, S., Kandels-Lewis, S., Tara Oceans Coordinators, Acinas,
2509 S. G., Bork, P., Boss, E., de Vargas, C., Gorsky, G., Ogata, H., Pesant, S.,
2510 Sullivan, M. B., Sunagawa, S., Wincker, P., Karsenti, E., Bowler, C., Not,
2511 F., Hingamp, P., and Iudicone, D. (2015). Environmental characteristics of
2512 Agulhas rings affect interocean plankton transport. *Science*, 348(6237).
- 2513 Visser, A. W. (1997). Using random walk models to simulate the vertical
2514 distribution of particles in a turbulent water column. *Marine Ecology
2515 Progress Series*, 158:275–281.
- 2516 Visser, A. W. (2008). Lagrangian modelling of plankton motion: From
2517 deceptively simple random walks to Fokker–Planck and back again. *Journal
2518 of Marine Systems*, 70(3-4):287–299.
- 2519 von Appen, W.-J., Koszalka, I. M., Pickart, R. S., Haine, T. W. N., Mastopole,
2520 D., and Magaldi, M. G. (2014). East Greenland Spill Jet as important part
2521 of the AMOC. *Deep Sea Res. I*, 192:75–84.
- 2522 Wallcraft, A. J., Metzger, E. J., and Carroll, S. N. (2009). Software design
2523 description for the HYbrid Coordinate Ocean Model (HYCOM) version
2524 2.2. Technical Report NRL/MR/7320-09-9166, NRL.
- 2525 Wang, B., Zhao, G., and Fringer, O. (2011). Reconstruction of vector fields
2526 for semi-lagrangian advection on unstructured, staggered grids. *Ocean
2527 Modelling*, 40(1):52–71.
- 2528 Wang, J., Mazloff, M. R., and Gille, S. T. (2016,a). Cross-stream transport
2529 near the Drake Passage. *Journal of Physical Oceanography (submitted)*, 88.

- 2530 Wang, Y., Beron-Vera, F. J., and Olascoaga, M. J. (2016b). The life cycle
2531 of a coherent Lagrangian Agulhas ring. *Journal of Geophysical Research: Oceans*, pages 1–11.
2532
- 2533 Waugh, D. W. and Abraham, E. R. (2008). Stirring in the global surface
2534 ocean. *Geophys. Res. Lett.*, 35(20).
- 2535 Waugh, D. W., Haine, T. W. N., and Hall, T. M. (2004). Transport times
2536 and anthropogenic carbon in the subpolar North Atlantic Ocean. *Deep Sea Research Part I: Oceanographic Research Papers*, 51(11):1475–1491.
2537
- 2538 Welander, P. (1955). Studies on the general development of motion in a
2539 two-dimensional, ideal fluid. *Tellus*, 7(2):141–156.
- 2540 Wilkins, D., van Sebille, E., Rintoul, S. R., Lauro, F. M., and Cavicchioli,
2541 R. (2013). Advection shapes Southern Ocean microbial assemblages independent
2542 of distance and environment effects. *Nature Communications*, 4:1–7.
2543
- 2544 Wolfram, P. J. and Ringler, T. D. (2017a). Computing eddy-driven effective
2545 diffusivity using lagrangian particles. *Ocean Modelling*, 118(Supplement
2546 C):94 – 106.
- 2547 Wolfram, P. J. and Ringler, T. D. (2017b). Quantifying nonlinearity of eddy-
2548 induced mixing in an idealized circumpolar current. *Journal of Physical
2549 Oceanography*, 47(8):1897–1920.
- 2550 Wolfram, P. J., Ringler, T. D., Maltrud, M. E., Jacobsen, D. W., and Petersen,
2551 M. R. (2015). Diagnosing isopycnal diffusivity in an eddying, idealized
2552 midlatitude ocean basin via lagrangian, in situ, global, high-performance
2553 particle tracking (light). *Journal of Physical Oceanography*, 45(8):2114–
2554 2133.
- 2555 Wood, S., Paris, C. B., Ridgwell, A., and Hendy, E. J. (2013). Modelling
2556 dispersal and connectivity of broadcast spawning corals at the global scale.
2557 *Global Ecology and Biogeography*, 23:1–11.
- 2558 Young, W. R. and Jones, S. (1991). Shear Dispersion. *Physics of Fluids
2559 a-Fluid Dynamics*, 3(5):1087–1101.

- 2560 Zhurbas, V. (2004). Drifter-derived maps of lateral diffusivity in the Pacific
2561 and Atlantic Oceans in relation to surface circulation patterns. *Journal of*
2562 *Geophysical Research: Oceans*, 109(C5):C05015.
- 2563 Zika, J. D., England, M. H., and Sipp, W. P. (2012). The Ocean Circulation
2564 in Thermohaline Coordinates. *Journal of Physical Oceanography*, 42(5):708–
2565 724.